Leptonic Flavour Symmetries and their Cosmological Dynamics

TURNER, JESSICA,MARGARET

Leptonic Flavour Symmetries and their Cosmological Dynamics

Jessica Turner

A Thesis presented for the degree of
Doctor of Philosophy

Institute of Particle Physics Phenomenology
Department of Physics
University of Durham
England

July 2017

Dedicated to

Helen, Katherine and Keat

Abstract

The discovery of neutrino oscillations provides indisputable evidence that neutrinos have non-zero masses and mixing. Measuring the fine structure of neutrino mixing is one of the foremost challenges in experimental neutrino physics and understanding the origin of the pattern of mixing is of great interest from a theoretical perspective.

The observed pattern of mixing in the lepton sector could be explained by the presence of a non-Abelian discrete symmetry and in this doctoral thesis, we study the phenomenological implications of applying a Non-Abelian, discrete flavour symmetry, $G_f = \mathrm{A}_5$, in combination with a generalised CP symmetry, to the lepton sector. We consider all possible Abelian residual symmetries in the charged lepton (G_ℓ) and neutrino (G_ν) sectors. In the more constrained scenario, the set of Abelian residual symmetries we study are $G_\ell = \{\mathbb{Z}_3, \mathbb{Z}_5, \mathbb{Z}_2 \times \mathbb{Z}_2\}$ and $G_\nu = \mathbb{Z}_2 \times \mathrm{CP}$. We focus on the mixing patterns that are compatible with experimental bounds and discuss in detail the testability of these predictions at upcoming accelerator, reactor and neutrinoless double-beta decay experiments. We find the synergy between upcoming oscillation facilities allows for this flavour symmetric approach to be fully tested. In addition, we consider a less constraining set of residual symmetries, $G_\ell = \mathbb{Z}_2$ and $G_\nu = \mathbb{Z}_2 \times \mathrm{CP}$, and find there are many more predictions with more complicated correlations between neutrino parameters.

In complement to the discussion of leptonic flavour symmetries, we present a new mechanism of leptogenesis which proceeds via lepto-bubble nucleation. This mechanism has direct connections with leptonic flavour models and low-energy neutrino parameters. We calculate the lepton asymmetry using the Closed-Time Path formalism and we find the phase transition temperature to be $T \sim 10^{11}$ GeV, similar to that of high-scale thermal leptogenesis.

Declaration

The work in this thesis is based on research carried out at the Institute of Particle Physics Phenomenology, Department of Physics, Durham University, England, U.K. No part of this thesis has been submitted elsewhere for any other degree or qualification and it is all my own work unless referenced to the contrary in the text.

The following chapters have been published in the form of papers:

- Chapter 2 is based on [1]

  P. Ballett, S. Pascoli, and J. Turner. 'Mixing angle and phase correlations from A_5 with generalized CP and their prospects for discovery' Phys.Rev. D92 (2015) no.9, 093008 [arXiv:1503.07543]

- Chapter 3 is based on [2]

  J. Turner. 'Predictions for leptonic mixing angle correlations and non-trivial Dirac CP violation from A_5 with generalized CP symmetry' Phys.Rev. D92 (2015) no.11, 116007 [arXiv:1507.06224]

- Chapter 4 is based on [3]

  S.Pascoli, J. Turner, Y.L. Zhou. 'Baryogenesis via leptonic CP-violating phase transition' [arXiv:1609.07969]

Acknowledgements

Firstly, I would like to thank my supervisor, Prof Silvia Pascoli, for her continued support and guidance throughout my PhD years. I have benefited greatly from the many opportunities you afforded me: your insight in theoretical physics, advice, freedom to explore, space to work and the chance to travel to many interesting places. I am lucky and grateful to be your student.

I would like to express my gratitude to Mrs Trudy Forster, Mrs Linda Wilkinson and Mr Oliver Smith for their good humour, kindness and organisational/technical skills which have helped me throughout my PhD years.

Thank you to collaborators, friends and colleagues who have been instrumental in teaching me physics and have stood next to me for various academic reasons. Dr Peter Ballett, thank you for patiently answering the many, many questions I asked you with a clarity and intelligence I try to aim for. Prof Celine Boehm, thank you for always having your door open for me, at those especially critical times, inspiring me with your creativity and good humour. Prof Serguey Petcov, thank you for your mentorship and encouragement, in particular with regards to finishing my second paper. I have thoroughly enjoyed our discussions on physics and life in general. Dr Ye-Ling Zhou, thank you for teaching me a great deal about physics, politics and culture; I value your friendship.

I am lucky to have good friends with whom I can discuss physics and other work-related topics: thank you to Helen Brooks, Davide Napoletano, Alexis Plascencia, Darren (Dazza) Scott and Dr Carlos Tamarit.

I am particularly grateful to those friends who made life outside physics much more enjoyable: Thomai Tsiftsi, thank you for your friendship, the many coffees, shared laughs and the opportunity to work in Mathlab. George Gazis, thank you for being a wonderful tango partner, sharing many glasses of wine, laughs and philosophical conversations with me. You have made the final year of my PhD infinitely brighter.

I am indebted to the enduring friendship of Kirsty Ireland and Gillian Ramage. Kirsty, thank you for always being there for me, for the laughs, walking hundreds, perhaps thousands, of miles with me and for taking the time to visit me in various locations. Gillian Ramage, thank you for offering both a listening ear and sound advice across the years, sharing your sharp wit and being a loving friend.

I would not be here without the unconditional love and support of my mother. I miss you very much. To my father, thank you for everything. My sister, Katherine, thank you for your humour, even in the darkest of hours; courage and compassion.

A final note to Holger: thank you for your love, support, laughter and acceptance, even when I am at my most intolerable. I am a better person for having you by my side. You know my gratitude and my love.

July 24, 2017

Contents

List of Figures

List of Tables

Chapter 1

Introduction

Since their discovery, neutrinos have played a pivotal role in revealing and probing the electroweak theory, the structure of the nucleon, the dynamics of the sun and violent cosmic phenomena such as core-collapse supernovae. However, in spite of their great abundance, relatively little is known about neutrinos as they are very weakly interacting.

There are a number of features of neutrinos which sets them apart from the menagerie of Standard Model particles: the neutrino is the only known neutral fermion, and therefore possibly its own anti-particle, leptonic CP-violation may be sizeable and neutrino masses are very small while mixing is large. Theories which hope to accommodate such features must go beyond the Standard Model and in doing so may reveal physics at a very high-energy scale.

In this chapter, we shall further elucidate and contextualise the aforementioned issues by reviewing the colourful history of neutrinos, outlining neutrino oscillation phenomenon and summarising the current status of neutrino observables. In addition, we shall discuss possible mechanisms of neutrino mass generation.

1.1 Neutrinos: A Brief Historical Overview

The existence of a very light, electrically neutral spin 1/2 particle was first postulated in 1930 by Pauli in order to explain the apparent non-conservation of energy observed in nuclear beta decay. Such a process was thought to proceed via a two-body decay of the unstable neutron into a proton and electron. To much consternation, it was discovered the energy spectrum of the radiated electron was continuous[1]. This observation puzzled Pauli and, unable to attend a physics meeting in Tübingen, he instead sent a letter in which he proposed a new, light particle as a "desperate remedy" to explain the missing energy in beta decay. Pauli initially dubbed this particle the neutron and later, Fermi suggested the name *neutrino* (this being derived from the Italian for *small, neutral one*).

In 1934, Fermi developed the first theory of beta decay where he considered the decay as a four-fermion process with a neutron decaying to proton, electron and anti-electron neutrino [4]. In the same year, Bethe and Peierls estimated the interaction cross section of a neutrino with a nuclei [5]. Their calculation showed the cross section to be so small that the detection of the neutrino was long thought to be impossible; Pauli bet a case of champagne that no one would ever detect the illustrious neutrino.

History proved otherwise. In 1946, Pontecorvo proposed a possible method of neutrino detection via chlorine

$$\nu + {}^{37}\mathrm{Cl} \rightarrow e^- + {}^{37}\mathrm{Ar}. \tag{1.1.1}$$

Moreover, he suggested fission reactors and the sun as intense sources of neutrinos. However it was not until 1956, that Reines and Cowan detected antineutrinos emitted from a nuclear reactor [6]. The detection was based on observation of the following reaction

$$\overline{\nu} + \mathrm{p} \rightarrow e^+ + \mathrm{n}. \tag{1.1.2}$$

[1] It was anticipated the energy spectrum would be a single monochromatic line corresponding to the mass difference between the neutron and proton.

Two years later (1958) Goldhaber, Grodzin, and Sunyar measured the handedness of the neutrino from an experiment which measured the circular polarisation of photons [7]. This experiment had important consequences as they established that neutrino particles were left-handed. As no right-handed neutrino has ever been detected, the finding of Goldhaber, Grodzin, and Sunyar implies that neutrinos are massless.

In spite of this result, Pontecorvo considered the possibility of massive neutrinos and the experimental implications [8]. If neutrinos had small masses then neutrino oscillations, similar to $K^0 - \overline{K^0}$ oscillations, could occur. In 1962, Pontecorvo's work was extended both theoretically and experimentally. In the former case, Maki, Nakagawa and Sakata introduced flavour oscillations (between electron and muon flavour) [9] and in the latter, the Brookhaven neutrino experiment led by Lederman, Schwartz and Steinberger, discovered that neutrinos which undergo charged current interactions with electron and muons are in fact different neutrinos. In short, they discovered the muon neutrino and were subsequently awarded the Physics Nobel Prize in 1988.

The next major experimental achievement in neutrino physics came in 1970 with the Homestake experiment pioneered by Davis and Bahcall [10]. In this experiment, they utilised the reaction initially proposed by Pontecorvo to measure high-energy solar neutrinos[2]. However, it was found that the observed rate of this reaction was two to three times smaller than predicted in the Minimal Solar Model and this deficit came to be known as the *solar neutrino problem*. This problem could only be fully resolved from improved understanding of neutrino properties and additional measurement by Super-Kamiokande (SK) and Sudbury Neutrino Oscillation (SNO) collaborations. Theoretically, a large deficit of electron neutrinos was to be expected due to the Mikheyev-Smirnov-Wolfenstein (MSW) effect which was formulated in 1985 [11, 12].

[2]The threshold of this reaction is 0.81 MeV and so only very high-energy neutrinos could partake.

In 1975, the tau lepton was discovered by Perl and colleagues at Stanford Linear Accelerator [13] and this hinted there may be a third generation of neutrino, the tau neutrino. The three-neutrino picture was later confirmed via Z-decays at LEP [14]. However, this species of neutrino was only directly observed in 2000 by the Direct Observation of NU Tau (DONUT) experiment [15] which used the decay of charmed particles to produce tau neutrinos.

As hinted at previously, SK [16] and SNO [17, 18] collaborations were the first oscillation experiments to confirm neutrino oscillations with high statistical significance. Since this time, there have been a plethora of neutrino experiments which have improved our understanding of neutrino properties and we shall discuss them further in Section 1.3

1.2 Neutrino Oscillations

An active neutrino, the particles we have been discussing thus far, is in an $SU(2)_L$ doublet with a charged lepton and therefore partakes in charged and neutral current interactions and comes in three varieties: electron, muon and tau flavour. As mentioned before, it was Pontecorvo who first proposed neutrino oscillations. He postulated such a phenomenon following the observation of particle mixing in kaon systems. This occurs because the flavour and mass eigenstates do not coincide and this mixing may be parametrised by the Cabbibo-Kobayashi-Maskawa (CKM) matrix [19, 20]. The analogous matrix in the neutrino sector is the Pontecorvo-Maki-Nakagawa-Saki (PMNS) matrix [9]. Denoting the mass eigenstates as ν_1, ν_2, ν_3 and the flavour eigenstates as $\nu_\mathrm{e}, \nu_\mu, \nu_\tau$, the matrix describing the misalignment of states is given by

$$\begin{pmatrix} \nu_\mathrm{e} \\ \nu_\mu \\ \nu_\tau \end{pmatrix} = \underbrace{\begin{pmatrix} U_{\mathrm{e}1} & U_{\mathrm{e}2} & U_{\mathrm{e}3} \\ U_{\mu 1} & U_{\mu 2} & U_{\mu 3} \\ U_{\tau 1} & U_{\tau 2} & U_{\tau 3} \end{pmatrix}}_{U_\mathrm{PMNS}} \begin{pmatrix} \nu_1 \\ \nu_2 \\ \nu_3 \end{pmatrix}. \tag{1.2.3}$$

If there are no additional states beyond the left-handed neutrinos, then the PMNS matrix is a 3×3, unitary matrix and therefore may be parametrised by three 2×2

rotation matrices

$$U_{\text{PMNS}} = \underbrace{\begin{pmatrix} 1 & 0 & 0 \\ 0 & c_{23} & s_{23} \\ 0 & -s_{23} & c_{23} \end{pmatrix}}_{\text{atmospheric}} \underbrace{\begin{pmatrix} c_{13} & 0 & s_{13}e^{i\delta_{\text{CP}}} \\ 0 & 1 & 0 \\ s_{13}e^{-i\delta_{\text{CP}}} & 0 & c_{13} \end{pmatrix}}_{\text{reactor}} \underbrace{\begin{pmatrix} c_{12} & s_{12} & 0 \\ -s_{12} & c_{12} & 0 \\ 0 & 0 & 1 \end{pmatrix}}_{\text{solar}} \underbrace{\begin{pmatrix} 1 & 0 & 0 \\ 0 & e^{i\alpha_{21}/2} & 0 \\ 0 & 0 & e^{i\alpha_{31}/2} \end{pmatrix}}_{\text{Majorana}}, \tag{1.2.4}$$

where $s_{ab} \equiv \sin(\theta_{ab}), c_{ab} \equiv \cos(\theta_{ab})$, δ_{CP} is the Dirac phase and α_{21}, α_{31} are the Majorana phases which are physical if and only if neutrinos are Majorana in nature [3]. It is worth stressing, the Majorana phases are only measurable in experiments in which the Majorana nature of the neutrinos is manifest e.g. in lepton-number violating processes such as neutrinoless double-beta decay. Therefore, the Majorana phases are not observable at oscillation experiments.

We shall briefly outline the standard derivation of the neutrino oscillation probability in vacuum. There are more rigorous derivations, such as using quantum mechanical wave packets, which drops the assumption of pure momentum eigenstates and instead superposes many momentum eigenstates [22]. However, for the purposes of illustration, is it sufficient to derive the oscillation probability using the equal-momentum approximation.

The physical states which propagate are the mass states $|\nu_1\rangle, |\nu_2\rangle, |\nu_3\rangle$ and evolve according to the time-dependent Schrödinger equation

$$\frac{\partial}{\partial t}|\nu_i\rangle = i\text{H}|\nu_i\rangle, \tag{1.2.5}$$

where $i = 1, 2, 3$ and the solutions are plane waves of the form $|e^{-iE_i t}\nu_i\rangle$. The quantity we would like to compute is the probability that a neutrino of flavour α oscillates into a neutrino of flavour β while propagating over a distance L. As it is the mass states, not the flavour states, which propagate the initial and final states

[3] There are a number of parametrisation of the PMNS matrix, however Eq. (1.2) follows the Particle Data Group [21] convention.

are given in terms of the mass states. The initial state is given by

$$|\Psi\left(x=0\right)\rangle = |\nu_\alpha\rangle = \sum_{i=1}^{3} U_{\alpha i}^{*}|\nu_i\rangle, \tag{1.2.6}$$

and after propagating for time, t, and distance L, the final state is written as

$$|\Psi\left(x=L\right)\rangle = \sum_{i=1}^{3} U_{\alpha i}^{*} e^{-iE_i t}|\nu_i\rangle. \tag{1.2.7}$$

Therefore the amplitude for $\nu_\alpha \to \nu_\beta$ is given by

$$\langle\nu_\beta|\Psi(L)\rangle = \sum_{i=1}^{3} U_{\alpha i}^{*} U_{\beta i} e^{-iE_i t}, \tag{1.2.8}$$

where we have applied the orthogonality of these states, $\langle\nu_j|\nu_i\rangle = \delta_{ij}$. The energy, E_i, may be written in terms of the mass and momentum

$$E_i = \sqrt{p_i^2 + m_i^2} \simeq p\left(1 + \frac{m_i^2}{2p^2}\right), \tag{1.2.9}$$

where p is the momentum common to all mass states[4]. In the relativistic limit, $L \sim t$, the amplitude of Eq. (1.2.8) may be rewritten as

$$\langle\nu_\beta|\Psi(L)\rangle = \sum_{i=1}^{3} U_{\alpha i}^{*} U_{\beta i} e^{-iL\left(p + \frac{m_i^2}{2p}\right)}. \tag{1.2.10}$$

To find the flavour oscillation probability, the amplitude is squared and the approximation, $p^{-1} \simeq E^{-1}$, is applied

$$P\left(\nu_\alpha \to \nu_\beta\right) = \Big|\sum_{i=1}^{3} U_{\alpha i}^{*} U_{\beta i} e^{-iL\left(p + \frac{m_i^2}{2E}\right)}\Big|^2. \tag{1.2.11}$$

Eq. (1.2.11) may be simplified by applying the unitary of the PMNS matrix and the formula, $2\sin^2\theta/2 = 1 - \cos\theta$. To this end, the oscillation probability is given by

$$\begin{aligned} P\left(\nu_\alpha \to \nu_\beta\right) = \delta_{\alpha\beta} &- 4\sum_{i>j} \mathrm{Re}\left[U_{\alpha i}^{*} U_{\beta i} U_{\alpha j} U_{\beta j}^{*}\right] \sin^2\left(\frac{\Delta m_{ij} L}{4E}\right) \\ &+ 2\sum_{i>j} \mathrm{Im}\left[U_{\alpha i}^{*} U_{\beta i} U_{\alpha j} U_{\beta j}^{*}\right] \sin\left(\frac{\Delta m_{ij} L}{2E}\right). \end{aligned} \tag{1.2.12}$$

From Eq. (1.2.12), we can see the oscillation probability is a function of the mixing angles, δ_{CP}, the mass squared splittings (e.g. $m_{ij}^2 = m_i^2 - m_j^2$), the neutrino energy,

[4]This is the equal-momentum approximation.

E, and the baseline, L, which is the distance between the site of production and detection of the neutrino. Therefore the determination of the oscillation probability of various different flavour transitions allows for the measurement of the oscillation parameters. In most oscillation experiments, the baseline is fixed but the energy of the neutrinos is varied. Moreover, the observation of neutrino oscillations indicates that at least two of the mass eigenstates are non-zero. The current status and method of measuring these parameters will be discussed in Section 1.3

1.3 Current Status of Neutrino Parameters

Over the past five decades, there has been impressive experimental progress made in neutrino physics which is made possible from the synergy of oscillation, neutrinoless double-beta decay, tritium end point experiments and cosmological constraints. The current best fit (and 3σ interval) values for neutrino parameters from the NuFit 3.0 group [23] are shown in Table 1.1 and shall be applied throughout the remainder of this thesis.

	best-fit value	3σ range
θ_{12}°	33.72	{31.52, 36.18}
θ_{13}°	8.47	{7.86, 9.11}
θ_{23}°	49.3	{38.6, 53.1}
δ°	272	{0, 360}
$\frac{\Delta m_{21}^2}{10^{-5}\mathrm{eV}^2}$	7.48	{7.02, 8.08}
$\frac{\Delta m_{31}^2}{10^{-3}\mathrm{eV}^2}$ (NO)	2.477	{2.351, 2.610}
$\frac{\Delta m_{32}^2}{10^{-3}\mathrm{eV}^2}$ (IO)	-2.465	{-2.594, -2.339}

Table 1.1: The best-fit points from NuFit 3.0 global analysis of oscillation data from May 2016.

In Sections. (1.3.1), (1.3.2) and (1.3.3) we provide a brief historical overview of the oscillation experiments used to measure the atmospheric, reactor and solar neutrino parameters and discuss their current status. Later, in Section 1.3.4 and Section 1.3.5 we discuss leptonic CP-violation and the neutrino mass spectra.

1.3.1 Atmospheric Parameters: θ_{23} and $\Delta m_{\mathbf{atm}}$

Atmospheric neutrinos are produced via cascades initiated by cosmic rays collisions in the Earth's atmosphere. The dominant production of these neutrinos follows the series of reactions

$$\pi^+ \to \mu^+ + \nu_\mu \quad \text{and} \quad \mu^+ \to e^+ + \nu_\text{e} + \overline{\nu_\mu}, \tag{1.3.13}$$

and their CP-conjugate decays. Typically, the neutrino energies range from MeV to GeV scale and for the lower-energy neutrinos, it was anticipated the ratio of muon to electron neutrinos would be 2:1[5]. A number of experiments were built to detect atmospheric neutrinos; these include NUSSEX, Frejus, Soudan [24] and SK [16]. In 1988, the Kamiokande collaboration noticed the expected ratio of muon to electron neutrino was approximately 60% of the expected number of events given the knowledge of atmospheric fluxes at that time [25]. To further confound the situation, in 1998, SK found an up-down asymmetry in addition to the already depleted muon neutrino flux reaching its detector. This finding was consistent with the up-going muon neutrinos oscillating into tau neutrinos while the down-going neutrinos do not propagate sufficient distance to oscillate into another flavour. From these results, the atmospheric parameters were found to be $\sin^2\theta_{23} \approx 1$ and $\Delta m_\text{atm} \approx 2.4\times10^{-3}$eV.

Three currently running experiments that have the greatest sensitivity to the atmospheric parameters are long baseline accelerator ν_μ disappearance experiments: Main Injector Neutrino Oscillation Search (MINOS), Tokai to Kamioka (T2K) and NuMI Off-Axis ν_e Appearance (NOνA). MINOS uses the Neutrinos at the Main Injector (NUMI) beam based at Fermilab and is an on-axis experiment with the far detector (magnetised steel scintillator) placed 735km away in Soudan mine, South Dakota. T2K is an off-axis, water Cherenkov detector which uses a 30 GeV proton beam based at J-PARC. The far detector, based in Kamioka, is approximately 295km from the neutrino source. NOνA also uses the NUMI beam but the detector (oil scintillator) is slightly off-axis. Moreover, the baseline is 810km with the far

[5]The ratio is expected to increase for higher energy neutrinos due to the fact that the fraction of higher energy muon that decay in flight is smaller.

detector based in Minnesota.

In the most recent results, data from MINOS and T2K is consistent with the maximal ($\theta_{23} = \pi/4$) atmospheric mixing angle while NOνA excludes maximal mixing at 2.6σ level. This *tension* between the two sets of experiments is shown in Fig. 1.1.

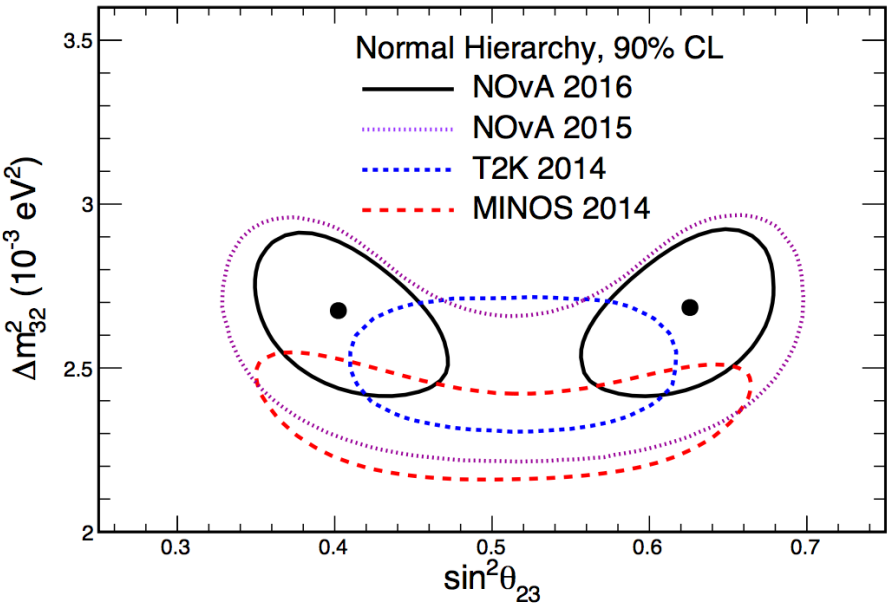

Figure 1.1: Measurement of atmospheric mass squared splitting and mixing angle. Contours display the 90% confidence region and shows there is tension between T2K, MINOS and NOνA [26].

1.3.2 Reactor Parameter: θ_{13}

Reactor neutrino experiments have played a key role in the precision measurement of θ_{13}. This is because fission reactors copiously produce neutrinos as by-products from beta decay of neutron-rich nuclei produced in the decay chains of uranium and plutonium. The flux of neutrinos from the reactors is isotropic and decreases rapidly ($\propto 1/L^2$) as the distance from the reactor to detector is increased. Moreover, the reactor neutrinos are typically of energies of several MeV and thus only one channel (anti-electron neutrino survival probability) may be studied as heavier charged lepton cannot be produced from such low energy neutrinos. In order to measure these

neutrinos, the reactor experiments rely upon inverse beta decay

$$\overline{\nu_e} + p \rightarrow n + e^+, \tag{1.3.14}$$

which has a neutrino energy threshold of 1.8 MeV. Importantly, any uncertainty in this cross section is related to the measured flux. Until 2011, it appeared the neutrino flux was well understood but this confidence was shaken as the absolute value of the measured flux is 6% below the theoretical prediction [27]. This issue has come to be known as the *reactor anomaly*.

Post-2002, eight reactor experiments had been proposed and three of them constructed: Daya Bay (China) [28, 29], Reactor Experiment for Neutrino Oscillation (RENO, South Korea) [30] and Double-Chooz (France) [31]. In addition, Kamioka Liquid Scintillator Antineutrino Detector (KamLAND, Japan) was built earlier and started data-taking in 2002. Daya Bay, RENO and Double-Chooz are similar in their setup: the near detectors have baselines $\mathcal{O}(100)$ m while the far detectors are $\mathcal{O}(1)$ km from the reactors. The design of the far and near detectors is similar, which allows the experiments to drastically reduce systematic uncertainties[6]. In addition, these three experiments are designed with a gadolinium doped liquid scintillator target surrounded by non-doped scintillator which is used to detect the gamma from the neutron capture. This allows the experiments to measure the reactor angle via the survival probability of the anti-electron neutrinos, which is largely independent of the other mixing angles

$$P\left(\overline{\nu_e} \rightarrow \overline{\nu_e}\right) \approx 1 - \sin^2 2\theta_{13} \sin\left(\frac{\Delta^2 m_{31} L}{4E_\nu}\right), \tag{1.3.15}$$

where E_ν is the energy of the neutrino and L is the baseline distance. These experiments were instrumental in the precision measurement of θ_{13} [29], which is the best measured mixing angle to date.

[6]Especially if those uncertainties are associated to the flux.

1.3.3 Solar Parameters: θ_{12} and $\Delta m_{\mathbf{sol}}$

Although neutrino physics is often considered as particle physics, the study of solar neutrinos is directly connected with the study of the sun. There are two key thermonuclear processes which produce solar neutrinos: the pp-chain starting with proton-proton fusion and the Carbon-Nitrogen-Oxygen cycle that fuses heavier elements. The reactions that dominate the solar neutrino production are the following

$$\begin{aligned} p + p &\rightarrow {}^{2}\mathrm{H} + e^{+} + \nu_e, \\ p + e^{-} + p &\rightarrow {}^{2}\mathrm{H} + \nu_e, \\ {}^{7}\mathrm{Be} + e^{-} &\rightarrow {}^{7}\mathrm{Li} + \nu_e, \\ {}^{8}\mathrm{B} &\rightarrow {}^{8}\mathrm{Be}^{*} + e^{+} + \nu_e, \end{aligned}$$

and energy of the neutrinos may vary depending on their production mode. However typically solar neutrinos are of the MeV energy scale. These neutrinos, and their deficit, were first measured by the radio-chemical experiment Homestake [10] in 1968. In the subsequent decades several other gallium-based experiments, such as GALLEX [32], GNO [33] and SAGE [34], also confirmed this deficit.

The resolution of this solar neutrino problem came from improved understanding of neutrino oscillations and application of the MSW effect. The MSW effect arises as neutrinos born in the centre of the sun, with the greatest matter density, must propagate to the surface through a decreasing matter density. For high-energy neutrinos (> 5 MeV), interactions with electron-dense solar matter causes resonant conversion between the mass states and reduces the neutrino flux by approximately one third, while for lower-energy neutrinos, the oscillation length is shorter than the size of the solar core and therefore the MSW effect is averaged, resulting in a flux half of what is expected. After many years of measuring a lower than expected flux of solar neutrinos, experiments SK and SNO unambiguously solved the solar neutrino problem by proving the ν_es were oscillating to other flavours.

Although the solar neutrino experiments were crucial, a terrestrial experiment with laboratory conditions was essential to improve the precision in the measurement

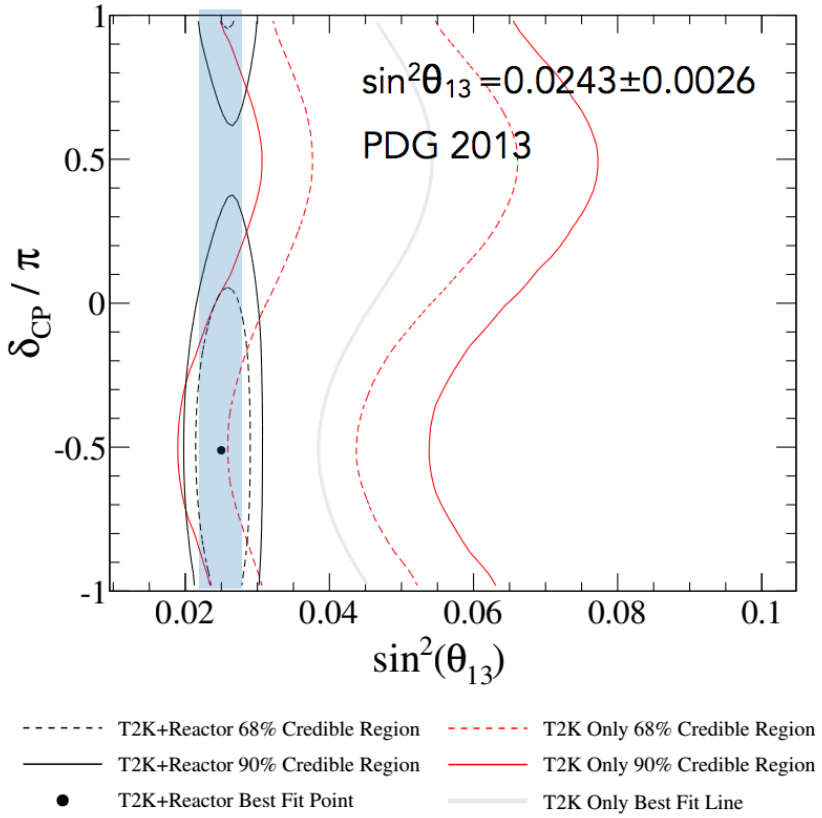

Figure 1.2: Current results from T2K shows slight preference for maximal CP-violation [35].

in the solar parameters. For this purpose, KamLAND was constructed in Japan. KamLAND detects MeV-scale reactor neutrinos at a baseline of 180km using liquid scintillator technology. Using global fit data from all solar neutrino experiments, the best fit values of the solar parameters are $\Delta m_{\text{sol}} \simeq 7.49 \times 10^{-5}\text{eV}^2$ and $\theta_{12} \simeq 33.72°$.

1.3.4 Leptonic CP-Violation

With the precision measurement of $\theta_{13} \simeq 8.5°$, it is possible to explore leptonic CP-violation from δ_{CP} at upcoming oscillation facilities[7]. To date, the 3σ interval of this phase allows for both CP-conservation and maximal CP-violation.

[7]Note that in oscillation probabilities, δ_{CP} is always associated to θ_{13} and therefore if this angle was zero then neutrino and anti-neutrino oscillations would be equal.

Currently, T2K is searching for the effects of this phase via comparison of the oscillation probability of $\nu_\mu \to \nu_e$ and $\overline{\nu_\mu} \to \overline{\nu_e}$. There has been exciting recent news from T2K showing a slight preference for maximal CP-violation as can be seen in Fig. 1.2 [35].

In order to improve the precision in the measurement of this observable, two experiments have been proposed: Deep Underground Neutrino Experiment (DUNE) will utilise the ν_μ beam produced at Fermilab and its far detector will be based 1300km away in South Dakota. The detector will use state-of-the-art Liquid Argon Time-Projection Chamber (LArTPC) technology for the neutrino detector planned at the far site. Likewise, Tokai-to-Hyper-Kamiokande (T2HK) has been proposed as the successor to T2K with similar water Cherenkov technology but with a detector volume of 250 kton. Both of these detectors, and their capabilities, are discussed at length in Section 2.4.2.

If neutrinos are Majorana particles, there are two phases in addition to δ_{CP}. However, these phases cannot be measured at oscillation experiments and it will be a formidable task to constrain them using neutrinoless double-beta decay, which will be further discussed in Section 2.4.4.

1.3.5 Mass Ordering

The neutrino mass spectrum may be ordered in two possible ways as illustrated in Fig. 1.3. In the case of normal ordering the masses are ordered such that $m_1 < m_2 < m_3$, while in the case of inverted ordering, $m_3 < m_1 < m_2$. The difference between the mass *ordering* and mass *hierarchy* is related to the absolute neutrino mass scale and normal and inverted hierarchy are defined as $m_1, m_2 \ll m_3$ and $m_3 \ll m_1, m_2$ respectively.

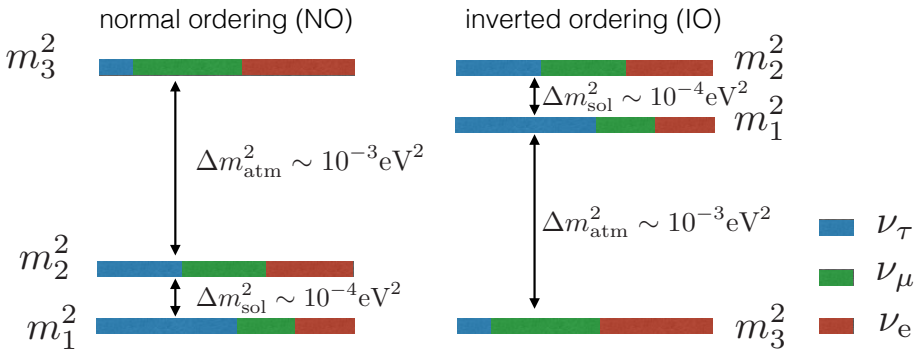

Figure 1.3: Normal (Inverted) ordering is shown on the left (right) diagram.

1.4 Neutrino Masses

As discussed in Section 1.2, there is overwhelming evidence that neutrinos oscillate and are therefore massive. The origin of neutrino mass is unknown and remains a central issue of neutrino physics. The nature of neutrinos, whether they are Dirac or Majorana particles, is intimately connected with their mass generation. For this purpose, we shall discuss Dirac and Majorana fermions in Section 1.4.1 before we proceed to discuss different neutrino mass mechanisms in Section 1.4.2 and Section 1.4.3.

1.4.1 Dirac and Majorana Fermions

- **Dirac Fermions**

  The Lie algebra of the Lorentz group, SO(3, 1), is isomorphic to SU(2)×SU(2). This has the consequence that any representation of the Lorentz algebra can be described by its transformation under SU(2) × SU(2) whose irreducible representations are labelled as (j_1, j_2) where $j_1, j_2 = \pm 1/2$. Importantly, in the language of chiral fermions [36], this means a left-handed chiral fermion is a doublet of one SU(2) factor and a singlet of the other and vice versa for a right-handed chiral fermion. Both of these states are known as *Weyl fermions*. Weyl fermions are the minimal fermionic degree of freedom and hence are the building blocks of Dirac and Majorana fields. This is because any fermionic field transforms under the following representation $(1/2, 0) + (0, 1/2)$ of SU(2) × SU(2).

To begin our discussion of Dirac fermions, we will first define the Dirac matrices in the chiral representation

$$\gamma^0 = \begin{pmatrix} 0 & -\mathbb{1} \\ -\mathbb{1} & 0 \end{pmatrix}, \quad \gamma^i = \begin{pmatrix} 0 & \sigma_i \\ -\sigma_i & 0 \end{pmatrix} \quad \text{and} \quad \gamma^5 = \begin{pmatrix} \mathbb{1} & 0 \\ 0 & -\mathbb{1} \end{pmatrix}, \tag{1.4.16}$$

where σ_i are the Pauli matrices and from Eq. (1.4.16), we define the left and right-handed projection operators

$$P_L = \frac{\mathbb{1} - \gamma^5}{2} \quad \text{and} \quad P_R = \frac{\mathbb{1} + \gamma^5}{2}, \tag{1.4.17}$$

respectively. We may consider a generic bi-spinor, Ψ, which is composed of two Weyl spinors, ξ and η. To identify the chiral components of the bi-spinor, the projection operators must be applied in the following manner

$$\Psi_L = P_L\Psi = \frac{\mathbb{1} - \gamma^5}{2}\begin{pmatrix} \xi \\ \eta \end{pmatrix} = \begin{pmatrix} 0 \\ \eta \end{pmatrix} \quad \text{and} \quad \Psi_R = P_R\Psi = \frac{\mathbb{1} + \gamma^5}{2}\begin{pmatrix} \xi \\ \eta \end{pmatrix} = \begin{pmatrix} \xi \\ 0 \end{pmatrix}. \tag{1.4.18}$$

Applying the free Dirac equation to the bi-spinor we find

$$\left(i\gamma_\mu\partial^\mu - m\right)\Psi = 0, \tag{1.4.19}$$

which may be decomposed in terms of the chiral components as

$$i\gamma_\mu\partial^\mu\Psi_L = m\Psi_R \quad \text{and} \quad i\gamma_\mu\partial^\mu\Psi_R = m\Psi_L. \tag{1.4.20}$$

Note the two Weyl spinors are mixed by the mass term of the Dirac equation and in the massless limit, we recover two uncoupled equations for each Weyl fermion. Regardless, the Dirac spinor may be written in terms of the chiral components

$$\Psi = \Psi_L + \Psi_R, \tag{1.4.21}$$

where the Dirac mass term is given by

$$m(\overline{\Psi_L}\Psi_R + \overline{\Psi_R}\Psi_L) \quad \text{with} \quad \overline{\Psi} \equiv \Psi^\dagger\gamma^0. \tag{1.4.22}$$

To summarise the Dirac fermion, Ψ, is a combination of two Weyl fermions where each Weyl fermion is labelled by chirality. Consequently, the Dirac spinor has four real degrees of freedom[8].

- **Majorana Fermions**

Without loss of generality, the charge conjugation operator may be written as

$$C = i\gamma^0\gamma^2. \tag{1.4.23}$$

The generic approach to define Majorana fermions is to start from the Majorana condition, which constrains the bi-spinor to be equivalent to its conjugate

$$\Psi = \Psi^C = \kappa C\overline{\Psi}^T, \tag{1.4.24}$$

where κ is an arbitrary phase which may be absorbed by rephasing Ψ. Applying the condition of Eq. (1.4.24) to the bi-spinors we find

$$\Psi = \Psi^C = \kappa C\overline{\Psi}^T \implies \begin{pmatrix}\xi\\ \eta\end{pmatrix} = i\begin{pmatrix}0 & \sigma_2\\ -\sigma_2 & 0\end{pmatrix}\begin{pmatrix}\xi^*\\ \eta^*\end{pmatrix}. \tag{1.4.25}$$

Eq. (1.4.25) allows the bi-spinor to be expressed as a function of a single Weyl spinor

$$\Psi = \begin{pmatrix}i\sigma_2\eta^*\\ \eta\end{pmatrix}. \tag{1.4.26}$$

As can be seen from Eq. (1.4.26), the Majorana fermion has only two degrees of freedom coming from the single Weyl fermion, η. From Eq. (1.4.26), we can derive the relation between the chiral components of Ψ

$$\Psi_L = C\overline{\Psi_R}^T \quad \text{and} \quad \Psi_R = C\overline{\Psi_L}^T. \tag{1.4.27}$$

This means the Majorana fermion may be defined purely in terms of the left-handed chiral component

$$\Psi = \Psi_L + C\overline{\Psi_L}^T, \tag{1.4.28}$$

which has the corresponding mass term

$$\frac{1}{2}m(\overline{\Psi_L}^C\Psi_L + \overline{\Psi_L}\Psi_L^C). \tag{1.4.29}$$

[8] At first glance it would seem to be eight (four real d.o.f. from each Weyl spinor), however four d.o.f. may be eliminated from equations of motion.

1.4.2 Dirac Mass

In the following we will (mostly) follow the conventions of [37]. As seen in Eq. (1.4.22), the Dirac mass connects two distinct chiralities of Weyl fermion. For a single generation of neutrino, a Dirac mass connects an active neutrino (ν_L) and a sterile neutrino (N_R)[9].

$$-\mathcal{L}_{\mathrm{D}} = m_D \left(\overline{\nu_L} N_R + \overline{N_R}\nu_L\right) = m_D \nu_D \overline{\nu_D}, \tag{1.4.30}$$

where $\nu_D = \nu_L + N_R$ is the Dirac field. From the global re-phasing, $\nu_L / N_R \to e^{i\theta}\nu_{L/R}$, it is evident that lepton-number is conserved. The Dirac mass of Eq. (1.4.30) may be generated when the Higgs acquires a vacuum expectation value (VEV), $\langle\phi\rangle = \left(0, v_H/\sqrt{2}\right)$ and the effective neutrino mass is given by

$$y_\nu v_H/\sqrt{2}, \tag{1.4.31}$$

where y_ν is the Yukawa coupling and $v_H = 246$ GeV. There persists the question of why the neutrino mass is so small compared with the other Standard Model (SM) fermion masses. If we compare the neutrino Yukawa to the top (tau) there are twelve (nine) orders of magnitude difference and such strong disparity in mass scales is thought to be rather unnatural[10]. For these reasons, it is a widely held belief there is an alternative mechanism of neutrino mass generation.

1.4.3 Majorana Mass

A Majorana mass term, as shown in Eq. (1.4.29), is rather economical as it uses only a single Weyl fermion

$$-\mathcal{L}_{\mathrm{M}} = \frac{m_M}{2}\left(\overline{\nu_L}\nu_R^C + \mathrm{h.c}\right) = \frac{m_M}{2}\left(\overline{\nu_L} C \overline{\nu_L}^T + \mathrm{h.c}\right) = \frac{m_M}{2}\overline{\nu_M}\nu_M \tag{1.4.32}$$

and describes the transition between a left-handed neutrino and a right-handed anti-neutrino (its CPT conjugate). Unlike the previous case, the Majorana mass violates

[9] The sterile neutrino we refer to is also known as a right-handed neutrino. This particle is an $SU(2)_L$ singlet and has not been observed as yet.

[10] This argument should be taken with a pinch of salt as we do not understand the hierarchy between the top and electron mass.

lepton number by two units. In the final expression of Eq. (1.4.32) the Majorana neutrino, $\nu_M = \nu_L + \nu_R^C$, is self-conjugate and therefore is its own anti-particle. Because of this property, such a particle could mediate neutrinoless double-beta decay, which is discussed at length in Chapter 2. It is worth noting that the sterile neutrino will have a Majorana mass (unless there is a symmetry strictly forbidding such a term) as this is completely consistent with SM gauge symmetries

$$-\mathcal{L}_{\rm S} = \frac{m_S}{2}\left(\overline{N_L}^C N_R + \overline{N_R} N_L^C\right). \tag{1.4.33}$$

1.4.4 Majorana Mass and Dirac Mass Terms

If active and sterile neutrinos are present, both Dirac and Majorana masses are allowed. For a single generation of neutrino, the Lagrangian in the weak basis is written as

$$-\mathcal{L} = \frac{1}{2}\begin{pmatrix}\overline{\nu_L}' & \overline{N_L^C}'\end{pmatrix}\begin{pmatrix} m_M & m_D \\ m_D & m_S\end{pmatrix}\begin{pmatrix}\nu_R^{C\prime} \\ N_R{}'\end{pmatrix} + \text{h.c}, \tag{1.4.34}$$

where the primed superscript refers to the flavour/weak eigenstates and each mass term is summarised as follows

- m_D: **Dirac** with $|\Delta L| = 0$,
- m_M: **Majorana** with $|\Delta L| = 2$,
- m_S: **Majorana** with $|\Delta L| = 2$.

Unitary transformations may be applied to rotate from the flavour to mass eigenstates

$$\begin{pmatrix}\nu_{1L} \\ \nu_{2L}\end{pmatrix} = U_L^{\nu\dagger}\begin{pmatrix}\nu_L{}' \\ N_L^{C\prime}\end{pmatrix}, \quad \text{and} \quad \begin{pmatrix}\nu_{1R}^C \\ \nu_{2R}^C\end{pmatrix} = U_R^{\nu\dagger}\begin{pmatrix}\nu_R^{C\prime} \\ N_R{}'\end{pmatrix}, \tag{1.4.35}$$

and diagonalise the mass matrix of Eq. (1.4.34) via the following transformation

$$U_L^{\nu\dagger}\begin{pmatrix} m_M & m_D \\ m_D & m_S\end{pmatrix} U_R^{\nu} = \begin{pmatrix} m_1 & 0 \\ 0 & m_2\end{pmatrix} \tag{1.4.36}$$

where m_1, m_2 are the Majorana mass eigenvalues which correspond to the mass eigenstates $\nu_{iM} = \nu_{iL} + \nu_{iR}^C, i = 1, 2$. There are several important limiting cases of Eq. (1.4.34):

- **Majorana**: $m_D = 0$. The mass matrix of Eq. (1.4.34) is diagonal and $m_1 = m_M$ and $m_2 = m_S$.

- **Dirac**: $m_M = m_S = 0$. The mass eigenvalues are $m_1 = m_D$ and $m_2 = -m_D$.

- **Pseudo-Dirac**: $m_D \gg m_M, m_S$. The mass eigenstates are a small perturbation from the Dirac mass $m_{1,2} = m_D \pm (m_M + m_S)/2$.

- **Seesaw**: $m_S \gg m_D, m_M$. A particularly interesting case will be $m_S \gg m_D$ and $m_M = 0$. The corresponding mass eigenvalues are $m_1 = m_D^2/m_S$ and $m_2 = m_S$ and therefore we have one light state suppressed by the heavy, sterile state. This is the well-known *seesaw* mechanism. This mechanism is important as it will provide a plausible explanation of small neutrino masses (and possibly the baryon asymmetry) without invoking very small Yukawa couplings.

1.5 The Seesaw Mechanism

As previously discussed, the generation of Majorana masses requires lepton-number to be violated. In order to construct lepton-number violating operators, which respect SM gauge symmetries, we will consider higher dimensional operators constructed from SM fields. Taking such an effective-field theory approach, the lowest order non-renormalisable operator to fulfil these criteria is the well-known Weinberg operator [38]

$$\mathcal{O}_5 = \frac{\lambda}{\Lambda}\left(\overline{L_L}\widetilde{\phi}\right)\left(\phi^\dagger \widetilde{L_R}\right), \tag{1.5.37}$$

where flavour indices have been suppressed, λ is a dimensionless coefficient, Λ is the New Physics scale and where the leptonic and Higgs doublets are written as

$$L_L = \begin{pmatrix} \nu_L \\ e_L \end{pmatrix}, \quad \widetilde{L_R} = \begin{pmatrix} e_R^C \\ -\nu_R^C \end{pmatrix}, \quad \phi = \begin{pmatrix} \phi^+ \\ \phi^0 \end{pmatrix}, \quad \widetilde{\phi} = \begin{pmatrix} \phi^{0\dagger} \\ -\phi^- \end{pmatrix}. \tag{1.5.38}$$

After electroweak symmetry breaking (EWSB), a Majorana mass term for the left-handed neutrinos is generated, $m_\nu = \lambda v_H^2/\Lambda$. An attractive feature of such an approach is that the small neutrino masses are the result of integrating out New Physics

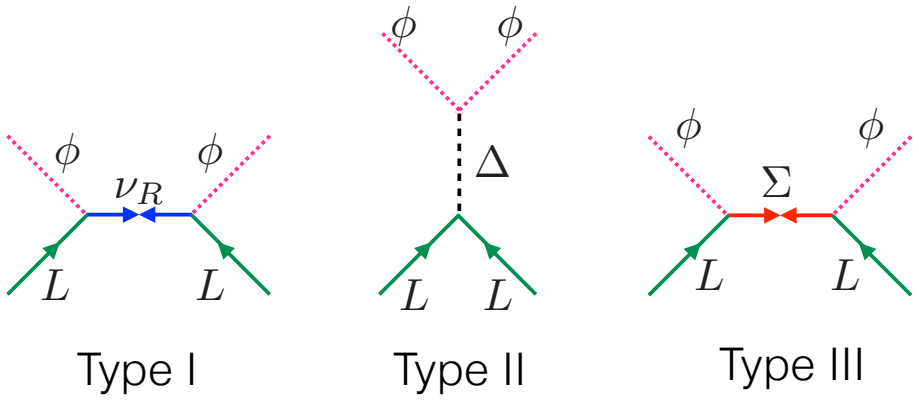

Figure 1.4: Feynman diagram of the three seesaw mechanisms.

at the high-energy scale. We will see there are three possible ways to ultra-violate (UV) complete this operator at tree-level and they correspond to type-I, II and III seesaw mechanisms.

1.5.1 Type-I

Type-I seesaw [39–42] introduces fermionic singlets, namely sterile neutrinos, as the seesaw mediators. In order to explain active neutrino masses minimally two sterile neutrinos are introduced[11]. These particles are singlets of the SM gauge group but couple to leptons and SM Higgs via a Yukawa term. For illustration, we will consider only one generation of neutrinos and therefore omit flavour indices. The mass terms for such a setup are written as

$$-\mathcal{L} = \frac{1}{2}\begin{pmatrix}\overline{\nu_L}' & \overline{N_L^C}'\end{pmatrix}\begin{pmatrix}0 & m_D\\ m_D & m_S\end{pmatrix}\begin{pmatrix}\nu_R^{C\prime}\\ N_R{}'\end{pmatrix} + \text{h.c}, \tag{1.5.39}$$

The mass eigenvalues are given by

$$m_{1,2} = \frac{m_S}{2} \pm \sqrt{\left(\frac{m_S}{2}\right)^2 + m_D^2}. \tag{1.5.40}$$

As the mass of the sterile neutrinos is not protected by any SM symmetry, it can be very large. The seesaw mechanism causes one mass eigenvalue to be light, via

[11] It is consistent with experimental observation that the lightest neutrino is massless and therefore only two sterile neutrino species are needed in the seesaw setup.

suppression by the sterile neutrino mass, and one to be heavy

$$m_1 \sim \frac{m_D^2}{m_S}, \quad m_2 \sim m_S \quad \text{with} \quad m_D = \frac{y_\nu v_H}{\sqrt{2}}. \tag{1.5.41}$$

If we assume $y_\nu \sim \mathcal{O}(1)$ and $m_\nu \sim \sqrt{\Delta m_{atm}} \sim 0.05$ eV, this implies $m_S \sim 10^{13}$ GeV, which is close to the GUT scale. Such heavy degrees of freedom may be *integrated out* and lead to the Weinberg operator as discussed earlier. Generalising the above discussion to three generations of light and heavy neutrinos, m_1, is now a complex, symmetric 3×3 matrix which is diagonalised by the PMNS matrix.

1.5.2 Type-II

In the type-II seesaw [43–48], the SM is enlarged by an SU(2) scalar triplet

$$\Delta = \begin{pmatrix} \frac{\Delta^+}{\sqrt{2}} & \Delta^{++} \\ \Delta^0 & -\frac{\Delta^+}{\sqrt{2}} \end{pmatrix}. \tag{1.5.42}$$

The corresponding terms added to the SM Lagrangian are

$$-\mathcal{L}_\Delta = \left(Y_\Delta \overline{L^C} i\sigma_2 \Delta L + \text{h.c}\right) - \left(\mu_\Delta \widetilde{\phi^T} \Delta^* i\sigma_2 \phi + \text{h.c}\right) - m_\Delta^2 \text{Tr}\left(\Delta^\dagger \Delta\right), \tag{1.5.43}$$

where Y_Δ is a symmetric Yukawa matrix, m_Δ is the mass scale of the triplet and μ_Δ is a parameter of unit mass dimension which characterises the lepton number violation. Again, we have suppressed flavour indices for ease of notation. The scalar triplet may be integrated out leading to the Weinberg operator with the following coefficient

$$C = Y_\Delta \frac{\mu_\Delta}{M_\Delta^2}, \tag{1.5.44}$$

and subsequently after EWSB the neutrino mass matrix is written as

$$m_\nu = Y_\Delta v_H^2 \frac{\mu_\Delta}{M_\Delta^2}. \tag{1.5.45}$$

The first key difference between type-II and the other varieties of seesaws is that m_ν is a linear function of the Yukawa matrix, not quadratic. This has the effect that measurement of m_ν would reveal the flavour structure of the high-scale theory. A second crucial difference is the introduction of two associated mass scales: μ_Δ and m_Δ. For $Y_\Delta \sim 1$, the scale of neutrino mass generation is approximated by

$$\Lambda_\Delta = \frac{M_\Delta^2}{\mu_\Delta}. \tag{1.5.46}$$

For $\Lambda_\Delta \sim 10^{13}$ GeV and $\mu_\Delta \sim 10^{-6}$, the mass of the scalar may be around the TeV scale.

1.5.3 Type-III

Type-III [49–52] involves the addition of a fermionic SU(2) triplet to the SM particle spectrum

$$\Sigma = \begin{pmatrix} \frac{\Sigma^0}{\sqrt{2}} & \Sigma^+ \\ \Sigma^- & -\frac{\Sigma^0}{\sqrt{2}} \end{pmatrix}. \tag{1.5.47}$$

The interactions of the new triplet is described by the Lagrangian

$$-\mathcal{L}_\Sigma = \sqrt{2} Y_\Sigma \overline{L} \Sigma \widetilde{\phi} + \frac{1}{2} M_\Sigma \mathrm{Tr}\left(\overline{\Sigma^C}\Sigma\right) + \mathrm{h.c}, \tag{1.5.48}$$

where again we have suppressed generational indices. Analogously to the type-I scenario, the light neutrino mass eigenvalue is

$$m_\nu \sim \frac{Y_\Sigma Y_\Sigma^T}{m_\Sigma}. \tag{1.5.49}$$

1.5.4 Inverse Seesaw

The seesaws of type-I, II and III offer a plausible explanation of light neutrino masses. However, a priori, the mass scale of the mediators could be very high. From a phenomenological perspective it would be interesting to explain neutrino masses with TeV scale physics. The Inverse seesaw [53–55] offers such possibility. In its minimal implementation it requires the introduction of two sets of fermionic singlets, N_R and N'_R, which couple to the left-handed SM neutrinos via the following mass matrix in the (ν_L, N_R, N'_R) basis

$$m_{\mathrm{ISS}} = \begin{pmatrix} 0 & m_D & 0 \\ m_D & \mu_N & m_N \\ 0 & m_N & \mu_{N'} \end{pmatrix}. \tag{1.5.50}$$

Naturally, for three generations of N_R and N'_R, m_{ISS} is a 9×9 matrix. Note that the parameters μ_N and $\mu_{N'}$ are *natural* in the sense as they tend to zero, the symmetry of the theory is enhanced and lepton number is conserved. In the limiting regime

where $\mu_N, \mu_{N'} \ll m_N, \mu_D$ the mass eigenvalues are given by

$$m_1 = \frac{m_D^2}{m_D^2 + m_N^2}\mu_{N'} \quad \text{and} \quad m_{2,3} = \pm\sqrt{m_N^2 + m_D^2} + \frac{m_N^2 \mu_{N'}}{2\left(m_D^2 + m_N^2\right)} + \frac{\mu_N}{2}. \quad (1.5.51)$$

The smallness of neutrino masses is directly connected with the smallness of lepton-number violating parameter $\mu_{N'}$. In the regime, $\mu_N, \mu_{N'} \ll \mu_D \ll m_N$, then the light neutrino mass is given by

$$m_\nu \sim \frac{m_D^T \mu_{N'} m_D^T}{M_R^T M_R}. \quad (1.5.52)$$

Because the smallness of the light neutrino mass is controlled by $\mu_{N'}$, M_R may be TeV scale and $Y_\nu \sim \mathcal{O}(1)$; crucially, this means sterile-active mixing may be non-negligible and the sterile states may sufficiently light such that they can be searched for at colliders.

As theoretically appealing as the seesaw mechanism may be, the origin of neutrino masses has not yet been confirmed and thus it is important to consider alternative explanations. It is possible the neutrino masses are generated radiatively. Neutrino masses may be small and indeed the lepton-number violating scale may be low, due to loop integrals [56–61]. Moreover, there have been proposals that neutrino masses stem from effective operators with mass dimension greater than five [62–65], from non-hermitian Yukawa matrices [66] or large-extra dimensions [67, 68].

1.6 Motivation and Outline of this Thesis

The SM explains the behaviour of visible matter remarkably well. However, there are a number of observational and aesthetical inconsistencies of this theory which demands New Physics. Perhaps the most immediate issues can be found when one considers the energy composition of the Universe: only 5% is comprised of ordinary, visible matter whose behaviour is governed by the SM. Approximately 72% of the Universe is comprised of Dark Energy, the mysterious energy needed to drive the accelerated expansion of the Universe. A further 23% of the cosmic energy budget is attributed to dark matter, whose composition and cosmic origin remain unknown.

Moreover, the asymmetry between matter and its counterpart, anti-matter, also remains a mystery. Other problems of the SM which include

- The observation and origin of non-zero neutrino masses,
- The presence of scale-invariant and acausal density perturbations consistent with a period of rapid inflation,
- The disparity between the electroweak and Planck scale,
- The strong CP-problem,
- The structure of fermionic masses and mixing,

amongst others. In this thesis, we shall primarily focus on the *Flavour Problem* which asks the question: are the parameters of the flavour sector (in particular the lepton sector) free parameters or do they exhibit structure? In this direction, we shall apply a Non-Abelian discrete and a generalised CP symmetry to the lepton sector in order to predict the structure of leptonic mixing. Such an approach was initially motivated, pre-reactor neutrino data, from the observation that the entries of the PMNS matrix resembled Clebsch-Gordon coefficients of non-Abelian discrete groups such as symmetric, alternating or dihedral groups. In addition, if the discrete groups have three-dimensional irreducible representations then this allows the leptonic doublets to be unified into a single representation of the group and thereby motivates the existence of three-generations. A particularly appealing aspect of the approach we shall consider in Chapter 2 and Chapter 3 is that a UV-complete flavour model need not be specified; a consideration of the high-scale non-Abelian and low-scale Abelian residual symmetries is all that is needed. Moreover, *sum rules* or correlations between observables are predicted from the particular choice of symmetries and this allows the flavour-symmetric models to be tested at upcoming oscillation facilities. We shall discuss the testability of such correlations at length.

Although there is a plethora of literature on the flavour models, there is a definite paucity in the study of the associated cosmology of such models. In Chapter 4, we discuss a new mechanism of leptogenesis (via lepto-bubbles) which has explicit

connections with leptonic flavour models and neutrino observables. Although we postulate neutrino masses derive from the Weinberg operator, and thereby assume neutrinos to be Majorana particles, it is not necessary to specify the particular completion of this dimension-five operator. The lepton asymmetry is generated from a phase transition which is strongly motivated by the breaking of an underlying flavour symmetry. During this phase transition, the coefficient of the Weinberg operator is time-dependent and the lepton asymmetry arises from the interference of the Weinberg operator at different times. To calculate the lepton asymmetry we apply the Closed-Time Path formalism which allows for a derivation of the kinetic equations from the first principles of quantum field theory. In addition, such a calculation incorporates memory-effects. There remains a number of interesting aspects of this mechanism to further explore and we present several possibilities before we summarise and conclude in Chapter 5.

Chapter 2

Mixing Angles and Phase Predictions from A_5 with Generalised CP and their Phenomenological Implications

2.1 Leptonic Flavour Models

The SM contains 18 free parameters:

- Nine fermion masses.
- Three CKM mixing angles and one phase.
- One electromagnetic, one strong and one weak coupling.
- Vacuum expectation value and mass of the Higgs.

Minimally extending the SM to include neutrino masses and mixing, adds seven (possibly nine depending on the nature of neutrinos) additional parameters and highlights the puzzling flavour structure of the quark and lepton sectors and the stark difference between the two. In short, quark masses are hierarchical and mixing is small while neutrino masses are rather degenerate and mixing is large as has been illustrated in Fig. 2.1. Generically, there are two ways to tackle the flavour

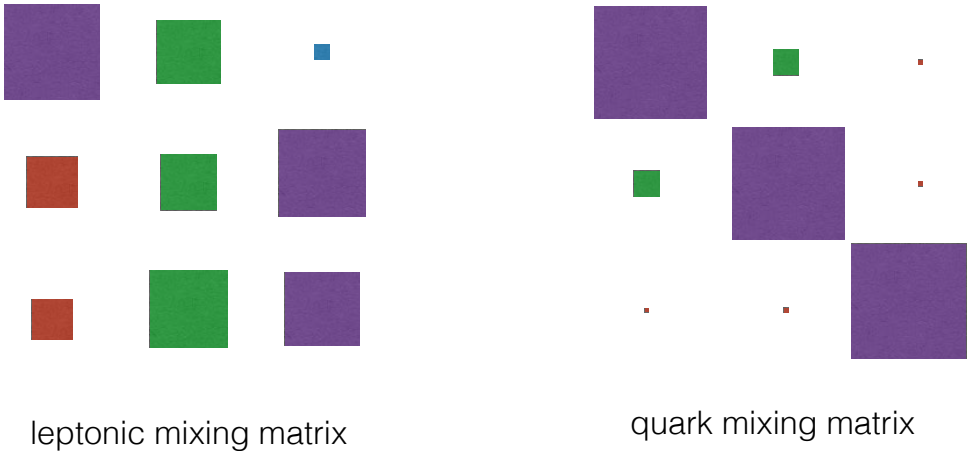

Figure 2.1: A pictorial representation of leptonic and quark mixing where the magnitude of the coloured square represents the magnitude of the CKM/PMNS matrix entry.

problem: either we assume the structure of mixing manifests from a symmetric principle or results from random, unbiased unitary matrices (henceforth referred to as the *anarchy paradigm* [69–71]). The physical intuition behind the latter approach is that the high-energy theory may be so complex and contain so many parameters all that can be observed at the low-scale is a statistical fluctuation in the magnitude of the mixing angles. Although anarchy agrees relatively well with leptonic mixing data, it is incompatible with quark mixing.

If an underlying flavour symmetry exists it may be continuous or discrete. In [72, 73], the authors explained the structure of masses and mixing, in both the quark and lepton sectors, via the flavour symmetry $\mathrm{U}(2) \cong \mathrm{SU}(2) \times U(1)$, where the SM fermions are assigned to doublets and singlets of this group respectively. However, this assignment implies the chosen flavour symmetry group cannot explain why there are three generations. There have been other applications of continuous flavour symmetries such as SU(3) [74, 75], where fermionic masses are explained via the VEVs of scalar which are SM-singlets but charged under the flavour symmetry. These scalars are known as *flavons* and are pervasive throughout flavour model-building and also appear in the prolifically used Froggatt-Nielsen mechanism [76]. This mechanism explains the hierarchy of the fermionic masses by assuming a U(1) under which each

of the fermions is charged differently. The role of the flavon is to break the U(1) symmetry with its VEV, $\langle v_{\rm FN} \rangle$. This breaking affects the fermions at different order in the small parameter $\epsilon = \langle v_{\rm FN} \rangle / M_*$, where M_* is the flavour dynamics scale which is set by integrating out heavy fermions.

These are just a few approaches which attempt to solve the flavour problem; in the remainder of this work we will particularly focus on the application of discrete, Non-Abelian flavour symmetries in the lepton sector.

Prior to 2012, before θ_{13} has been measured [28–30, 77, 78], many classes of discrete symmetry flavour models predicted bi-maximal (BM) [79–82], tri-bimaximal (TBM) [83, 84] or GR (golden ratio) [85] mixing which result from using small flavour groups such as A_4, A_5 and S_4 (an in-depth review of discrete groups can be found in [86]). In these flavour models the larger non-Abelian flavour group (for example A_4) is broken into residual symmetries groups in the charged lepton ($\mathbb{Z}_3$) and neutrino ($\mathbb{Z}_2$) sectors. Subsequently, the combination of the low-scale symmetries constrain leptonic mixing and in this case TBM mixing is achieved. To accommodate post-2012 experimental data, these flavour models could slightly break the residual symmetry in the neutrino or charged lepton sector via higher-dimensional flavon operators. There have been many studies where corrections to leading order mixing patterns have been investigated [87–92]. In addition, larger groups such as $\Delta(96)$ [93, 94], $\Delta(150)$ [95], $\Delta(600)$ [96] and $\Delta(1536)$[97], were also used to be consistent with leptonic mixing.

In general, there are two possible implementations of flavour symmetries and they are often referred to as direct and semi-direct (e.g. see [86]). The distinction between the two approaches is the low-energy residual symmetry of the Majorana mass matrix: in the direct approach the Klein group, $\mathbb{Z}_2 \times \mathbb{Z}_2$, is a subgroup of the underlying flavour symmetry whilst in the semi-direct approach, $\mathbb{Z}_2$ emerges as a residual symmetry of the flavour group. In the semi-direct models a continuous parameter is introduced, derived from the freedom to rotate in the degenerate sub-

space of the neutrino residual symmetry, allowing the prediction of a non-zero θ_{13}. There are several attractive features of implementing such an approach: firstly a UV-complete theory is not necessary in order to predict leptonic observables [98–104]. Secondly, correlations between the observables can be derived and provide specific signatures which allow the comparison of a range of models to experimental data [100–107].

These models can successfully predict mixing angles consistent with data and a Dirac phase, δ. However, due to the constraints imposed on the mass matrices used to construct the PMNS matrix, a number of degrees of freedom cannot be eliminated and therefore these models cannot predict Majorana phases. By extending the flavour group to include generalised CP (gCP) symmetry, the three mixing angles and three phases can be determined using a small number of input parameters [108]. This idea of combining CP with a flavour symmetry is not a recent one and was originally discussed in [109–113] together with a μ-τ symmetry. There have been a number of interesting works on the consistent relation between gCP and flavour symmetry [108, 114, 115] and many plausible groups have been studied such as A_4 [108, 116], S_4 [108, 117–119], $\Delta(96)$ [93, 94], $\Delta(150)$ [95], $\Delta(600)$ [96], $\Delta(1536)$[97], $\Delta(3n^2)$ [120], $\Delta(6n^2)$ [120, 121] and A_5 [1, 122, 123].

The work presented in this chapter follows that of [1] where an A_5 flavour symmetry is assumed in conjunction with a generalised CP-symmetry. In Section 2.2 and Section 2.2.3 we explain the assumptions behind the theoretical framework and define necessary group theoretic terms. In Section 2.3 we focus on the predictions, present some simplified relations between leptonic mixing observables and highlight interesting phenomenological signatures. Finally, in Section 2.4 we investigate the testability of such correlations at upcoming reactor, accelerator and neutrinoless double-beta decay experiments.

2.2 Theoretical Framework

There are two key assumptions applied throughout this section. First, we assume neutrinos are Majorana in nature and therefore the leptonic mass terms of the low-energy effective theory are given by

$$\mathcal{L} = \overline{(e_{\mathrm{L}})_\alpha}(m_\ell)_{\alpha\beta}(e_{\mathrm{R}})_\beta + \overline{(e_{\mathrm{R}})_\alpha}(m_\ell^\dagger)_{\alpha\beta}(e_{\mathrm{L}})_\beta + \frac{1}{2}\overline{(\nu_{\mathrm{L}}^c)_\alpha}(m_\nu)_{\alpha\beta}(\nu_{\mathrm{L}})_\beta + \frac{1}{2}\overline{(\nu_{\mathrm{L}})_\alpha}(m_\nu^\dagger)_{\alpha\beta}(\nu_{\mathrm{L}}^c)_\beta, \tag{2.2.1}$$

where Greek subscripts denote flavour indices and the mass matrices are 3×3 and complex-valued. Second, we conjecture the existence of a finite, discrete flavour symmetry, G_f, at the high-energy scale. The purpose of this symmetry is to unify the three flavours of leptonic doublets into a single mathematical structure, namely a three-dimensional irreducible representation of the flavour group, Ψ. The flavour group acts on Ψ such that

$$\Psi \to \rho(g)\Psi, \tag{2.2.2}$$

where $\rho(g)$ is a three-dimensional unitary representation of the group element $g \in G_f$. The non-Abelian flavour symmetry must be broken at the low-energy scale as leptonic masses are distinct. This implies that if a flavour symmetry is operational in the high-energy regime then only its Abelian residual symmetries would be observable at the scale of mass generation. Therefore, we assume that the non-Abelian flavour symmetry is broken into Abelian residual symmetries of the charged lepton, G_ℓ, and the neutrino sector, G_ν respectively. For the group elements $g_\ell \in G_\ell$ and $g_\nu \in G_\nu$, the charged lepton and neutrino fields transform under the residual symmetries according to

$$e_{\mathrm{L}} \to \rho\left(g_\ell\right) e_{\mathrm{L}} \quad \text{and} \quad \nu_{\mathrm{L}} \to \rho\left(g_\nu\right) \nu_{\mathrm{L}}, \tag{2.2.3}$$

where generational indices have been suppressed. These transformations enforce the following constraints on the charged lepton and neutrino mass matrices

$$m_\ell m_\ell^\dagger = \rho\left(g_\ell\right)^\dagger \left(m_\ell m_\ell^\dagger\right) \rho\left(g_\ell\right), \tag{2.2.4}$$

$$m_\nu = \rho\left(g_\nu\right)^{\mathrm{T}} m_\nu \rho\left(g_\nu\right). \tag{2.2.5}$$

To deduce the possible forms of the residual symmetries, we must consider the largest possible symmetry of each sector and the structure inherited from the larger

non-Abelian flavour group. In the basis of a diagonal charged lepton mass matrix, the largest symmetry of this sector is $U(1)^3$. This derives from the freedom to rephase each generation of the charged leptons. The most general discrete residual symmetry of this sector must be a subgroup of $U(1)^3$ and is therefore a direct product of cyclic groups, $\mathbb{Z}_n$. In contrast, the largest symmetry of the Majorana neutrino mass matrix is the Klein group (K_4), which is significantly more constrained. This conclusion follows from the fact that the diagonalised neutrino mass matrix is left invariant by the following transformation

$$K^T{}_{n,m} m_\nu^{diag} K_{n,m} = m_\nu{}^{diag} \quad \text{where} \quad K_{n,m} = \begin{pmatrix} -1^n & 0 & 0 \\ 0 & -1^m & 0 \\ 0 & 0 & -1^{n+m} \end{pmatrix}, \tag{2.2.6}$$

where $n, m = 0, 1$. The four possible combinations of n and m correspond to the four elements of K_4. Explicitly, in this representation, the four group elements are

$$K_{0,0} = \begin{pmatrix} 1 & 0 & 0 \\ 0 & 1 & 0 \\ 0 & 0 & 1 \end{pmatrix}, K_{1,0} = \begin{pmatrix} -1 & 0 & 0 \\ 0 & 1 & 0 \\ 0 & 0 & -1 \end{pmatrix}, K_{0,1} = \begin{pmatrix} -1 & 0 & 0 \\ 0 & 1 & 0 \\ 0 & 0 & -1 \end{pmatrix}$$
$$\text{and} \quad K_{1,1} = \begin{pmatrix} -1 & 0 & 0 \\ 0 & -1 & 0 \\ 0 & 0 & 1 \end{pmatrix}. \tag{2.2.7}$$

However, in the basis where the charged lepton mass matrix is diagonal (m_ν is non-diagonal) the elements of K_4 are clearly non-diagonal and are given by

$$\overline{K_{n,m}} = U^*_{PMNS} K_{n,m} U^T_{PMNS}. \tag{2.2.8}$$

In a few lines [86], we verify the invariance of m_ν under $\overline{K_{n,m}}$

$$\begin{aligned} \overline{K_{n,m}}^T m_\nu K_{n,m} &= U_{PMNS} K^T_{n,m} U^\dagger_{PMNS} m_\nu U^*_{PMNS} K_{n,m} U^T_{PMNS} \\ &= U_{PMNS} \left(K^T_{n,m} m_\nu^{diag} K_{n,m} \right) U^T_{PMNS} \\ &= U_{PMNS} m_\nu^{diag} U^T_{PMNS} \\ &= m_\nu. \end{aligned} \tag{2.2.9}$$

Hence, we conclude the symmetric Majorana neutrino mass is left invariant by K_4 or a subgroup thereof, namely $\mathbb{Z}_2$. In the remainder of this discussion, we will consider the residual flavour symmetry of the neutrino sector to be $\mathbb{Z}_2$.

2.2.1 Group Theory Definitions

In this short interlude, we define the necessary group theoretic terms to clarify their usage in proceeding sections.

- **Group homomorphism** Let G and G' be two groups. A map f of group G into G' is a homomorphism if the following property holds

$$f(ab) = f(a)f(b), \tag{2.2.10}$$

  $\forall a, b \in G$. From this definition, the identity elements of G and G' are identified and inverse elements of G are mapped to inverse elements of G'. Therefore, a homomorphism is a mapping that preserves the group structure.

- **Automorphism** A bijective (one-to-one and onto) homomorphism from the group G to itself is an automorphism. This is a way of mapping a group to itself whilst preserving its structure.

- **Automorphism Group** The automorphism group is the group of automorphism of G under composition. We will denote this group as $\mathrm{Aut}(G)$.

- **Inner Automorphism** The automorphism $f_C : G \to G$ where $f_C(x) = gxg^{-1} \quad \forall x \in G$, is the inner automorphism of G by g. The action of f_C on x is called conjugation of x by g.

- **Conjugacy Class** The group elements which are related by conjugation with a group element form a conjugacy class.

- **Inner Automorphism** A subgroup H of group G is normal if the following condition is satisfied

$$H = g^{-1}Hg \quad \forall g \in G. \tag{2.2.11}$$

  This is equivalent to stating H is invariant under all inner automorphisms.

- **Quotient Group** For a normal subgroup N in group G, the quotient group is the set of all left cosets of N in G given by

$$G/N := \{gN, g \in G\}. \tag{2.2.12}$$

  G/N is the quotient group of G by N. An intuitive way of understanding the the quotient group G/N is collapsing all of N to the identity element in G.

- **Centre** The centre of group G, denoted as $Z(G)$, is the set of all elements in G that commute with all other elements in G. By definition, $Z(G)$ is a normal subgroup of G. Moreover, the inner automorphism group can be found in the following manner

$$\text{Inn}(G) \cong G/Z(G). \tag{2.2.13}$$

- **Outer Automorphism** An automorphism in $\text{Aut}(G)$ that is not inner is an outer automorphism. The outer automorphism group can be constructed using the following quotient group

$$\text{Out}(g) = \text{Aut}(g)/\text{Inn}(G). \tag{2.2.14}$$

2.2.2 Generalised CP Symmetry

In addition to the non-Abelian flavour symmetry operational at the high-energy regime, we assume the presence of a generalised CP (gCP) symmetry[1]. This symmetry parity transforms and charge-conjugates the field as well as acting on its generational indices [124]. The gCP transformation acts on the multiplet of fields, Ψ, such that

$$\Psi_\alpha \to X_{\alpha\beta}\Psi^C_\beta, \tag{2.2.15}$$

where $X_{\alpha\beta}$ is assumed to be unitary in order to preserve the kinetic terms of the Lagrangian and Ψ^C denotes the CP-conjugate of Ψ. The gCP transformation is involutary meaning that two gCP transformations are equivalent to the identity: $XX^* = \mathbb{1}$. It is worth noting this condition, together with the unitary constraint,

[1]The presence of this symmetry allows the Majorana phases to be predicted, as well as the Dirac phase.

implies X is also a symmetric matrix. In order for the gCP symmetry to leave the Lagrangian invariant, the mass matrices must satisfy further constraints. The gCP transformation swaps the hermitian conjugate terms in Lagrangian Eq. (2.2) and subsequently the Lagrangian remains invariant if the following conditions are satisfied

$$X^{\mathrm{T}} m_\nu X = m_\nu^*, \tag{2.2.16}$$

$$X^\dagger (m_\ell m_\ell^\dagger) X = (m_\ell m_\ell^\dagger)^*. \tag{2.2.17}$$

It has been demonstrated [117, 125] that if gCP remains unbroken at the low-energy scale in both the charged lepton and neutrino sectors no CP-violating effects will be observed. Therefore, we assume that gCP is broken in the charged lepton sector and remains a preserved symmetry of the neutrino sector. To assure the consistency of this assumption, the X matrix must map the elements of the neutrino residual symmetry to themselves,

$$X \rho(g_\nu)^* X^* = \rho(g_\nu). \tag{2.2.18}$$

To summarise, we assume a discrete flavour symmetry G_f and a gCP symmetry (implemented by the X-matrix) at the high-energy scales. These symmetries are broken to subgroup G_ℓ acting on the charged-lepton mass terms and another subgroup G_ν which along with the gCP symmetry acts on the neutrino mass terms. This leads to a system of constraints which the mass matrices must fulfil: Eq. (2.2.4), Eq. (2.2.5), Eq. (2.2.16) and Eq. (2.2.18). These constraints on the charged lepton and neutrino mass matrices in turn constrain their diagonalising matrices and hence the PMNS matrix. In this theoretical framework, details of the flavour model[2] need not be specified in order to predict leptonic mixing observables: simply the high and low scale symmetries. In Section 2.2.4, we demonstrate how such symmetry considerations alone can be used to predict the PMNS matrix including the Majorana phases.

[2] A UV-complete model with a flavour-invariant scalar potential and a specific way of (spontaneously) breaking the flavour symmetry.

2.2.3 Basic Group Structure of A_5

Geometrically, A_5 is the rotational symmetries of an icosahedron. More formally, A_5 is the alternating group of five elements which is the group of even permutations of five objects. This implies the order of A_5 is half the order of the symmetric group of order 5 (as half the elements of a symmetric group are even and the other half are odd) and therefore we determine the order of A_5 to be

$$\mathrm{Ord}(A_5) = \frac{\mathrm{Ord}(S_5)}{2} = \frac{5!}{2} = 60. \tag{2.2.19}$$

All 60 elements of A_5 can be constructed from the following abstract presentation

$$\langle S, T | S^2 = T^5 = (ST)^3 = \mathbb{1} \rangle, \tag{2.2.20}$$

where S and T are the *generators* of the group and the *relations* are the combinations of the generators which give the identity element. This group has been employed as a flavour symmetry [126–128] and gives rise to *golden-ratio* (GR) mixing: $\sin^2\theta_{13} = 0$, $\sin^2\theta_{23} = 1/2$ and $\tan\theta_{12} = 1/\varphi$ where $\varphi = (1+\sqrt{5})/2$ is the golden ratio.

For our purposes, the most important features of this symmetry group are the three-dimensional representations. This is because we assume, at sufficiently high energies, the leptonic doublets are assigned to a three-dimensional representation of the group. There are two three-dimensional representations of A_5: 3 and 3′. We have chosen to work with the real representation of 3, however naturally the conclusions we reach are representation-independent. In our chosen representation, the generators S and T take the form

$$T = \frac{1}{2}\begin{pmatrix} 1 & -\varphi & -\varphi_g \\ \varphi & -\varphi_g & -1 \\ -\varphi_g & 1 & \varphi \end{pmatrix} \quad \text{and} \quad S = \begin{pmatrix} -1 & 0 & 0 \\ 0 & -1 & 0 \\ 0 & 0 & 1 \end{pmatrix}, \tag{2.2.21}$$

where φ the golden ratio and φ_g its Galois conjugate ($\varphi_g = \left(1-\sqrt{5}\right)/2$). A_5 has non-identity elements of order 2, 3 and 5 and has four conjugacy classes. For the interested reader, further details can be found in the Appendix.

2.2.4 PMNS Matrix from Symmetry Considerations

In Section 2.2 and Section 2.2.2 we investigated the transformation of fields, specifically charged lepton and neutrinos, under a flavour and gCP symmetry respectively. These symmetries constrain the form of the corresponding mass matrices and consequently the PMNS matrix.

Firstly, we shall derive U_ℓ from symmetry constraints. To begin with, we re-express the first condition of Eq. (2.2.4) in the form of a commutator

$$[\rho(g_\ell), m_\ell m_\ell^\dagger] = 0. \tag{2.2.22}$$

As the unitary matrix $\rho(g_\ell)$ commutes with the hermitian matrix $m_\ell m_\ell^\dagger$, there must exist a basis where these matrices are simultaneously diagonalisable [129]. This implies there is a unitary matrix, U_ℓ, that simultaneously diagonalises both

$$\left(m_\ell m_\ell^\dagger\right)_{diag} = U_\ell^\dagger m_\ell m_\ell^\dagger U_\ell \quad \text{and} \quad \rho(g_\ell)_{diag} = U_\ell^\dagger \rho(g_\ell) U_\ell, \tag{2.2.23}$$

where $\left(m_\ell m_\ell^\dagger\right)_{diag}$ and $\rho(g_\ell)_{diag}$ are the diagonalised form of the mass and residual symmetry matrices respectively. This statement of commutativity is powerful: by computing the diagonalising matrix of the residual symmetry group element, $\rho(g_\ell)$, we constrain the form of the mass matrix, $m_\ell m_\ell^\dagger$. In the scenario where $\rho(g_\ell)$ has degenerate eigenvalues, i.e. is not full rank, then there does not exist a unique diagonalising matrix of $\rho(g_\ell)$ but rather a complex rotation can be performed in the degenerate eigenspace. With these considerations in mind, the most general diagonalising matrix of $\rho(g_\ell)$ and $m_\ell m_\ell^\dagger$ takes the form

$$U_\ell = U_e R_\ell\left(\omega, \gamma\right), \tag{2.2.24}$$

where U_e diagonalises $\rho(g_\ell)$ and $R_\ell\left(\omega, \gamma\right)$ is an SU(2) rotation in the degenerate eigenspace, if indeed such a subspace exists. In the neutrino sector, we have three constraints to consider on the mass terms: the flavour symmetry, the gCP symmetry and consistency between these two. Under a change of flavour basis, the matrix X transforms in the following way

$$X \to U^\dagger X U^*. \tag{2.2.25}$$

As X is unitary and symmetric we may apply the Takagi factorization which allows us to express it as $X = \Omega\Omega^{\mathrm{T}}$ for some unitary matrix Ω. This implies we may choose a basis where X becomes trivial [108]. This basis is not unique and the remaining freedom can be used to further diagonalise $\rho(g_\nu)$. In such a basis, the constraint in Eq. (2.2.16) implies the mass matrix is real

$$\left(\Omega^{\mathrm{T}} m_\nu \Omega\right)_{\alpha\beta} \in \mathbb{R}. \tag{2.2.26}$$

As $\rho(g_\nu)$ is diagonal and commutes with this matrix, the mass matrix in this basis must be diagonal up to a basis change in the degenerate subspace of $\rho(g_\nu)$. As it is purely real, the most general additional basis transformation required to bring it into diagonal form is a rotation in two dimensions

$$U_\nu = \Omega R_\nu(\theta), \tag{2.2.27}$$

where θ is the angle describing real rotation. There remains the possibility that the diagonal mass matrix is not positive definite, in which case a diagonal re-phasing must occur. As a consequence, the Majorana phases may only be predicted only up to multiples of $\pm\pi$. This will be explicitly shown in later sections. Combining the results for the charged-lepton and the neutrino sector, the PMNS matrix is given by

$$U_{\mathrm{PMNS}} = \Phi R_\ell(\phi, \gamma) U_e^\dagger \Omega R_\nu(\theta), \tag{2.2.28}$$

where R_ℓ and R_ν denote two unspecified rotations ($R_\ell = \mathbb{1}$ if $\mathrm{ord}\,(g_\ell) > 2$). We make two further simplifications: Φ is removed by re-phasing the charged leptons, and we note that the angles θ and ϕ need only be defined over the interval $\theta, \phi \in [0, \pi)$, as shifts by π can be absorbed by unphysical redefinitions of the complex phases.

2.2.5 Deriving X

The matrix, X, which implements the generalised CP symmetry must satisfy $XX^* = \mathbb{1}$. Moreover, this transformation is related to a class-inverting automorphism of the group [115],

$$\forall g \in \mathrm{A}_5,\ \exists h_g \in \mathrm{A}_5 \ \text{ s.t. } \ (X^*\rho(g)X)^* = \rho(h_g^{-1})\rho(g^{-1})\rho(h_g), \tag{2.2.29}$$

where ρ is our chosen irreducible representation, generated by the matrices S and T. To find the X matrices associated to physical gCP transformations we must apply our knowledge of the automorphism structure of the group. The automorphism group of A_5 is S_5. The next step is to identify the *inner* and *outer* automorphisms. The inner automorphism group, $\mathrm{Inn}(A_5)$, comprises those automorphisms which can be represented by conjugation by a group element,

$$\phi_h \in \mathrm{Inn}(A_5) \quad \Longleftrightarrow \quad \forall\, g \in A_5, \quad \phi_h(g) = h^{-1}gh. \tag{2.2.30}$$

This group can be found by considering the map from element ($h \in A_5$) to inner automorphism ($\phi_h(g) = h^{-1}gh$). Using the First Isomorphism Theorem we find

$$\mathrm{Inn}(A_5) \cong A_5/\mathcal{Z}(A_5) \cong A_5, \tag{2.2.31}$$

where the final step uses the fact that the centre of A_5 is trivial, $\mathcal{Z}(A_5) = 1$. Hence, the inner automorphisms of A_5 are given by A_5 itself. The outer automorphism group is the quotient of the full automorphism group by the inner automorphism group. For A_5 it follows from above that this is the unique group of two elements $\mathbb{Z}_2$. As each element of A_5 is conjugate to its inverse (such a group is said to be *ambivalent*) finding X is simplified. For such groups, the class-inverting automorphisms are also class-preserving. For the case of A_5 we have a single non-trivial outer automorphism to consider and this automorphism maps elements of order 5 from one conjugacy class to the other. In this case, we conclude that the class-preserving automorphisms are precisely the inner automorphisms. The constraint on X can then be simplified

$$\exists h \in A_5,\ \forall g \in A_5 \qquad (X^*\rho(g)X)^* = \rho(h^{-1})\rho(g)\rho(h), \tag{2.2.32}$$

where the element h is the same for all elements g. Recalling we chose to work with the real representation of the group and using the condition $XX^* = \mathbb{1}$, an additional simplification can be made such that

$$\forall g \in A_5 \qquad X\rho(g)X^* = \rho(h^{-1})\rho(g)\rho(h),$$

which is equivalent to a commutation relation,

$$[\rho(h)X, \rho(g)] = 0.$$

We invoke Schur's lemma to deduce that as $\rho(h)X$ commutes with all the elements of A_5 and must be a scalar matrix: $\rho(h)X = \lambda\mathbb{1}$, for some complex constant λ. Requiring that $XX^* = \mathbb{1}$ constrains $\rho(h^2) = 1/|\lambda|^2$. By closure the group, we conclude that λ is just a complex phase, $\lambda = e^{i\theta}$ for $\theta \in \mathbb{R}$. Hence, h is an order 2 element and the most general form of X that implements an involutory class-inverting automorphism for A_5 is given by

$$X = e^{i\theta}\rho(h) \qquad \text{s.t.} \qquad \text{ord}(h) = 2. \tag{2.2.33}$$

The consistency relation in Eq. (2.2.18) implies that the X matrix must commute with the generator S of the residual $\mathbb{Z}_2$ symmetry in the neutrino sector. Therefore not all choices of h can be consistently implemented, and there will be only three non-trivial X matrices for any given S. These are the three elements of the Klein group associated with S. If we work in the basis where this group is diagonal, we find that

$$X_{23} = e^{i\theta}\begin{pmatrix} 1 & 0 & 0 \\ 0 & -1 & 0 \\ 0 & 0 & -1 \end{pmatrix}, \tag{2.2.34}$$

and X_{12} and X_{13} can be defined as permutations of this matrix, where the row of the negative entry is denoted by the subscript. It is necessary for us to find the basis in which X is trivial. The necessary change of basis is given for X_{ij} by Ω_{ij}, where

$$\Omega_{12} = e^{i\theta}\begin{pmatrix} i & 0 & 0 \\ 0 & i & 0 \\ 0 & 0 & 1 \end{pmatrix}, \qquad \Omega_{13} = e^{i\theta}\begin{pmatrix} i & 0 & 0 \\ 0 & 1 & 0 \\ 0 & 0 & i \end{pmatrix} \quad \text{and} \quad \Omega_{23} = e^{i\theta}\begin{pmatrix} 1 & 0 & 0 \\ 0 & i & 0 \\ 0 & 0 & i \end{pmatrix}. \tag{2.2.35}$$

Due to the degenerate subspace in the $\mathbb{Z}_2$ generator, it remains possible that the neutrino mass matrix is only block diagonal and requires an orthogonal transformation to fully diagonalise it. This rotation must be in the plane of the degenerate subspace for the matrix S. Given these two elements, the most general form of the matrix which maps between neutrino flavour and mass bases is given by

$$U_\nu = \Omega R(\theta), \tag{2.2.36}$$

where $R(\theta)$ is an orthogonal matrix effecting a rotation in either the 12-, 13- or 23-plane. We note that the overall phase of Ω has no physical effect and henceforth will be set to zero.

2.3 Results from $G_\ell = \{\mathbb{Z}_3, \mathbb{Z}_5, \mathbb{Z}_2 \times \mathbb{Z}_2\}$ and $G_\nu = \mathbb{Z}_2 \times$ CP

In the following sections of this chapter, we detail the work of [1] in which the combination of Abelian residual symmetries studied were $G_\ell = \{\mathbb{Z}_3, \mathbb{Z}_5, \mathbb{Z}_2 \times \mathbb{Z}_2\}$ and $G_\nu = \mathbb{Z}_2 \times$ gCP. The observables are a function of one continuous parameter, derived from the freedom to make a real rotation in the degenerate subspace of the $\mathbb{Z}_2$ residual symmetry of the neutrino sector. We find there are 10 distinct predictions which agree with global fit data to a 3σ level [23]. The authors of [1] also considered the combination $G_\ell = \{\mathbb{Z}_3, \mathbb{Z}_5, \mathbb{Z}_2 \times \mathbb{Z}_2\}$ and $G_\nu = \mathbb{Z}_2 \times \mathbb{Z}_2 \times$ CP. It is worth stressing these predictions are completely fixed by the flavour symmetry and are not dependent on any internal parameter. It was found that none of these predictions were inconsistent with data. Finally, [1] also considered the combination $G_\nu = \mathbb{Z}_2 \times \mathbb{Z}_2 \times$ CP and $G_\ell = \mathbb{Z}_2$. In this case, each observable is a function of two input parameters which is obtained from the ability to make an SU(2) transformation in the degenerate eigenspace of the $\mathbb{Z}_2$ charged lepton residual symmetry. This was fully explored and there were no predictions that agreed with data at the 3σ level. A further consideration of $G_\ell = \mathbb{Z}_2$ and $G_\nu = \mathbb{Z}_2 \times$ CP was proposed in [1]. Moreover, there were predictions that agreed to a 3σ level with global fit data, however these correlations were not analysed further.

2.3.1 Predictions from $G_\ell = \mathbb{Z}_3$ and $G_\nu = \mathbb{Z}_2 \times$ CP

In this first example we shall provide full calculational details from the explicit symmetry-constrained PMNS matrix, extraction of the mixing angles and phases to calculating the sum rules. As the exact same procedure will be applied for the

remaining combinations of residual symmetries, we shall avoid repetition and simply provide the final result.

We have considered all 20 elements of order 3 in A_5. Many different group elements lead to a pattern of mixing which agrees with global fit data to a 3σ level. However, there is only one unique and valid mixing pattern and therefore it is sufficient to consider one representative element of $\mathbb{Z}_3$. We label this element $\mathbb{Z}_3 5$:

$$\mathbb{Z}_3 5 = \begin{pmatrix} 0 & -1 & 0 \\ 0 & 0 & -1 \\ 1 & 0 & 0 \end{pmatrix}. \tag{2.3.37}$$

In order to construct the leptonic mixing matrix, we first find the diagonalising matrix, U_ℓ, of $\mathbb{Z}_3 5$. This diagonalising matrix is combined with the gCP symmetry and a rotation in the degenerate eigenspace of G_ν. To diagonalise the matrix of equation Eq. (2.3.37), the eigenvectors of matrix Eq. (2.3.37) are calculated and arranged to form the following diagonalising matrix

$$U_\ell = \frac{1}{\sqrt{3}} \begin{pmatrix} -1 & 1 & 1 \\ 1 & e^{\frac{-i\pi}{3}} & e^{\frac{i\pi}{3}} \\ -1 & e^{\frac{-2i\pi}{3}} & e^{\frac{2i\pi}{3}} \end{pmatrix}, \tag{2.3.38}$$

where the ordering of the eigenvectors is arbitrary. As discussed earlier, one such X-matrix associated to the gCP symmetry is $X_{13} = \text{diag}(1, -1, 1)$. This X can be decomposed into the product of two unitary matrices, $\Omega_{13} = \text{diag}(1, i, 1)$. Hence, the leptonic mixing matrix may be written as

$$\begin{aligned} U_{PMNS} = U_\ell^\dagger \Omega_{13} R(\theta_{13}) &= \frac{1}{\sqrt{3}} \begin{pmatrix} -1 & 1 & -1 \\ 1 & e^{\frac{i\pi}{3}} & e^{\frac{2i\pi}{3}} \\ 1 & e^{\frac{-i\pi}{3}} & e^{\frac{-2i\pi}{3}} \end{pmatrix} \begin{pmatrix} 1 & 0 & 0 \\ 0 & i & 0 \\ 0 & 0 & 1 \end{pmatrix} \begin{pmatrix} c_\theta & 0 & s_\theta \\ 0 & 1 & 0 \\ -s_\theta & 0 & c_\theta \end{pmatrix} \\ &= \frac{1}{\sqrt{3}} \begin{pmatrix} -c_\theta + s_\theta & i & (-c_\theta - s_\theta) \\ c_\theta - s_\theta e^{\frac{2i\pi}{3}} & i e^{\frac{i\pi}{3}} & s_\theta + c_\theta e^{\frac{2i\pi}{3}} \\ c_\theta - s_\theta e^{\frac{-2i\pi}{3}} & i e^{\frac{-i\pi}{3}} & s_\theta + c_\theta e^{\frac{-2i\pi}{3}} \end{pmatrix}. \end{aligned} \tag{2.3.39}$$

Because the ordering of the eigenvectors that diagonalise the residual symmetries of the charged lepton and neutrino sector is arbitrary, the resulting matrices must be

permuted in 36 possible ways (both U_ℓ and U_ν may have their columns ordered in six ways). These 36 permutations are realised by left and right multiplication of the above matrix by the following permutation matrices

$$\begin{aligned} p_1 &= \begin{pmatrix} 1 & 0 & 0 \\ 0 & 1 & 0 \\ 0 & 0 & 1 \end{pmatrix}, \quad p_2 = \begin{pmatrix} 1 & 0 & 0 \\ 0 & 0 & 1 \\ 0 & 1 & 0 \end{pmatrix}, \quad p_3 = \begin{pmatrix} ,1 & 0 & 0 \\ 0 & 0 & 1 \\ 0 & 1 & \end{pmatrix}, \\ p_4 &= \begin{pmatrix} 0 & 1 & 0 \\ 0 & 0 & 1 \\ 1 & 0 & 0 \end{pmatrix}, \quad p_5 = \begin{pmatrix} 0 & 0 & 1 \\ 1 & 0 & 0 \\ 0 & 1 & 0 \end{pmatrix}, \quad p_6 = \begin{pmatrix} 0 & 0 & 1 \\ 0 & 1 & 0 \\ 1 & 0 & 0 \end{pmatrix}. \end{aligned} \tag{2.3.40}$$

In this theoretical framework, the need to perform permutations to the above matrix means multiple permutations of Eq. (2.3.39) provide valid mixing patterns. There are four permutations of Eq. (2.3.39) which are consistent with data: $p_1 U_{PMNS} p_1$, $p_2 U_{PMNS} p_1$, $p_1 U_{PMNS} p_6$ and $p_2 U_{PMNS} p_6$. The mixing angles are extracted from such matrices using the following set of equations

$$\sin^2(\theta_{13}) = U_{e3} {U_{e3}}^*, \quad \sin^2(\theta_{12}) = \frac{U_{e2} {U_{e2}}^*}{1 - U_{e3} {U_{e3}}^*} \quad \text{and} \quad \sin^2(\theta_{23}) \quad = \frac{U_{\mu 3} {U_{\mu 3}}^*}{1 - U_{e3} {U_{e3}}^*}. \tag{2.3.41}$$

Using this method to extract the mixing angles, it becomes clear why multiple permutations yield the same mixing pattern. For example, $p_2 U_{PMNS} p_1$ differs from $p_1 U_{PMNS} p_1$ by interchanging the second and third row. Therefore, the $(1,3)$ and $(1,2)$ entries of Eq. (2.3.39) are unchanged and thus the predictions of θ_{13} and θ_{12} are identical. As the $(2,3)$ and $(3,3)$ entries of Eq. (2.3.39) are conjugate, θ_{23} remains unaltered as well.

Calculating the CP phases of the PMNS matrix is complicated by the presence of unphysical phases which derive from the freedom to rephase the charged leptons. This has the consequence of transforming the PMNS matrix in the following manner

$$U_{ab} \to e^{i\phi} U_{ab}. \tag{2.3.42}$$

Such a rephasing is unphysical and in order to evade this issue the δ and Majorana phases must be calculated using rephasing invariants. The δ phase of the PMNS

matrix is extracted using the Jarlskog invariant [130–132]

$$\begin{aligned} J_{CP} = \mathrm{Im}[U_{\mu 3} U_{e3}^* U_{e2} U_{\mu 2}^*] &= \frac{1}{8}\cos(\theta_{13})\sin(2\theta_{12})\sin(2\theta_{23})\sin(2\theta_{13})\sin\delta, \\ \implies \sin(\delta) &= \frac{\mathrm{Im}[U_{e1} U_{e3}^* U_{\tau 1}^* U_{\tau 3}]}{\frac{1}{8}\cos(\theta_{13})\sin(2\theta_{12})\sin(2\theta_{23})\sin(2\theta_{13})}. \end{aligned} \tag{2.3.43}$$

Likewise, the Majorana phases are reconstructed using the following set of invariants [133]

$$\begin{aligned} I_1 = \mathrm{Im}[U_{e2}^2 \left(U_{e1}^2\right)^*] = {s_{12}}^2 {c_{12}}^2 {c_{13}}^4 \sin\alpha_{21} &\implies \sin\alpha_{21} = \frac{\mathrm{Im}[U_{e2}^2 \left(U_{e1}^2\right)^*]}{{s_{12}}^2 {c_{12}}^2 {c_{13}}^4}, \\ I_2 = \mathrm{Im}[U_{e3}^2 \left(U_{e1}^2\right)^*] = s_{13}^2 c_{12}^2 c_{13}^4 \sin(\alpha_{31} - 2\delta) &\implies \sin(\alpha_{31} - 2\delta) = \frac{\mathrm{Im}[U_{e3}^2 \left(U_{e1}^2\right)^*]}{s_{13}^2 c_{12}^2 c_{13}^4}. \end{aligned} \tag{2.3.44}$$

Applying formulae Eq. (2.3.41), we calculate the mixing angles as a function of θ

$$\begin{aligned} \sin^2(\theta_{13}) &= \frac{1}{3}(-c_\theta - s_\theta)^2 = \frac{1}{3}(1 + s_{2\theta}) \\ \sin^2(\theta_{12}) &= \frac{\frac{1}{3}}{1 - \frac{1}{3}(1 + s_{2\theta})} = \frac{1}{2 - s_{2\theta}} \\ \sin^2(\theta_{23}) &= \frac{\frac{1}{3}(s_\theta + c_\theta e^{\frac{2i\pi}{3}})(s_\theta + c_\theta e^{\frac{-2i\pi}{3}})}{1 - \frac{1}{3}(1 + s_{2\theta})} = \frac{1}{2}. \end{aligned} \tag{2.3.45}$$

As θ is an unphysical, internal parameter we rephase $\theta \to \theta + 3\pi/4$. This allows the above equations to be rewritten as

$$\sin^2(\theta_{13}) = \frac{2}{3}{s_\theta}^2, \quad \sin^2(\theta_{12}) = \frac{1}{3 - 2s_\theta^2}, \quad \text{and} \quad \sin^2(\theta_{23}) = \frac{1}{2}. \tag{2.3.46}$$

The pattern of mixing angles above is continuously connected to tribimaximal mixing which is recovered at $\theta = 0°$.

To calculate δ, we write the LHS of Eq. (2.3.43) as

$$\begin{aligned} J_{CP} &= \mathrm{Im}[U_{e1} U_{e3}^* U_{\tau 1}^* U_{\tau 3}] \\ &= \frac{1}{\sqrt{3}}^4 [(c_\theta^2 - s_\theta^2)(-s_\theta^2 e^{\frac{2i\pi}{3}} + c_\theta^2 e^{-\frac{2i\pi}{3}})] \\ &= \frac{-1}{6\sqrt{3}} c_{2\theta}, \end{aligned} \tag{2.3.47}$$

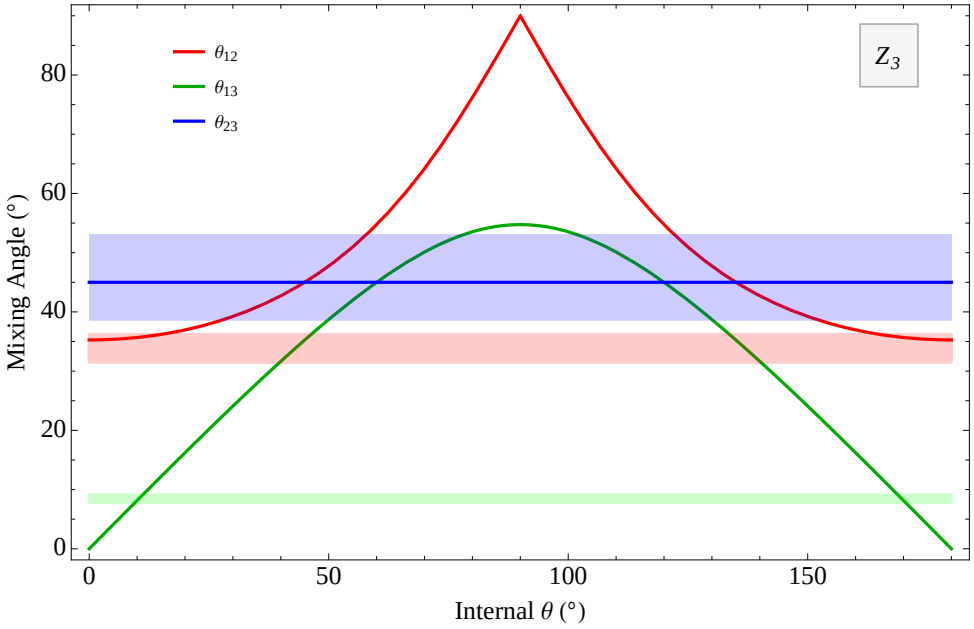

Figure 2.2: Mixing angles prediction for $\mathbb{Z}_3$ as a function of θ. This mixing pattern is associated to $|\sin\delta| = 1$ and $\sin\alpha_{21} = \sin\alpha_{31} = 0$. The blue, red and green-coloured bands show the 3σ allowed region for θ_{23}, θ_{12} and θ_{13} respectively [23].

and the RHS as

$$\begin{aligned} J_{CP} &= \frac{1}{8}\cos(\theta_{13})\sin(2\theta_{12})\sin(2\theta_{23})\sin(2\theta_{13})\sin\delta \\ &= \sin(\theta_{13})\cos^2(\theta_{13})\sin(\theta_{12})\cos(\theta_{12})\sin(\theta_{23})\cos(\theta_{23})\sin(\delta) \\ &= \pm\frac{(1+s_{2\theta})^{\frac{1}{2}}}{\sqrt{3}}\left(\frac{2-s_{2\theta}}{3}\right)\left(\frac{1}{2-s_{2\theta}}\right)^{\frac{1}{2}}\left(\frac{1-s_{2\theta}}{2-s_{2\theta}}\right)^{\frac{1}{2}}\left(\frac{1}{\sqrt{2}}\right)^2\sin(\delta) \\ &= \pm\frac{1}{6}\left(\frac{1-{s^2}_{2\theta}}{3}\right)^{\frac{1}{2}}\sin(\delta) \\ &= \pm\frac{1}{6}\left(\frac{{c^2}_{2\theta}}{3}\right)^{\frac{1}{2}}\sin(\delta). \end{aligned} \tag{2.3.48}$$

Equating Eq. (2.3.47) and Eq. (2.3.48), we find that $\sin(\delta) = \pm 1 \implies \delta = \frac{\pi}{2}, \frac{3\pi}{2}$ and therefore δ is maximally CP-violating. Using Eq. (2.3.44) the Majorana phases are constrained to be CP-conserving

$$\sin\alpha_{21} = \sin\alpha_{31} = 0, \tag{2.3.49}$$

but their precise value cannot be determined using this particular symmetry approach. We have plotted correlations Eq. (2.3.46) as a function of the parameter, θ,

in Fig. 2.2. The coloured bands represent the 3σ range in the mixing angles from recent global fit data [23]. From Fig. 2.2, we see there are two intervals of the θ parameter which leads to mixing angles consistent with 3σ data. As Eq. (2.3.46) are symmetric expressions, the mixing angles predictions for these two regions are identical. However, it can be shown that

$$\delta = \begin{cases} \frac{3\pi}{2} & \theta \in (0, \frac{\pi}{2}), \\ \frac{\pi}{2} & \theta \in (\frac{\pi}{2}, \pi), \end{cases} \tag{2.3.50}$$

and the Majorana phases are CP-conserving Eq. (2.3.49) for all values of θ. It is worth noting that if the upper limit in the measurement of θ_{12} shifts downwards, towards the best fit value, then this prediction can be easily excluded. Because two of the mixing angles are a function of θ, we may eliminate the unphysical parameter and construct a relation between θ_{12} and θ_{13}. Such relations between mixing angles and phases are generally referred to as *sum rules*. We use the notation of [134] which has introduced the following parameters

$$\sin\theta_{12} = \frac{1+s}{\sqrt{3}}, \quad \sin\theta_{13} = \frac{r}{\sqrt{2}} \quad \text{and} \quad \sin\theta_{23} = \frac{1+a}{\sqrt{2}}. \tag{2.3.51}$$

These solar, reactor and atmospheric parameters were originally introduced to describe the deviation of leptonic mixing from tribimaximality [83]. Using Eq. (2.3.51) to write $s^2_\theta = 3r^2/4$, we find that

$$s^2_{\theta 12} = \frac{1}{3 - \frac{3r^2}{2}} \implies \sin\theta_{12} = \frac{1}{\sqrt{3}} \left(\frac{1}{1 - \frac{r^2}{2}} \right)^{\frac{1}{2}}. \tag{2.3.52}$$

As r is a small parameter ($r \sim 0.2$) we Taylor expand Eq. (2.3.52) such that

$$\sin\theta_{12} = \frac{1}{\sqrt{3}} \left(1 + \frac{r^2}{4} + \mathcal{O}(r^4) \right). \tag{2.3.53}$$

We may re-express the above sum rule in terms of the angles themselves

$$\theta_{12} = 35.27^\circ + 10.13^\circ r^2. \tag{2.3.54}$$

Later in Section 2.4, we will discuss the testability of the above relation.

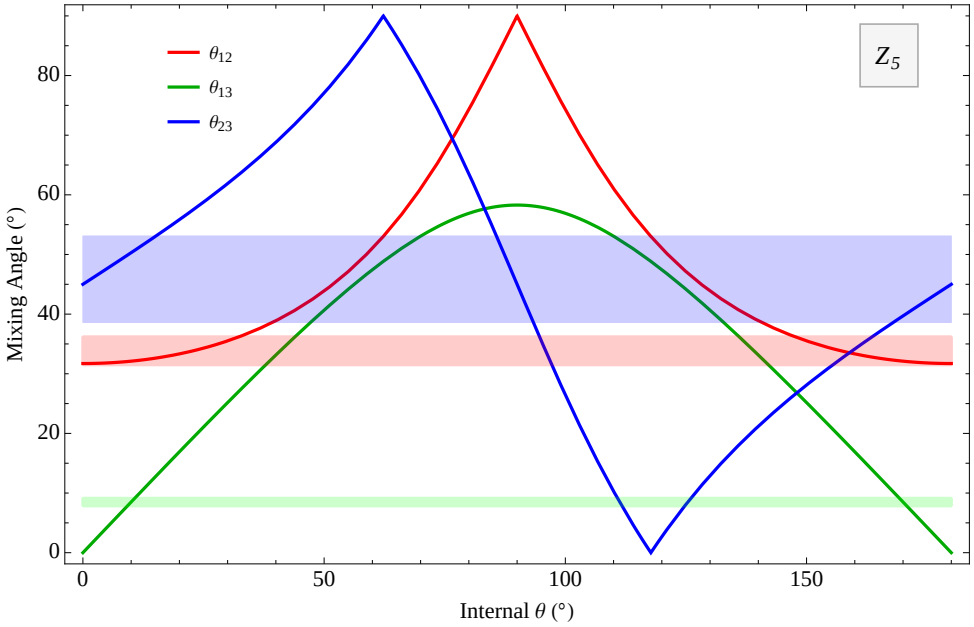

Figure 2.3: Mixing angles prediction for $\mathbb{Z}_5$ as a function of internal parameter, θ. This mixing pattern is associated to $|\sin\delta| = 1$ and $\sin\alpha_{21} = \sin\alpha_{31} = 0$. The blue, red and green-coloured bands show the 3σ allowed region for θ_{23}, θ_{12} and θ_{13} respectively [23].

2.3.2 Predictions from $G_\ell = \mathbb{Z}_5$ and $G_\nu = \mathbb{Z}_2 \times$ CP

In the case of a residual symmetry $G_\ell = \mathbb{Z}_5$, there are two sets of correlations which lead to three distinct predictions for the mixing angles. The first set of predictions corresponds to the following PMNS matrix

$$U_{PMNS} = U_\ell^\dagger \Omega_{13} R(\theta_{13}) = \begin{pmatrix} \frac{\phi}{\sqrt{2+\phi}} & \frac{-1}{\sqrt{2+\phi}} & 0 \\ \frac{-i}{\sqrt{4+2\phi}} & \frac{-i\phi}{\sqrt{4+2\phi}} & \frac{1}{\sqrt{2}} \\ \frac{i}{\sqrt{4+2\phi}} & \frac{i\phi}{\sqrt{4+2\phi}} & \frac{1}{\sqrt{2}} \end{pmatrix} \begin{pmatrix} 1 & 0 & 0 \\ 0 & i & 0 \\ 0 & 0 & 1 \end{pmatrix} \begin{pmatrix} c_\theta & 0 & s_\theta \\ 0 & 1 & 0 \\ -s_\theta & 0 & c_\theta \end{pmatrix}$$
$$= \begin{pmatrix} \frac{c_\theta \phi}{\sqrt{2+\phi}} & \frac{-i}{\sqrt{2+\phi}} & \frac{s_\theta \phi}{\sqrt{2+\phi}} \\ -\frac{c_\theta i}{\sqrt{4+2\phi}} - \frac{s_\theta}{\sqrt{2}} & \frac{\phi}{\sqrt{4+2\phi}} & \frac{-i s_\theta}{\sqrt{4+2\phi}} + \frac{c_\theta}{\sqrt{2}} \\ \frac{i c_\theta}{\sqrt{4+2\phi}} - \frac{s_\theta}{\sqrt{2}} & \frac{-\phi}{\sqrt{4+2\phi}} & \frac{i s_\theta}{\sqrt{4+2\phi}} + \frac{c_\theta}{\sqrt{2}} \end{pmatrix}. \tag{2.3.55}$$

From this particular matrix there are three additional permutations which produce a pattern of mixing that agrees with data to a 3σ level: $p_2 U_{PMNS} p_1$, $p_1 U_{PMNS} p_6$ and $p_2 U_{PMNS} p_6$. From these sets of PMNS matrices, we follow the exact same procedure

as before and the mixing angles may be written as

$$\begin{aligned} \sin^2(\theta_{13}) &= \frac{\phi^2 c_\theta^2}{2+\phi}, \quad \sin^2(\theta_{12}) = \frac{1}{2+\phi-\phi^2 c_\theta^2} \quad \text{and} \\ \sin^2(\theta_{23}) &= \frac{1}{2}\frac{\left((1+\phi^2)\, s_\theta^2 + c_\theta^2 + 2 c_\theta s_\theta \sqrt{1+\phi^2}\right)}{1+\phi^2 s_\theta^2}. \end{aligned} \tag{2.3.56}$$

Rephasing $\theta \to \theta + \pi/2$ allows the mixing angles of Eq. (2.3.56) to be re-expressed as

$$\sin^2(\theta_{13}) = \frac{s_\theta^2}{1+\phi_g^2}, \quad \sin^2(\theta_{12}) = \frac{1}{1+\phi^2 c_\theta^2} \quad \text{and} \quad \sin^2(\theta_{23}) = \frac{1}{2}\frac{\left(s_\theta + c_\theta\sqrt{1+\phi^2}\right)^2}{1+\phi^2 c_\theta^2}. \tag{2.3.57}$$

which permits the sum rules to be written in a concise and closed form. The mixing angles of Eq. (2.3.57) are shown as a function of θ in Fig. 2.3. As we have seen in the case of $G_\ell = \mathbb{Z}_3$, there are two ranges of θ which yield the same results. However, unlike $G_\ell = \mathbb{Z}_3$, θ_{23} is non-maximal and θ-dependent: for $\theta \in (0, \frac{\pi}{2}), \theta_{23} > 45^\circ$ while $\theta \in (\frac{\pi}{2}, \pi), \theta_{23} < 45^\circ$. All three phases are CP-conserving and the precise value of δ is dependent upon θ

$$\delta = \begin{cases} 0 & \theta \in (0, \frac{\pi}{2}), \\ \pi & \theta \in (\frac{\pi}{2}, \pi), \end{cases} \tag{2.3.58}$$

and again the Majorana phases cannot be uniquely be determined, $\sin\alpha_{21} = \sin\alpha_{31} = 0$, but are CP-conserving. The CP-conservation originates from the CP symmetry remaining accidentally unbroken in the charged lepton sector. Using the correlations Eq. (2.3.57), we may write the following sum rules for the atmospheric and solar angle respectively

$$\theta_{23} = 45^\circ \pm 25.04^\circ r + \mathcal{O}(r^4) \quad \text{and} \quad \theta_{12} = 31.72^\circ + 8.85^\circ r^2 + \mathcal{O}(r^4). \tag{2.3.59}$$

The second set of correlations is given by the following PMNS matrix

$$U_{PMNS} = U_\ell^\dagger \Omega_{12} R(\theta_{23}) = \begin{pmatrix} \frac{1}{\sqrt{2+\phi}} & 0 & \frac{-\phi}{\sqrt{2+\phi}} \\ \frac{i\phi}{\sqrt{4+2\phi}} & \frac{1}{\sqrt{2}} & \frac{i}{2\sqrt{2+\phi}} \\ \frac{-i\phi}{\sqrt{4+2\phi}} & \frac{1}{\sqrt{2}} & \frac{-i}{2\sqrt{2+\phi}} \end{pmatrix} \begin{pmatrix} 1 & 0 & 0 \\ 0 & i & 0 \\ 0 & 0 & i \end{pmatrix} \begin{pmatrix} 1 & 0 & 0 \\ 0 & c_\theta & s_\theta \\ 0 & -s_\theta & c_\theta \end{pmatrix}. \tag{2.3.60}$$

The permutations which yield PMNS matrices consistent with data are $p_1 U_{PMNS} p_3$, $p_2 U_{PMNS} p_3$, $p_1 U_{PMNS} p_4$ and $p_2 U_{PMNS} p_4$. The predictions for θ_{13} and θ_{12} are the

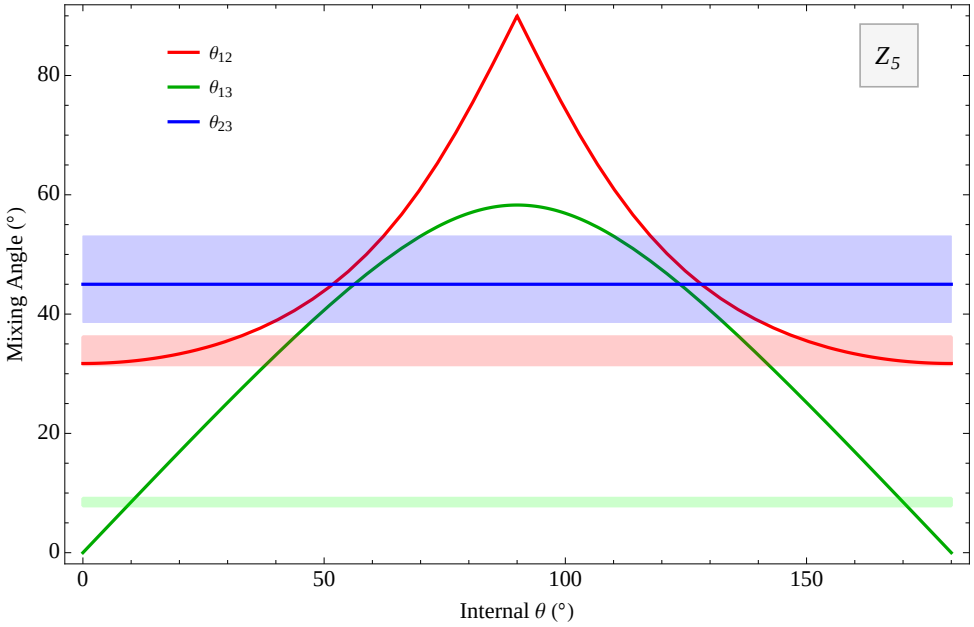

Figure 2.4: Mixing angles prediction for $\mathbb{Z}_5$ as a function of internal parameter, θ. This mixing pattern is associated to $|\sin\delta| = 1$ and $\sin\alpha_{21} = \sin\alpha_{31} = 0$. The blue, red and green-coloured bands show the 3σ allowed region for θ_{23}, θ_{12} and θ_{13} respectively [23].

identical to the first case, but now θ_{23} is maximal

$$\sin^2(\theta_{13}) = \frac{s_\theta^2}{1+\phi_g^2}, \quad \sin^2(\theta_{12}) = \frac{1}{1+\phi^2 c_\theta^2} \quad \text{and} \quad \sin^2(\theta_{23}) = \frac{1}{2}. \tag{2.3.61}$$

The mixing angles predictions are shown as a function of θ in Fig. 2.4. Similarly to the case of $\mathbb{Z}_3$ predictions, the sign of δ is also θ-dependent

$$\delta = \begin{cases} \frac{3\pi}{2} & \theta \in (0, \frac{\pi}{2}), \\ \frac{\pi}{2} & \theta \in (\frac{\pi}{2}, \pi), \end{cases} \tag{2.3.62}$$

and likewise $\sin\alpha_{21} = \sin\alpha_{31} = 0$. Both mixing patterns Eq. (2.3.57) and Eq. (2.3.61) are continuously connected to the GR mixing pattern (also known as GRA or GR1) [135, 136] which is recovered at $\theta = 0°$. However, their predictions for θ_{23} differ. The latter prediction has a similar feature to that of Section 2.3.1: maximal θ_{23} associated to maximal CP-violation in δ. Henceforth, we refer to this prediction as *maximal-maximal*. Although the $\mathbb{Z}_3$ and $\mathbb{Z}_5$ predictions share this feature, they may be distinguished by their θ_{12} predictions. In the $\mathbb{Z}_5$ case, the preferred values for θ_{12} are close to the lower allowable range whilst $\mathbb{Z}_3$ prefers values of θ_{12} close

to the upper boundary of the allowable range. In a simplistic way, the origin of the maximal-maximal predictions arises from $\mu - \tau$ symmetry of the neutrino mass matrix [137][3]. However, a more rigorous mathematical examination the origin of this ubiquitous prediction is found in [138] where additional conditions are deduced.

2.3.3 Predictions from $G_\ell = \mathbb{Z}_2 \times \mathbb{Z}_2$ and $G_\nu = \mathbb{Z}_2 \times$ CP

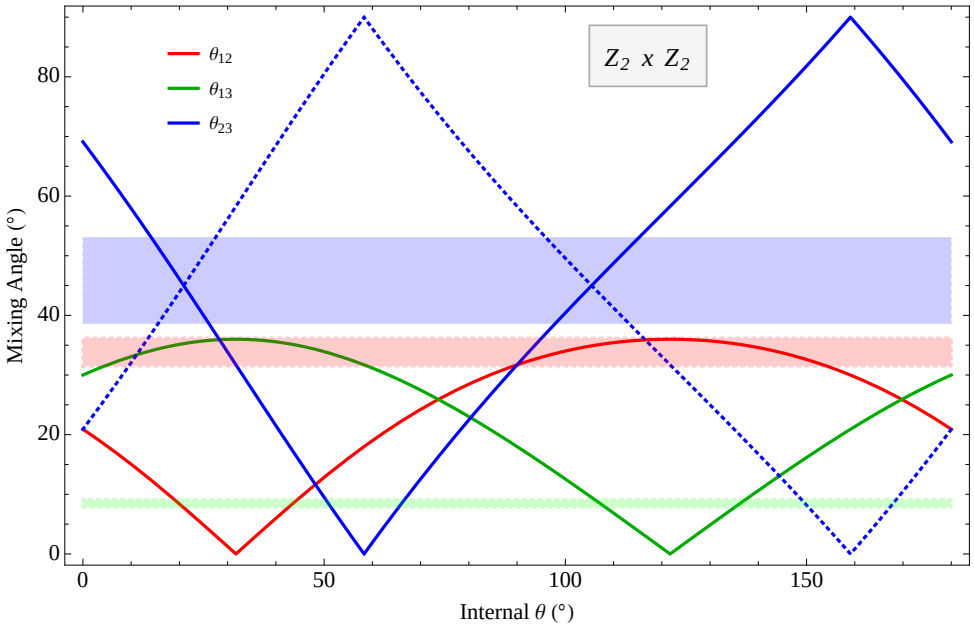

Figure 2.5: Allowed mixing angles for $G_\ell = \mathbb{Z}_2 \times \mathbb{Z}_2$ as a function of the unphysical parameter θ. There are two possible sets of predictions of the mixing angles which have the same θ_{12} and θ_{13} predictions but distinct θ_{23} predictions (solid and dotted lines) related by the mapping $\theta_{23} \to \frac{\pi}{2} - \theta_{23}$. All complex phases are CP-conserving for these patterns: $\sin\delta = \sin\alpha_{21} = \sin\alpha_{31} = 0$. The shaded regions show the 3σ allowed region for the corresponding mixing angle according to current global data [23].

The only non-cyclic subgroup of A_5 is the Klein group. In the case of this residual

[3]Defining the neutrino mass matrix from the see-saw mechanism in the following simple way: $m_\nu = Y_\nu Y_\nu^T v_H^2/\text{diag}(M)$, we obtain the diagonal neutrino mass matrix via $m_\nu = U\text{diag}(m)U^T$. The $\mu - \tau$ symmetry is defined as the interchanging of the indices 2 and 3 of Y_ν such that $(Y_\nu)_{12} = (Y_\nu)_{13}$, $(Y_\nu)_{22} = (Y_\nu)_{33}$ etc. Solving this set of equations one can deduce $\theta_{23} = \pi/4$ and $\delta = \pi/2$.

symmetry in the charge lepton sector, there are two patterns of mixing which differ only by their prediction for θ_{23}. The first pattern of mixing can be derived from the following representative matrix

$$\begin{aligned} U_{PMNS} &= \frac{1}{2}\begin{pmatrix} \frac{1}{\phi} & -1 & \phi \\ \phi & \frac{-1}{\phi} & -1 \\ -1 & -\phi & \frac{-1}{\phi} \end{pmatrix}\begin{pmatrix} i & 0 & 0 \\ 0 & 1 & 0 \\ 0 & 0 & i \end{pmatrix}\begin{pmatrix} c_\theta & 0 & s_\theta \\ 0 & 1 & 0 \\ -s_\theta & 0 & c_\theta \end{pmatrix} \\ &= \frac{1}{2}\begin{pmatrix} i\frac{c_\theta}{\phi} - i\phi s_\theta & -1 & \frac{i(\phi^2 c_\theta + s_\theta)}{\phi} \\ i(\phi c_\theta + s_\theta) & -\frac{1}{\phi} & -i(c_\theta - \phi s_\theta) \\ -i(c_\theta - \frac{s_\theta}{\phi}) & -\phi & \frac{-i(c_\theta + \phi s_\theta)}{\phi} \end{pmatrix}, \end{aligned} \tag{2.3.63}$$

where the permutations which produce mixing consistent with data are: $p_5 U_{PMNS} p_3$, $p_6 U_{PMNS} p_3$, $p_5 U_{PMNS} p_5$ and $p_6 U_{PMNS} p_5$. From these matrices, the mixing angles can be expressed as

$$\begin{aligned} &s^2_{13} = \frac{1}{4}\left(\phi_g^2 - \phi_g\left(s^2_\theta + s_{2\theta}\right)\right), \quad s^2_{12} = \frac{1 - (\phi_g^2 - 1)s^2_\theta + \phi_g s_{2\theta}}{4 - \phi_g^2 + \phi_g\left(s^2_\theta + s_{2\theta}\right)} \quad \text{and} \\ &s^2_{23} = \frac{\phi^2 + (\phi_g - \phi)s^2_\theta + s_{2\theta}}{4 - \phi_g^2 + \phi_g\left(s^2_\theta + s_{2\theta}\right)}. \end{aligned} \tag{2.3.64}$$

We rephase Eq. (2.3.64) so that the sum rules can be written in a closed form. As a consequence, the mixing angles may be expressed as

$$\begin{aligned} &s^2_{13} = \frac{1 + \phi_g\left(s^2_\theta - s_{2\theta}\right)}{4}, \quad s^2_{12} = \frac{1 + \phi_g\left(\cos^2\theta + s_{2\theta}\right)}{3 - \phi_g\left(s^2_\theta - s_{2\theta}\right)} \quad \text{and} \\ &s^2_{23} = \frac{1 + \varphi\left(\cos^2\theta - s_{2\theta}\right)}{3 - \phi_g\left(s^2_\theta - s_{2\theta}\right)}. \end{aligned} \tag{2.3.65}$$

For this pattern, the complex phases are given by CP-conserving values: $\sin\delta = 0$ and $\{\alpha_{21}, \alpha_{31}\} \subseteq \{0, \pi\}$. The true value of δ can be shown to depend on θ

$$\delta = \begin{cases} 0 & 31.7^\circ < \theta < 58.3^\circ \text{ or } 121.7^\circ < \theta < 159.1^\circ, \\ \pi & \text{else.} \end{cases} \tag{2.3.66}$$

This dependence on θ looks complex, but the boundaries of the $\delta = 0$ regions can be seen in Fig. 2.5 to be those values of θ for which one mixing angle is either 0° or 90°, and closed form of the expressions can be derived for these values from the mixing angle formulae above. For the matrix shown here, this means that only the $\delta = \pi$ solution agrees with the global data. However, when considering all permutations the

alternative CP-conserving solution can also be found. A permutation of Eq. (2.3.63) ($p_6 U_{PMNS} p_3$) has the effect of mapping: $\theta_{23} \to \pi/2 - \theta_{23}$ which has been shown as a dashed line in Fig. 2.5. Using the correlations Eq. (2.3.65), the sum rules of the atmospheric and solar angle are given by

$$\begin{aligned} &\theta_{23} = 31.72^\circ + 55.76^\circ r + \mathcal{O}(r^2), \quad \theta_{23} = 58.28^\circ + 55.76^\circ r + \mathcal{O}(r^2) \quad \text{and} \\ &\theta_{12} = 36^\circ - 19.72^\circ r^2 + \mathcal{O}(r^4), \end{aligned} \tag{2.3.67}$$

respectively.

2.4 Phenomenological Prospects

In the preceding sections we derived all patterns of mixing angles and phases which are possible with an A_5 symmetry with generalised CP broken into residual symmetries $G_\ell = \{\mathbb{Z}_3, \mathbb{Z}_5, \mathbb{Z}_2 \times \mathbb{Z}_2\}$ and $G_\nu = \mathbb{Z}_2 \times \text{CP}$. They depend upon a single real angle, θ, and can all be brought into agreement with current global data [23] for a suitable restriction of its range. Eliminating the unphysical parameter θ leads to a set of correlated predictions between observables which are testable by oscillation experiments and searches for neutrinoless double-beta decay. In the proceeding sections, we shall discuss the prospects for present and future experiments to constrain these patterns and derive simple versions of the predicted parameter correlations which may be useful experimentally. A summary of the 10 possible predictions thus far is shown in Table 2.1.

2.4.1 Precision Measurement of θ_{12}

Upcoming medium-baseline reactor experiments such as the Jiangmen Underground Neutrino Observatory (JUNO) [139, 140] and Reactor Experiment for Neutrino Oscillation (RENO-50) [30, 141] expect to make very precise, sub-percent measurement of θ_{12}. JUNO is a multi-purpose experiment which will be built in Jiangmen city in the Guangdong province of China. The location is conveniently situated 53km from nuclear power plants (NPPs) in Yangjiang and Taishan. The survival probability of anti-electron neutrinos, copiously produced by these NPPs, will be used by JUNO to

G_ℓ	θ_{12}	θ_{23}	$\sin\alpha_{ji}$	δ
$\mathbb{Z}_3$	$35.27^\circ + 10.13^\circ\, r^2$	45°	0	90°
				270°
$\mathbb{Z}_5$	$31.72^\circ + 8.85^\circ\, r^2$	$45^\circ \pm 25.04^\circ\, r$	0	0°
				180°
		45°	0	90°
				270°
$\mathbb{Z}_2 \times \mathbb{Z}_2$	$36.00^\circ - 34.78^\circ\, r^2$	$31.72^\circ + 55.76^\circ\, r$	0	0°
				180°
		$58.28^\circ - 55.76^\circ\, r$	0	0°
				180°

Table 2.1: The dimensionless parameter $r \equiv \sqrt{2}\sin\theta_{13}$ is constrained by global data to lie in the interval $0.19 \lesssim r \lesssim 0.22$ at 3σ. The predictions for θ_{12} and θ_{23} shown here neglect terms of order $\mathcal{O}(r^4)$ and $\mathcal{O}(r^2)$, respectively.

determine the mass ordering. The approach applied by JUNO to determine the mass ordering is reliant upon being able to distinguish between the oscillation probability of normally or invertedly ordered mass spectra [142]. However, in order to resolve the difference between the spectral distortion, a greater than 3% energy resolution is required [140]. As a consequence of the planned excellent energy resolution, JUNO will be well placed to make unprecedented measurements of oscillation parameters such as θ_{12} and Δm^2_{21} with better than 1% precision. RENO-50 is another MR experiment which has very similar physics goals to JUNO. RENO-50 will use the same method to determine the mass ordering as JUNO and likewise the necessary high-energy resolution will enable precise measurements of θ_{12} and Δm^2_{21}. The precision on θ_{13}, currently dominated by measurements from Daya Bay [28, 29] and RENO [30], is not expected to be significantly improved by the next generation of reactor facilities. Therefore, the first significant test of these predictions will come from increased precision on θ_{12} independently of θ_{13}. There are three distinct predictions identified for θ_{12}, if we fix θ_{13} to its current best-fit value [23]. These are

$$\theta_{12} = 35.71^\circ, \quad \theta_{12} = 32.10^\circ \quad \text{and} \quad \theta_{12} = 35.14^\circ, \tag{2.4.68}$$

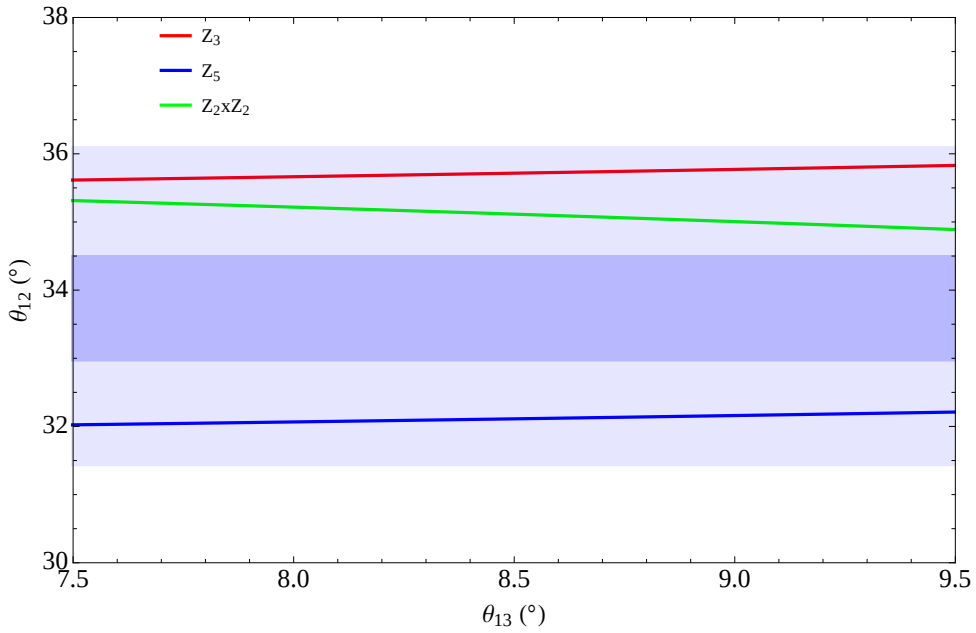

Figure 2.6: Predictions for θ_{12} as a function of θ_{13}. The linearised predictions for all charged lepton residual symmetries are shown in the coloured lines. The blue and pale blue bands show the 1 and 3σ allowed regions for θ_{12} from current global fit [23].

for preserved charged-lepton subgroups $\mathbb{Z}_3$, $\mathbb{Z}_5$ and $\mathbb{Z}_2 \times \mathbb{Z}_2$, respectively. As the expected precision of the MR experiments is at the level of 0.1° or around 0.3% for θ_{12}, a strong discriminatory power exists between the values of the mixing angles predicted by these correlations. The difference between the predicted values of all models under consideration is always greater than 0.26° over the current 3σ interval for θ_{13}, and in many cases significantly greater. Therefore we expect these experiments to identify if any of the charged-lepton residual symmetries are consistent with observation. In the framework of this discussion, each model predicts a continuous correlation between the values of θ_{13} and θ_{12}. If one of the predictions above agrees with data, the next step would be to test the correlation between parameters itself. These correlations can be conveniently re-expressed as expansions in the dimensionless parameter $r \equiv \sqrt{2}\sin\theta_{13}$ [134]. The current best fit value from global fit data is $\theta_{13} \approx 8.47^\circ$ [23] and translates to $r \approx 0.21$; the second-order corrections are therefore suppressed by a factor of $1/25$. Expressed in this way, the predictions for $\sin\theta_{12}$ associated with the charged-lepton subgroups $\mathbb{Z}_3$, $\mathbb{Z}_5$ and $\mathbb{Z}_2 \times \mathbb{Z}_2$

(respectively) can be expanded in the following relations from Table 2.1,

$$\sin\theta_{12} = \frac{1}{\sqrt{3}}\left(1+\frac{r^2}{4}\right)+\mathcal{O}\left(r^4\right), \quad \sin\theta_{12} = \frac{1}{\sqrt{1+\varphi^2}}\left(1+\frac{r^2}{4}\right)+\mathcal{O}\left(r^4\right), \quad \text{and}$$
$$\sin\theta_{12} = \frac{\sqrt{2+\phi_g}}{2} - \frac{2-\phi_g}{\sqrt{2+\phi_g}}\frac{r^2}{8}+\mathcal{O}\left(r^4\right). \tag{2.4.69}$$

Expressing the above in terms of the angles themselves, we find that

$$\theta_{12} = 35.27^\circ + 10.13^\circ\, r^2 + \mathcal{O}\left(r^4\right), \quad \theta_{12} = 31.72^\circ + 8.85^\circ\, r^2 + \mathcal{O}\left(r^4\right) \quad \text{and}$$
$$\theta_{12} = 36.00^\circ - 19.72^\circ\, r^2 + \mathcal{O}\left(r^4\right). \tag{2.4.70}$$

The approximations of Eq. (2.4.70) have been plotted against θ_{12} in Fig. 2.6. We see that these relations depend only slightly on θ_{13}, which appears at order $\mathcal{O}(r^2)$, leading to sub-degree-level corrections. The formulae above show that the predictions for θ_{12} only vary by 0.07°, 0.06° and 0.13° (for $\mathbb{Z}_3$, $\mathbb{Z}_5$ and $\mathbb{Z}_2 \times \mathbb{Z}_2$, respectively) over the current 3σ region for θ_{13}. This is around the target precision of the MR experiments, and therefore it is unlikely that the θ_{12}–θ_{13} correlations themselves will be tested at a significant level even if precision on θ_{13} was to be significantly improved. There are no currently planned facilities which could further improve the precision on θ_{12}.

2.4.2 Maximal-Maximal Predictions for θ_{23} and δ

The currently running and future planned long-baseline accelerator oscillation experiments will be able to make important constraints on θ_{23} and δ. In the context of A_5 flavour symmetry with residual symmetries of the charged lepton and neutrino sectors, $G_\ell = \{\mathbb{Z}_3,\ \mathbb{Z}_5,\ \mathbb{Z}_2 \times \mathbb{Z}_2\}$ and $G_\nu = \mathbb{Z}_2 \times \mathrm{CP}$, respectively, we find that four of the ten predictions are maximal-maximal. Moreover, the maximal-maximal prediction is ubiquitous in gCP and flavour model-building [1, 117, 122, 123, 143–145] and therefore the joint determination of these parameters is crucially important.

As previously mentioned, there are two currently running experiments, T2K and NOνA, which will be able to test the maximality of θ_{23}. T2K has the ability to exclude maximal θ_{23} with a 90% confidence level (C.L.) for $|\sin^2(2\theta_{23}) - 0.5| >$

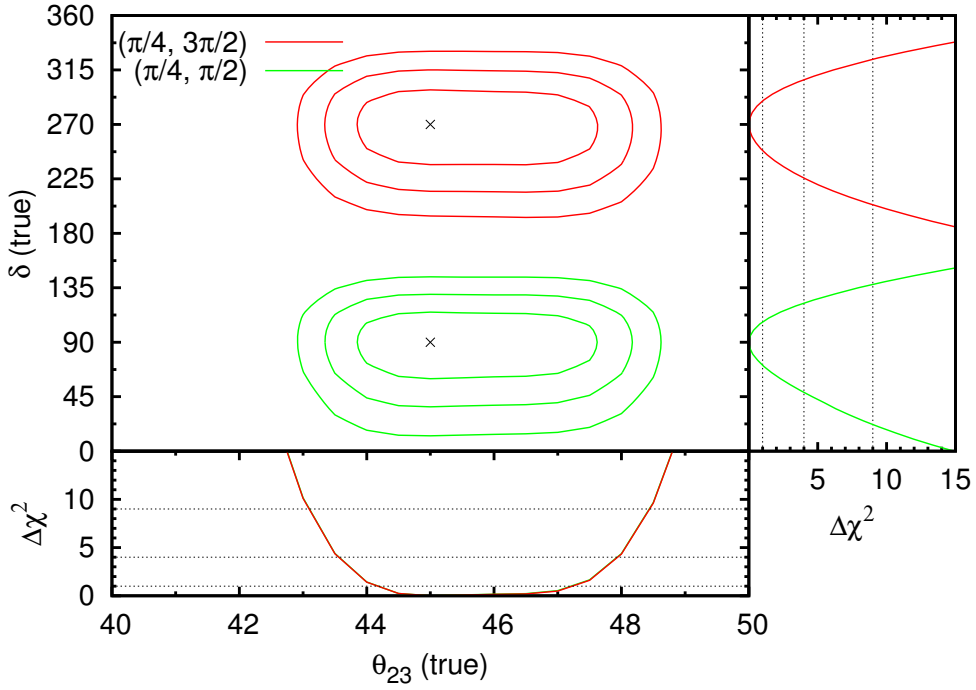

Figure 2.7: Red (green) lines show the exclusion regions at 1, 2 and 3σ for $\theta_{23} = \pi/4$ and $\delta = 3\pi/2$ ($\delta = \pi/2$) expected at DUNE with a 34 kton LAr detector after $5+5$ years running. In this region outside the curves, the two sets of predictions can be excluded at the given confidence. The side panels show the appropriate marginalised $\Delta\chi^2$ and the 1, 2 and 3σ confidence levels (1 d.o.f.).

$0.05 - 0.07$, largely independently of the value of δ [146]. The determination of δ is more difficult; however, maximally CP-violating values are the most accessible. T2K expects to exclude $0 \lesssim \delta \lesssim \pi$ ($\pi \lesssim \delta \lesssim 2\pi$) at the 90% C.L. for a true value of $\delta = 3\pi/2$ ($\delta = \pi/2$) [146]. This would enable T2K to differentiate between $\delta = \pi/2$ and $\delta = 3\pi/2$ if one of them is true at least at the 90% C.L. NOνA also has a similar power for exclusion of maximally CP-violating δ [147].

In the long term, there are several planned experiments which aim to improve the sensitivity to δ and therefore permit the further testing of the maximal-maximal prediction. In order to estimate the capabilities of such experiments in excluding this prediction, we ran a simulation of DUNE [148, 149] using the GLoBES package [150, 151]. The simulation is based on the detector fluxes and response files made available by the LBNE collaboration [152]. At the time this simulation was completed, the

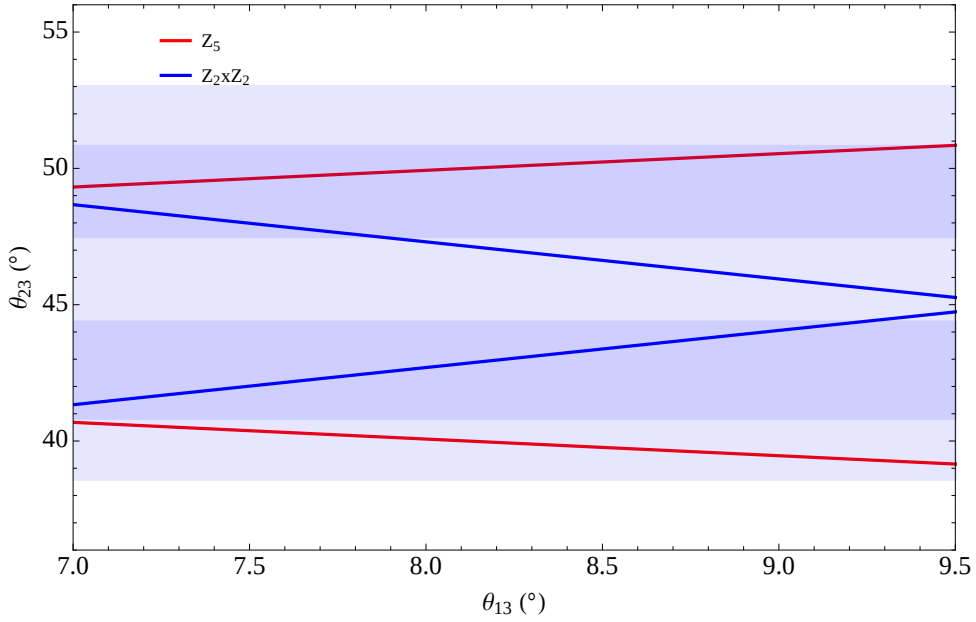

Figure 2.8: Predictions for θ_{23} as a function of θ_{13}. The linearised predictions for all charged lepton residual symmetries are shown in the coloured lines. The blue and pale blue bands show the 1 and 3σ allowed regions for θ_{12} from current global fit [23].

design specifications of DUNE were not finalised. In light of this, we used the following specifications in the GLoBES simulation: 700kW beam operating at 120 GeV, a liquid argon TPC detector of fiducial mass 34 kton and overall systematic error of 5% for signal and background normalisations. The results of the simulation are shown in Fig. 2.7, where the region of parameter space for which the maximal-maximal prediction can be excluded after five years of neutrino and five years of anti-neutrino run time. This prediction can be excluded if $\theta_{23} < 43°$ or $\theta_{23} > 48.3°$ or if δ lies outside the ranges $90°^{+48°}_{-69°}$ or $270°^{+53°}_{-67°}$.

2.4.3 CP-Conservation and Precision Measurements of θ_{23}

Six of our ten predictions have non-maximal θ_{23} and CP-conserving values of δ such that $|\cos\delta|=1$. Such predictions will be constrained by attempts to discover leptonic CP-violation. There are two currently running experiments which can constrain δ; these include NOνA and T2K whose capabilities have been discussed in 2.4.2. Future planned experiments which will have increased sensitivity to leptonic

CP-violation include DUNE and T2HK. T2HK has shown that it expects to make a discovery of CP-violation over 76% (58%) of the parameter space at 3σ (5σ) [153]. Likewise, DUNE (using conceptual design report reference design with an exposure of 1320 kt.MW.year) is sensitive to CP-violation for 75% of δ values at 3σ (5σ) [154].

If the currently running experiments do not discover leptonic CP-violation then six of our predictions would remain in agreement with data. These predictions have non-maximal θ_{23} and may be further tested by the increased precision in the measurement of θ_{23} by future long baseline experiments. The model associated with $\mathbb{Z}_5$ residual symmetry predicts

$$45^\circ \pm 25.04^\circ\, r + \mathcal{O}(r^2), \tag{2.4.71}$$

whilst $\mathbb{Z}_2 \times \mathbb{Z}_2$ predicts

$$31.72^\circ + 55.76^\circ r + \mathcal{O}(r^2) \quad \text{and} \quad 58.28^\circ - 55.76^\circ r + \mathcal{O}(r^2). \tag{2.4.72}$$

Unlike the θ_{12} sum rules of Eq. (2.4.70), the above sum rules are a linear function of r. Consequently, the θ_{23}-θ_{13} correlation is more experimentally accessible as θ_{23} is sensitive to r. These sum rules are shown in Fig. 2.8. Clearly, the predictions which are most difficult to distinguish are $\mathbb{Z}_2 \times \mathbb{Z}_2$: θ_{23} deviates from maximal by 2.5° and 0.8° over the 3σ range of θ_{13}. On the other hand, $\mathbb{Z}_5$ prediction differs from 45° by between 4.8° and 5.6° over the same range.

Studies of the current generation of oscillation experiments, of which T2K and NOνA will be most important, suggest that the octant may be established at 3σ (2σ) for deviations from maximality greater than around 6° (4°) [155, 156]. This excludes the current generation from separating between the two predictions of $\mathbb{Z}_2 \times \mathbb{Z}_2$, but would allow for 2σ evidence for those predictions coming from our model based on $\mathbb{Z}_5$. The ability to distinguish between these predictions will be improved by the next generation of oscillation experiments. The best bounds may come from T2HK by studying atmospheric neutrino data. A 3σ determination of the octant is expected to be possible after 10 years of data-taking for true values $\left|\sin^2\theta_{23} - 0.5\right| > 0.04$–$0.06$ corresponding to deviations between 2°–3° [157]. Although exclusion of the $\mathbb{Z}_2 \times \mathbb{Z}_2$

pattern would be unlikely, the two predictions from $\mathbb{Z}_5$ would be distinguishable.

To go beyond the octant determination, high resolution of θ_{23} would be necessary to differentiate between the $\mathbb{Z}_5$ and $\mathbb{Z}_2 \times \mathbb{Z}_2$ predictions, or in fact test the correlation with θ_{13} at all. The difference between these predictions varies between 2.4° and 4.8° and therefore degree-level precision is required to distinguish between them, even if θ_{13} is very well measured. T2HK has shown that around the point where they have expect to have the lowest sensitivity to θ_{23}, the 90% C.L. width is approximately 2-3°. This implies significant discrimination between these models would be very challenging even from upcoming experiments, however evidence in favour of these models would be possible, at low significance, if leptonic CP-conservation was observed. This would present a solid hypothesis for future work.

2.4.4 Neutrinoless Double-Beta Decay

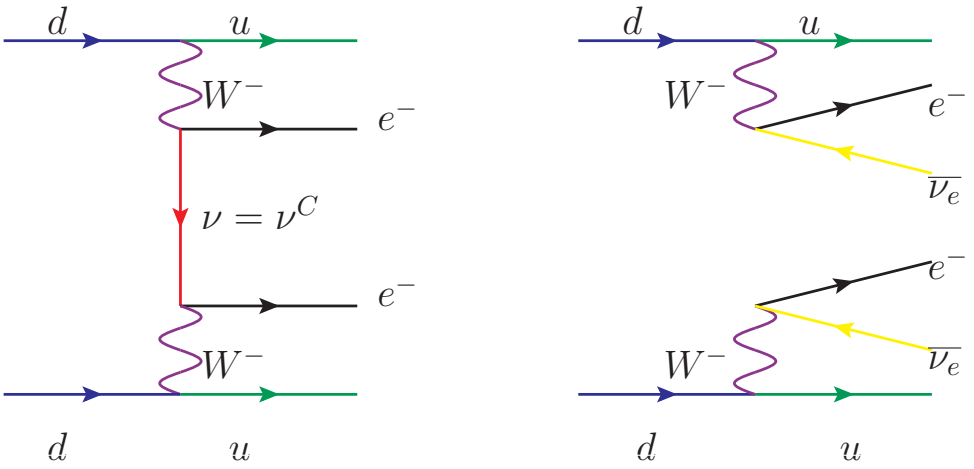

Figure 2.9: On the right (left) is the diagram contributing to $2\nu\beta\beta$ ($0\nu\beta\beta$) decay. The internal propagator of the $0\nu\beta\beta$ diagram represents a Majorana fermion denoted by ν.

Standard beta decay proceeds via the decay of nuclei of mass number A and atomic number Z in the following manner

$$(A, Z) \to (A, Z + 1) + e^- + \overline{\nu_e}. \tag{2.4.73}$$

This process arises from the decay of a bound d-quark. There is a significantly rarer process, two neutrino double-beta decay ($2\nu\beta\beta$), which is also mediated by known physics and manifests in the following decay

$$(A, Z) \rightarrow (A, Z + 2) + 2e^{-} + 2\overline{\nu_e}. \tag{2.4.74}$$

This four-body leptonic final-state decay, as shown in Fig. 2.9, preserves lepton number. In contrast, the observation of neutrinoless double-beta ($0\nu\beta\beta$) decay would signal violation of total lepton number. This process may be mediated by the exchange of a massive, Majorana neutrino, or possibly by other particles. However, the existence of this decay would indicate neutrinos are Majorana in nature, independent of the actual mechanism. Over the next decade, the new generation of $0\nu\beta\beta$ decay experiments will significantly increase the sensitivity to this rare process. For the first time these experiments will probe the region of parameter space associated with the inverse hierarchical spectrum. These experiments aim to establish that neutrinos are Majorana in nature, but can also provide valuable information on the neutrino mass spectrum and in principle, measure the Majorana phases themselves. Assuming a three-neutrino mixing paradigm, the $0\nu\beta\beta$ decay rate is proportional to the effective Majorana mass $|m_{ee}|$ which is given by

$$\begin{aligned} |m_{ee}| &= \left| \sum_{k=1}^{3} U_{ek}^2 m_k \right| \\ &= \left| m_1 \cos^2\theta_{12} \cos^2\theta_{13} + m_2 \sin^2\theta_{12} \cos^2\theta_{13} e^{i\alpha_{21}} + m_3 \sin^2\theta_{13} e^{i(\alpha_{31} - 2\delta)} \right|, \end{aligned} \tag{2.4.75}$$

where α_{21} and α_{31} are Majorana phases and δ is the Dirac phase.

The predicted values of $|m_{ee}|$ depend crucially on the neutrino masses. As the parameters Δm^2_{21} and $|\Delta m^2_{31}|$ are known from oscillation physics, there is a single degree of freedom remaining amongst the masses. This is typically taken to be the lightest neutrino mass, m_1 (m_3) for NO (IO), which we will denote in both cases by m_l [158]. The parameter space available to $|m_{ee}|$ can be further divided into three particularly interesting regions based on the true value of m_l. The first is for *quasi-degenerate* masses (QD) where $m_l \gtrsim 0.1$ eV, in which the splitting between masses is

a small correction to approximately degenerate values. For smaller values of m_l there are two parameter regions: one for *normal hierarchical* masses (NH; $m_1 < m_2 \ll m_3$) and the other for *inverted hierarchical* masses (IH; $m_3 \ll m_1 < m_2$). In order to better understand the predictions of our models, we have first computed the predicted values of $|m_{ee}|$ in the generic case, assuming only that the mixing parameters lie in their current 3σ allowed ranges [23]. These predictions for NO (IO) are shown as the blue (red) region in Fig. 2.10. For quasi-degenerate and IH spectra, there exist lower bounds on $|m_{ee}|$ [159]: for IH $|m_{ee}| \gtrsim 0.015$ eV, and for QD $|m_{ee}| \gtrsim 0.03$–0.04 eV. For NO there is no non-zero lower bound as $|m_{ee}|$ can vanish due to a cancellation between terms in Eq. (2.4.75).

There are many experiments that are searching for $0\nu\beta\beta$ decay or are in various stages of planning and construction. The most recent experiments that have set upper limits on the effective Majorana mass are CUORICINO, GERDA, EXO–200 and KamLAND-Zen. CUORICINO, based in Gran Sasso National Laboratories in Italy, was an experiment used to test the feasibility of its successor, CUORE. Using data taken from 2003–2004 they achieved a bound on $|m_{ee}|$ of 200–1100 meV [160]. As with all $0\nu\beta\beta$ experiments, a key uncertainty on their limits comes from the nuclear matrix element. GERDA (The Germanium Detection Array) is also located in the Gran Sasso Laboratory LNGS in Italy [161]. During phase I of their data-taking period they acquired sufficient data to attain an upper limit of $|m_{ee}| \lesssim 200$–400 meV. They intend to increase their sensitivity by a factor of approximately ten during GERDA Phase II. EXO (Enriched Xenon Observatory)–200, located in Carlsbad, New Mexico, has placed upper bounds for $|m_{ee}|$ of 69–163 meV [162]. KamLAND-Zen (Kamioka Liquid Scintillator Anti-Neutrino Detector-Zero neutrino double-beta decay search) has had two phases of data acquisition and using the combined data they found an upper limit of $|m_{ee}| \lesssim 140$–280 meV [163]. Both EXO–200 and KamLAND-Zen have ambitious long-term plans to upgrade their experiments in order to explore the inverted hierarchical region of parameter space. EXO–200 intends to upgrade to nEXO (next Enriched Xenon Observatory) which, with ten years of data-taking, is expected to cover the full IO region [164]. In its next phase,

KamLAND-Zen aims to increase its sensitivity to around 50 meV after approximately two years' running time [163]. As this limit will only begin to probe the IH region, KamLAND-Zen has proposed KamLAND2-Zen. This upgraded detector (with a running time of five years) has a target sensitivity of $|m_{ee}| \simeq 20$ meV and will allow the exploration of the majority of the IO region and all of the QD parameter space. In addition to EXO–200 and KamLAND-Zen, other future $0\nu\beta\beta$ decay experiments are CUORE, SNO+ and NEXT. CUORE started taking data in 2015. Over the course of five years, they hope to reach a sensitivity of 50–120 meV [165]. SNO+, a multi-purpose experiment located in Sudbury, Canada, aims to achieve a similar upper bound on $|m_{ee}|$. After two years of data-taking they expect to be able to set the upper bound $|m_{ee}| < 100$ meV [166]. The NEXT (Neutrino Experiment with Xenon TPC) experiment, based at CanFranc Underground Laboratory (LSC), will commence data-taking in 2018 using the NEXT-100 detector. Despite their late start compared with that of EXO–200 and KamLAND-Zen, they intend to achieve a $|m_{ee}|$ sensitivity of approximately 100 meV by 2020 [167]. The next stage will be the development of BEXT which proposes to fully cover the predicted values of $|m_{ee}|$ for IO [168]. Although they are not discussed here, there are other experiments which aim to improve the current bounds on $|m_{ee}|$; for example, COBRA [169], the Majorana Demonstrator [170], SuperNEMO [171] and the DCBA experiment [172], amongst others.

The predicted values of $|m_{ee}|$ for the case of A_5 with gCP can be calculated from the leptonic mixing matrices of Eq. (2.3.39), Eq. (2.3.60) and Eq. (2.3.63) for both IO and NO. The complex phases only influence $|m_{ee}|$ through the combinations $e^{\mathrm{i}\alpha_{21}}$ and $e^{\mathrm{i}(\alpha_{31}-2\delta)}$, and we will denote the phases of our predictions by an ordered pair of $\pm$ signs e.g.˙ $(+-)$ when $\alpha_{21} = 0$ and $\alpha_{21} - 2\delta = \pi$. As $|m_{ee}|$ does not depend on θ_{23}, patterns which only differ by this angle will be degenerate and each preserved charged-lepton subgroup leads to a single prediction for each mass ordering and phase assignment. Fig. 2.10 shows the predicted values from the mixing patterns in this paper for each charged-lepton residual symmetry G_ℓ. In these plots, we have neglected a small width to each line which comes from varying θ_{13} and the neutrino

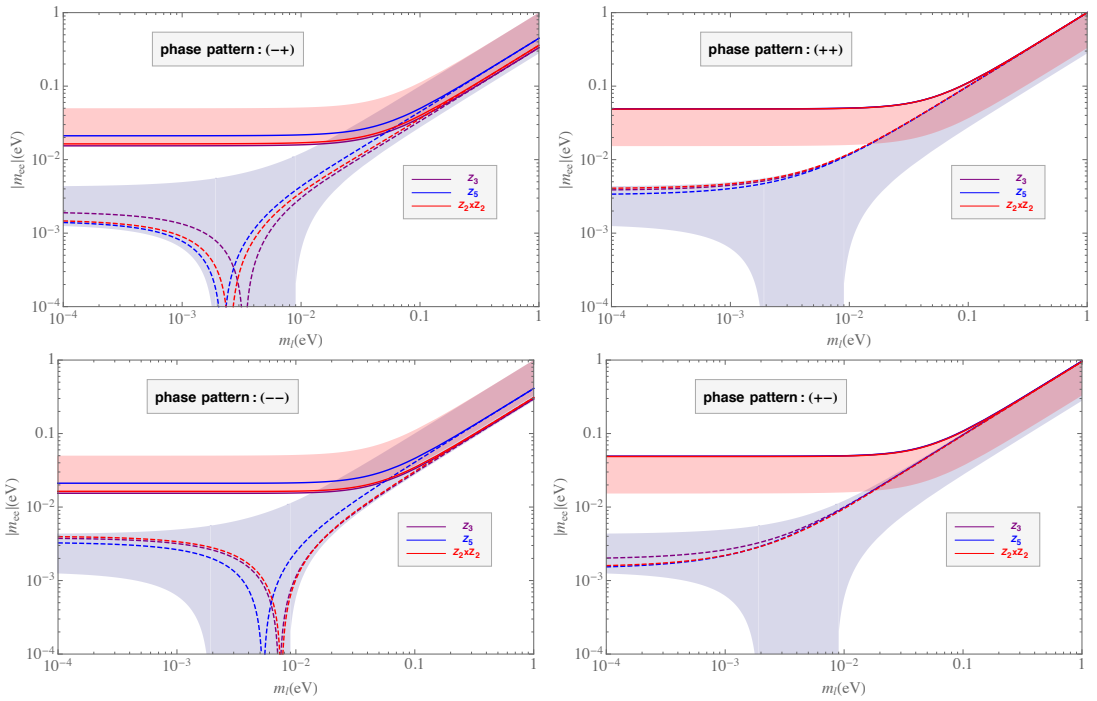

Figure 2.10: $|m_{ee}|$ versus the lightest neutrino mass for the IO (NO) for the solid (dashed) lines. The predictions in a given panel all have the same phase assignment, shown in the top left of the plot. The red (blue) shaded region shows the most general predictions for $|m_{ee}|$ with IO (NO) obtained by varying the oscillation parameters over their current 3σ global ranges [23].

mass-squared splittings over their allowed ranges, instead fixing these at their best-fit values from [23].

We focus first on the IO spectra. The phase assignments $(++)$ and $(+-)$, shown on the top row of Fig. 2.10, predict large values of $|m_{ee}|$, close to the upper boundary of the IO region obtained using the 3σ global data. These predictions are very similar for all models. This can be understood as the term in $|m_{ee}|$ proportional to m_3 only has a subdominant effect: it is not only multiplied by the small number ${s_{\theta_{13}}}^2$, but is further suppressed for IH by the small value of m_3 itself. If we neglect this term, the resulting approximation at leading-order is independent of θ_{12} up to corrections of the order $\mathcal{O}\left(\Delta m^2_{21}/\Delta m^2_{31}\right)$. It is feasible that experiments such as CUORE and KamLAND-Zen, and to a much greater extent BEXT and nEXO will be able to explore this topmost region of the IH parameter space and test these

predictions. Furthermore, distinguishing between them will be beyond their scope due to the small predicted differences and substantial experimental and theoretical uncertainties on $|m_{ee}|$. For the phase assignments $(-+)$ and $(--)$, shown on the bottom row of Fig. 2.10, we see values of $|m_{ee}|$ that are further suppressed and which exhibit more model dependence. Once again, the suppression of the m_3 term explains the similarity between the two phase assignments. The lower values compared to the $(++)$ case arise from the relative phase difference between the m_1 and m_2 terms: at leading order $|m_{ee}| = \sqrt{|\Delta m^2_{31}|}\cos^2\theta_{13}\cos^2(2\theta_{12})$ [159, 173]. This effect is evident if we compare $\mathbb{Z}_5$ and $\mathbb{Z}_3$ cases: the larger θ_{12} value of $\mathbb{Z}_3$ accounts for the more pronounced cancellation and therefore lower $|m_{ee}|$ than that of $\mathbb{Z}_5$. These predictions are beyond the reach of many of the facilities discussed so far; although KamLAND2-Zen, aims to set limits near the predictions for $\mathbb{Z}_5$ and, if capable of testing the full IO region, should be accessible to nEXO and BEXT. Although lying in a region of parameter space that is harder to explore, the greater model dependence for these phase assignments would make it easier to distinguish between models than with the $(++)$ and $(+-)$ cases. There exists a separation of around 5 meV between the predictions for $\mathbb{Z}_5$ and the other subgroups; however, it is unlikely such a resolution on $|m_{ee}|$ would be attainable in the foreseeable future.

For NO, we see quite different behaviour. In the quasi-degenerate region, the mass-squared splittings are negligible and the predictions for the IO and NO cases effectively coincide. However, in the limit of vanishing m_l the situation is very different. In this limit it is the relative phase between the m_2 and m_3 terms which dominates the magnitude of $|m_{ee}|$, which leads to larger predictions for the phase assignments $(++)$ and $(--)$, while suppressing the predictions of $(-+)$ and $(+-)$. Although exploring the NH region experimentally is beyond the scope of any planned experiment, if $0\nu\beta\beta$ decays are not observed and oscillation physics establishes that the neutrino masses are NO, it would be of paramount importance to try and test $|m_{ee}|$ values in the NH region. Due to the rich interplay between relative phases, these models make quite different predictions across this parameter space. In fact, all mixing angle patterns discussed in this paper could accommodate a value of $|m_{ee}|$

near the top of the current NH region allowed by global data. Although such an observation would add further support to any prediction of this paper which was still consistent with experimental data, to further discriminate between these models it would be necessary to provide complementary information on the absolute mass scale.

2.5 Summary

Testing the viability of leptonic flavour models is an accessible target for precision measurements from present and future neutrino oscillation experiments. In this chapter, we have presented a detailed analysis of a particular theoretical scenario: the flavour symmetry A_5 with a generalised CP symmetry breaking into residual symmetries $G_\ell = \{\mathbb{Z}_3, \mathbb{Z}_5, \mathbb{Z}_2 \times \mathbb{Z}_2\}$ and $G_\nu = \mathbb{Z}_2 \times \text{CP}$ at low energies.

We have identified the most general form of the generalised CP transformation, and studied the full group for consistent residual symmetries. Our analysis results in 10 distinct predictions as shown in Table 2.1. These depend on a single real parameter and therefore predict testable correlations between certain parameters.

We find the Majorana phases for all of our predictions are CP-conserving. These patterns can be classified by the residual symmetry in the charged-lepton mass terms: $\mathbb{Z}_3$, $\mathbb{Z}_5$ and $\mathbb{Z}_2 \times \mathbb{Z}_2$. A symmetry of $\mathbb{Z}_3$ predicts maximal θ_{23}, maximal CP violation from δ and a value of θ_{12} that lies close to the upper boundary of the 3σ global fit data. There are two distinct patterns which arise from a preserved $\mathbb{Z}_5$ residual symmetry. These share a common θ_{12} prediction which lies close to the lower boundary of the 3σ global fit data; however, one prediction has maximal θ_{23} and a maximally CP-violating value of δ whilst the other has non-maximal θ_{23} and CP-conserving values of δ. The patterns arising from a preserved subgroup $\mathbb{Z}_2 \times \mathbb{Z}_2$ also share a common θ_{12} which lies above the current 1σ region. In this case both θ_{23} predictions are non-maximal and the value of δ is CP-conserving. We discussed the phenomenology of these predictions, with an emphasis on the role played by cur-

rent and future reactor, superbeam and neutrinoless double-beta decay experiments.

The θ_{12} predictions are testable at high significance by the next generation of reactor neutrino experiments, such a JUNO and RENO-50. These experiments can be expected to differentiate between the different symmetry predictions, however, testing the precise correlations between θ_{12} and θ_{13} will most probably remain beyond the reach of any foreseen experiment.

A particularly interesting feature of the patterns found in this paper is the correlated maximality of θ_{23} and δ, and also non-maximal θ_{23} and CP-conserving values of δ. Testing such correlations is a feasible goal for current and future superbeam experiments. T2K and NOνA can be expected to collect early evidence and we have demonstrated that DUNE will be able to identify such a pattern over a significant part of the parameter space. For the CP-conserving patterns, the deviations from $\theta_{23} = \pi/4$ are expected to be measurable at 3σ by the next generation of superbeams for the preserved subgroup $\mathbb{Z}_5$, but not for $\mathbb{Z}_2 \times \mathbb{Z}_2$. However, in order to separate these models at 3σ significance, across the whole parameter space, would require a Neutrino Factory.

An appealing feature of this theoretical scenario is its ability to predict Majorana phases, and therefore, observables for neutrinoless double beta decay experiments. We have demonstrated in the case of inverted mass ordering, two of the possible Majorana phase combinations predict the discovery of neutrinoless double-beta decay at upcoming experiments. In the long-term, the exploration of the full parameter space for inverted hierarchical mass spectra could allow all of our patterns with this mass spectrum to be confirmed independently of oscillation physics.

To summarise, we find that the combination of the flavour symmetry A_5 with a generalised CP symmetry allows for a number of viable predictions to be made for the mixing angles and phases. These predictions specify parameter correlations which present good targets for currently running and upcoming experiments.

Chapter 3

Mixing Angles and Non-trivial Dirac CP Phase Predictions from A_5 with Generalised CP Symmetry

3.1 General Setup

In the previous chapter we studied the mixing angle and phase predictions from an A_5 flavour and gCP symmetry with residual symmetries $G_\ell = \{\mathbb{Z}_3, \mathbb{Z}_5, \mathbb{Z}_2 \times \mathbb{Z}_2\}$ and $G_\nu = \mathbb{Z}_2 \times \text{CP}$ [1]. In this chapter, we will focus on the predictions with less constraining residual symmetry combination $G_\ell = \mathbb{Z}_2$ and $G_\nu = \mathbb{Z}_2 \times \text{CP}$, which has been discussed in [2]. The six neutrino observables are now a function of three internal parameters so naturally there are many more predictions with more complex correlations. There are of the order 50 predictions, we shall not list them all but rather discuss some representative predictions and draw general conclusions. The method of constructing the symmetry-constrained PMNS is identical to the previous chapter but now we allow for a complex rotation in the diagonalising matrix of the charged lepton mass matrix. Consequently, the PMNS may be written

$$U_{PMNS} = R(\omega, \gamma) U_\ell^\dagger \Omega R(\theta). \tag{3.1.1}$$

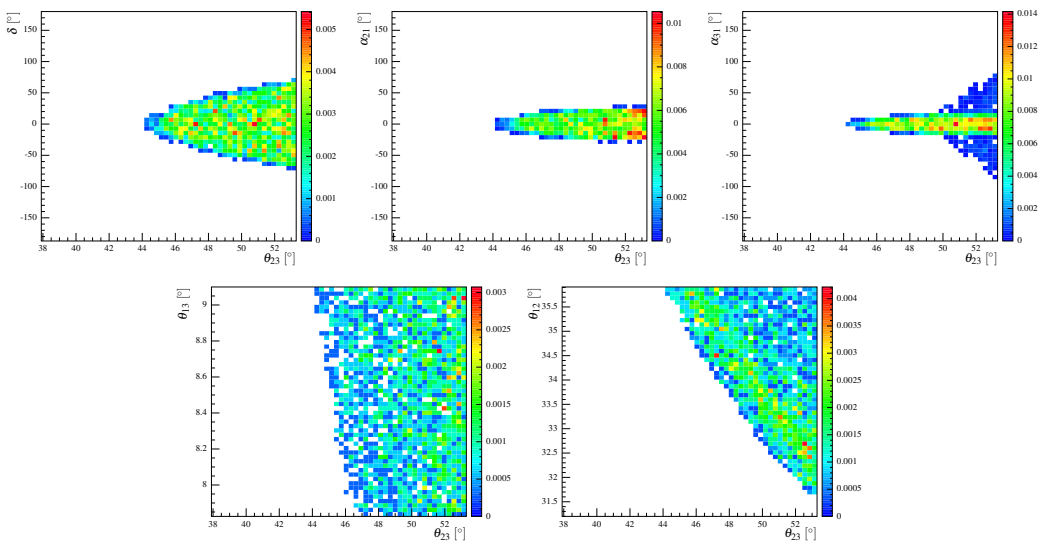

Figure 3.1: Two-dimensional histograms showing the phases and mixing angles as a function of θ_{23} for predictions that agree to a 3σ level with global fit data [23]. The colour chart shows relative frequencies of solutions where red (dark blue) represents a higher (lower) frequency.

3.2 An Example

In order to construct U_ℓ, let us first consider a $\mathbb{Z}_2$ group elements of A_5 in the three-dimensional real representation

$$\mathbb{Z}_2 = \frac{1}{2}\begin{pmatrix} -1 & \phi & \frac{-1}{\phi} \\ \phi & \frac{1}{\phi} & -1 \\ \frac{-1}{\phi} & -1 & -\phi \end{pmatrix}, \tag{3.2.2}$$

where $\phi = \frac{(1+\sqrt{5})}{2}$ is the golden ratio. A diagonalising matrix of Eq. (3.2.2) is

$$U_e \sim \begin{pmatrix} 0.665 & -0.555 & -\frac{1}{2} \\ -0.58 & -0.025 & -\frac{\phi}{2} \\ 0.461 & 0.832 & -\frac{1}{2\phi} \end{pmatrix}, \tag{3.2.3}$$

where the degenerate eigenvalues of the matrix of Eq. (3.2.2) are in the 12-plane. Therefore, $U_\ell^\dagger$ takes the form

$$U_\ell^\dagger \sim \begin{pmatrix} c_\omega & e^{i\gamma}s_\omega & 0 \\ -e^{-i\gamma}s_\omega & c_\omega & 0 \\ 0 & 0 & 1 \end{pmatrix} \begin{pmatrix} 0.665 & -0.58 & 0.461 \\ -0.555 & -0.025 & 0.832 \\ -\frac{1}{2} & -\frac{\phi}{2} & -\frac{1}{2\phi} \end{pmatrix}, \tag{3.2.4}$$

where $c_\omega \equiv \cos(\omega)$ and $s_\omega \equiv \sin(\omega)$. Not all combinations of Ω and $R(\theta)$ produce predictions within 3σ of the global fit data. However, one such combination that does is

$$U_\nu = \begin{pmatrix} 1 & 0 & 0 \\ 0 & i & 0 \\ 0 & 0 & i \end{pmatrix} \begin{pmatrix} 1 & 0 & 0 \\ 0 & c_\theta & s_\theta \\ 0 & -s_\theta & c_\theta \end{pmatrix}. \tag{3.2.5}$$

Combining Eq. (3.2.4) and Eq. (3.2.5), we construct the PMNS matrix and perform a random scan over the three continuous parameters (θ, ω, γ) in the interval $[0, \pi]$. The points of this parameter space that agree to a 3σ level with global fit data are retained and the phases are calculated. In Fig. 3.1, we plot the three leptonic phases, θ_{12} and θ_{13} as a function of θ_{23}. This PMNS matrix requires $44.2^\circ \leq \theta_{23} \leq 53.3^\circ$ and the δ phase reaches a maximal value of 69° for large values of θ_{23} (53°). A CP-conserving value of δ is possible for all viable θ_{23} and for maximal θ_{23}, $-20^\circ \leq \delta \leq 20^\circ$. From Fig. 3.1, there appears to be no preferred δ phase within the viable parameter space. The values of the Majorana phases range from $\alpha_{21} \sim \pm 25^\circ$ and $\alpha_{31} \sim \pm 80^\circ$. In the case of α_{31}, small values ($< 15^\circ$) are strongly preferred over the whole range θ_{23}. However for $\theta_{23} > 49^\circ$, α_{31} can take large values. The consequences of this prediction on neutrinoless double-beta ($0\nu\beta\beta$) decay would be interesting to explore. The magnitudes of α_{21} and $(\alpha_{31} - 2\delta)$ of this prediction can be small and this results in little cancellation between the mass terms of m_{ee}. This would imply the prediction for m_{ee} can be close to the CP-conserving upper boundary of the inverted ordering region, which experiments hope to explore. Therefore, it would be feasible to use $0\nu\beta\beta$ decay to study this particular prediction.

As the 3σ range of θ_{13} is highly constrained compared with the other mixing angles, there is little discernible structure in the θ_{13}-θ_{23} correlation, however the θ_{12}-θ_{23} dependence has greater predictivity. For near-maximal values of θ_{23}, θ_{12} is predicted to be at the very upper boundary of its 3σ range ($\sim 36^\circ$). For larger values of θ_{23}, close to the upper 3σ boundary, the range of predicted θ_{12} increases (31.6°-35.9°). Although for most viable values of θ_{23} there are a range of θ_{12} predictions, the density of solutions clusters near the boundary of the viable region of the

δ-θ_{23} parameter space.

3.3 Lower Octant Predictions

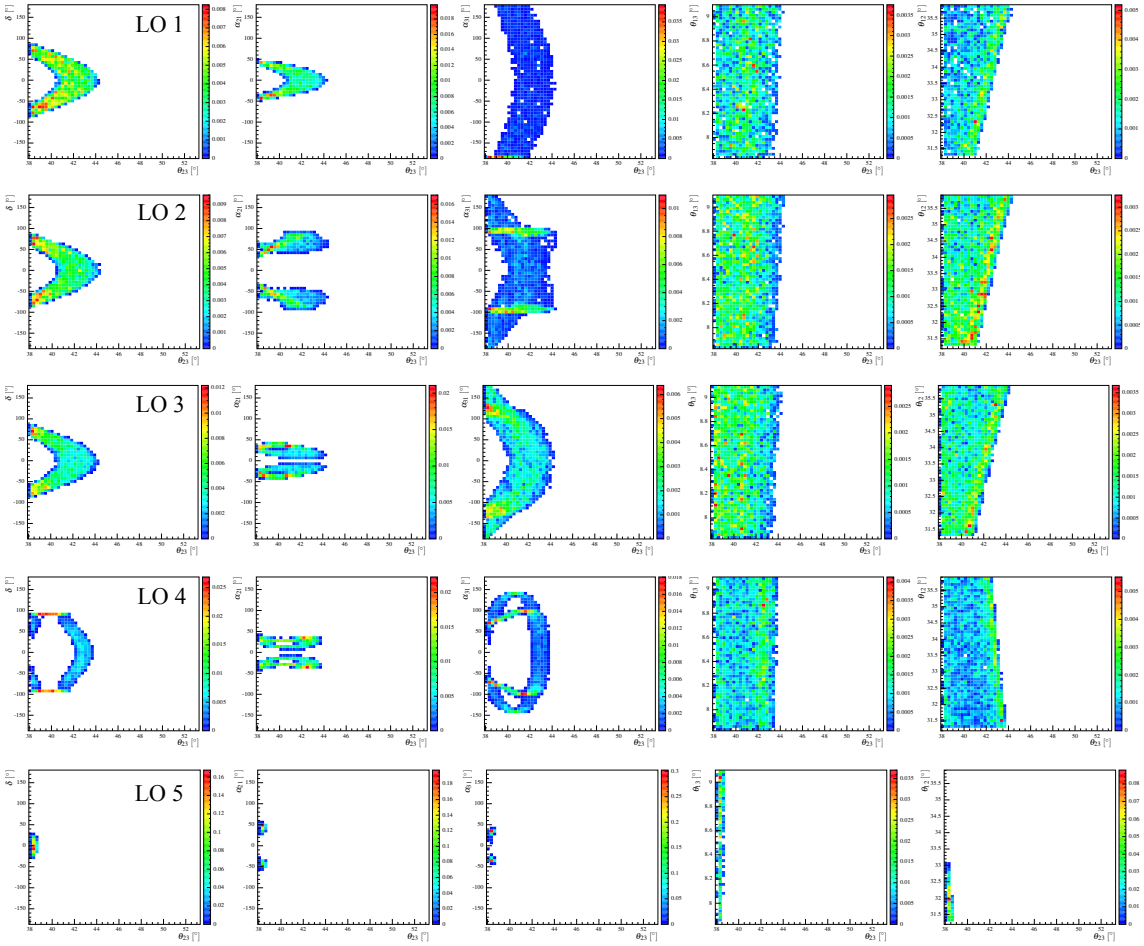

Figure 3.2: Two-dimensional histograms showing the phases and mixing angles as a function of θ_{23} for predictions that agree to a 3σ level with global fit data[23]. The colour chart shows relative frequencies of solutions where red (dark blue) represents a higher (lower) frequency. Each prediction is labelled lower octant (LO) 1-5.

The chosen lower octant predictions are presented in Fig. 3.2 and it can be seen that the possible range of θ_{23} values differs between the various cases: LO 1-3 have viable predictions for the entire lower octant (38.8°-45°) whilst LO 4 is somewhat more constrained as θ_{23} spans only 3° (40°-43°). LO 5 is the most highly constrained

and therefore most easily testable with $38° \leq \theta_{23} \leq 38.8°$. LO 1-3 share the same δ-θ_{23} correlation, which attains a maximal δ (85°) for θ_{23} close to the lower 3σ allowed region. The CP-conserving values of δ requires $40.6° \leq \theta_{23} \leq 44.2°$. In the case of LO4, although the δ-θ_{23} correlation structure is similar to that of LO 1-3, the maximal value of δ is slightly greater, reaching 90°, and solutions tend to cluster at these points. In contrast to LO 1-4, the δ value of LO 5 is close to zero. However it reaches a maximum of 26°.

LO 1-3 have a common θ_{12}-θ_{23} dependence: for values of θ_{23} close to the lower 3σ boundary, all values of θ_{12} are allowed. For near-maximal θ_{23}, the θ_{12} prediction becomes increasingly constrained: for example, for the current best fit value of θ_{23} (42.3°) [23], only values of $33.5° \leq \theta_{12} \leq 35.91°$ are predicted. In the case of LO 4, for $38.8° \leq \theta_{23} \leq 42.3°$, the predicted θ_{12} spans the 3σ range of θ_{12}. Similarly to LO 1-3, the range of predicted θ_{12} becomes more constrained for near-maximal θ_{23} (smaller θ_{12} is preferred). Using the θ_{12}-θ_{23} correlation as a means of differentiating between LO 1-3 and LO 4 would be problematic in the regions $\theta_{23} \leq 41°$, as the predictions are indistinguishable. As the viable parameter space of LO 5 is significantly smaller than that of the previous four predictions, there is no discernible correlation between θ_{12} and θ_{23}; in this regard its most discriminating feature is that θ_{12} can only range between 31°-33°.

The Majorana phases are the only observables that differ amongst LO 1-3. It is worth noting that LO 1 is the only lower octant prediction of this sample that has a CP-conserving value of α_{21}. It would be an interesting future study to investigate the effect that this would have on $0\nu\beta\beta$ decay and feasibility of discriminating between predictions.

In summary, there are several general features which are shared amongst these cases; the most striking of these is the prediction of non-trivial leptonic phases. Moreover, the δ and α_{21} phases are bound between $\pm 90°$. If δ is measured to be maximally CP-violating, as hinted at by T2K [174], the only remaining viable

prediction is LO 4. Some predictions cannot be discriminated between by using δ and θ_{12} alone and access to the Majorana phases is necessary. Moreover, the ability to discriminate between LO 4 and LO 1-3 is highly dependent upon the value of θ_{23}: in the scenario of maximal or near-maximal θ_{23}, this is possible. Of the cases presented, LO 5 is the most easily testable as its θ_{23} values are highly constrained and lie at the extreme lower boundary of the 3σ range. The combinations of matrices used to find these predictions are listed in Table 3.1.

Result	U_{PMNS}
LO 1	$p_4 R_{23} C U_1{}^{\dagger} \Omega_{12} R_{12} p_2$
LO 2	$p_2 R_{13} C U_2{}^{\dagger} \Omega_{12} R_{13} p_3$
LO 3	$p_1 R_{12} C U_3{}^{\dagger} \Omega_{12} R_{23} p_4$
LO 4	$p_2 R_{13} C U_2{}^{\dagger} \Omega_{12} R_{13} p_1$
LO 5	$p_4 R_{23} C U_1{}^{\dagger} \Omega_{12} R_{13} p_3$

Table 3.1: PMNS matrices corresponding to lower octant predictions as shown in Fig. 3.2

3.4 Upper Octant Predictions

Similarly to the lower octant results, we have chosen three cases (UO -1-3) presented in Fig. 3.3, for which the mixing angle and δ phase correlations are indistinguishable and only the Majorana phases differ. UO 1-3 share the feature of viable predictions over the entire upper octant (45°-53.3°). The θ_{23} allowed range UO 4 is slightly more constrained with $46.3° \leq \theta_{23} \leq 53.3°$. UO 5 is an analogous case to LO 5, where its θ_{23} prediction span is small and occurs at the very upper limit of the 3σ boundary, $51.2° \leq \theta_{23} \leq 53.3°$.

Maximal CP violation is possible in UO 1-3 and UO 5, however the δ-θ_{23} correlations structure differs between cases. UO 1-3 share the same pattern where the maximal δ value (90°) occurs for large θ_{23} values and CP-conserving values of δ are associated with $45.6° \leq \theta_{23} \leq 48.4°$. The δ correlation of UO 5 differs significantly from UO 1-3 as CP-conserving values of δ are not predicted and maximal δ favoured.

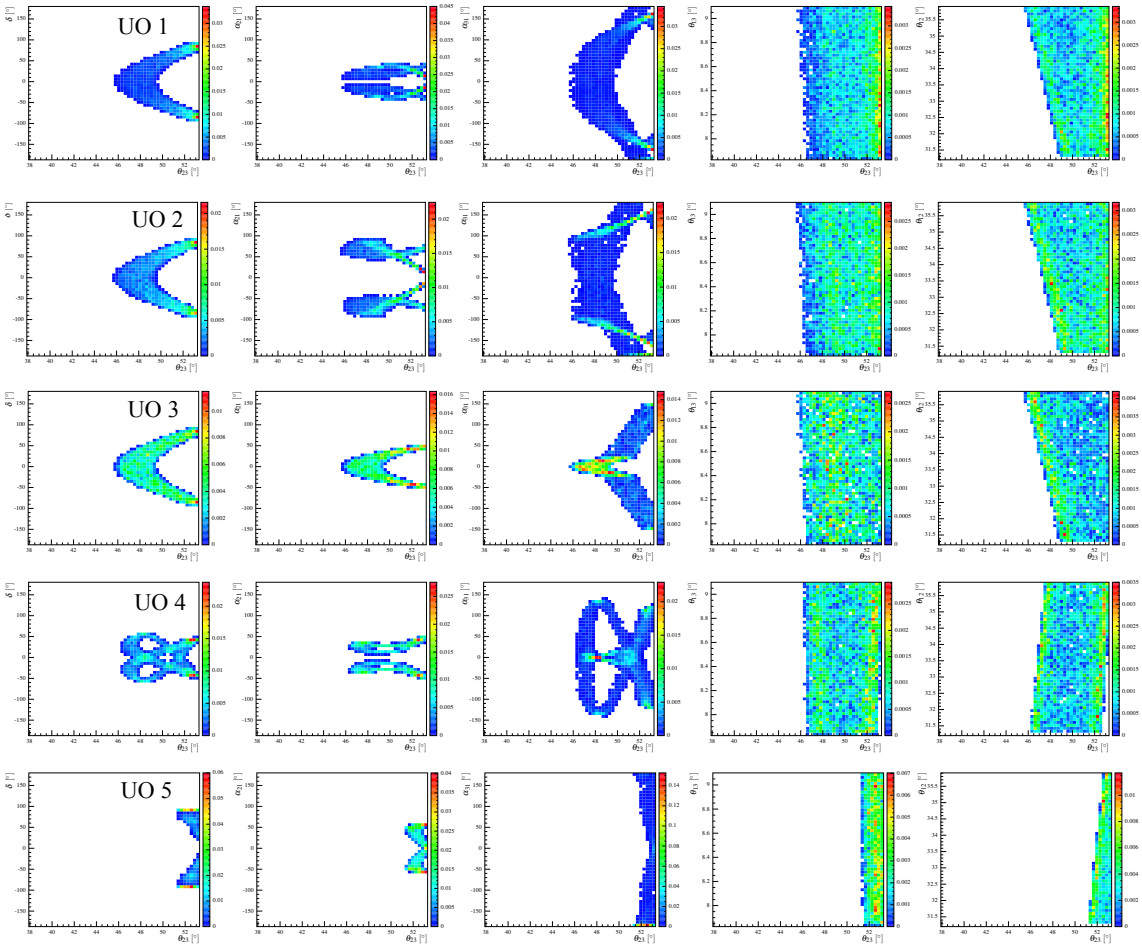

Figure 3.3: Two-dimensional histograms showing the phases and mixing angles as a function of θ_{23} for predictions that agree to a 3σ level with global fit data[23]. The colour chart shows relative frequencies of solutions where red (dark blue) represents a higher (lower) frequency. Each prediction is labelled upper octant (UO) 1-5.

In the case of UO 4, the correlation structures are particularly distinctive and unlike the previously discussed cases, the maximal δ value (55°) is much smaller. A unique aspect of LO 4 is that there are two distinct regions of θ_{23} where CP-conserving values of δ can occur: $47.4° \leq \theta_{23} \leq 49.2°$ and $51° \leq \theta_{23} \leq 52°$.

With regards to the θ_{12}-θ_{23} correlation of UO 1-3, all regions of the 3σ range of θ_{12} are allowed for $49° \leq \theta_{23} \leq 53.3°$. Larger values of θ_{12} are favoured for near-maximal θ_{23}. It is worth noting this dependence (large θ_{12} associated with near-maximal val-

ues of θ_{23}) is similar to the lower octant predictions LO 1-3. For $49^\circ \leq \theta_{23} \leq 52^\circ$, the θ_{12} predictions of UO 4 are indistinguishable from UO 1-3. In spite of this, for certain θ_{23}, these cases can be differentiated. For example, $\theta_{23} > 52.6^\circ$ UO 4 predicts large-valued θ_{12} ($\sim 36^\circ$) whereas the θ_{12} of UO 1-3 can attain any value in the 3σ range. Moreover, at near-maximal values of θ_{23} (46°), UO 4 predicts smaller θ_{12} values (31.3°) than UO 1-3. Discrimination between UO 1-3 and UO 5 is not possible using θ_{12}-θ_{23} correlations (as there is complete overlap in the predictions) and therefore a combination of θ_{23} and δ measurements in conjunction with $0\nu\beta\beta$ decay study would be required to disentangle these predictions.

In summary, δ and α_{21} are bounded between $\pm 90^\circ$. Moreover, the ability to discriminate between predictions is often dependent upon the value of θ_{23} and in certain cases predictions are only differentiable with knowledge of the Majorana phases. As before, the combinations of matrices used to find these predictions are listed in Table 3.2.

Result	U_{PMNS}
UO 1	$p_1 R_{13} C U_2^\dagger \Omega_{12} R_{13} p_1$
UO 2	$p_1 R_{13} C U_4^\dagger \Omega_{12} R_{13} p_3$
UO 3	$p_4 R_{12} C U_3^\dagger \Omega_{12} R_{23} p_4$
UO 4	$p_3 R_{23} C U_5^\dagger \Omega_{12} R_{13} p_3$
UO 5	$p_3 R_{23} C U_1^\dagger \Omega_{12} R_{12} p_2$

Table 3.2: PMNS matrices corresponding to upper octant predictions as shown in Fig. 3.3

3.5 Predictions Spanning Both Octants

We have chosen five representative cases that span both the upper and lower octants of θ_{23}. The predicted regions of θ_{23} vary amongst these cases: BO 1 has the greatest viable range, which fully covers the 3σ region of θ_{23}. BO 2 and BO 5 also have a wide range of θ_{23}: $38.2^\circ \leq \theta_{23} \leq 49^\circ$ and $38.2^\circ \leq \theta_{23} \leq 51^\circ$ respectively. BO 3 and BO 4 have the smallest viable range of θ_{23} with $44.3^\circ \leq \theta_{23} \leq 53.3^\circ$ and

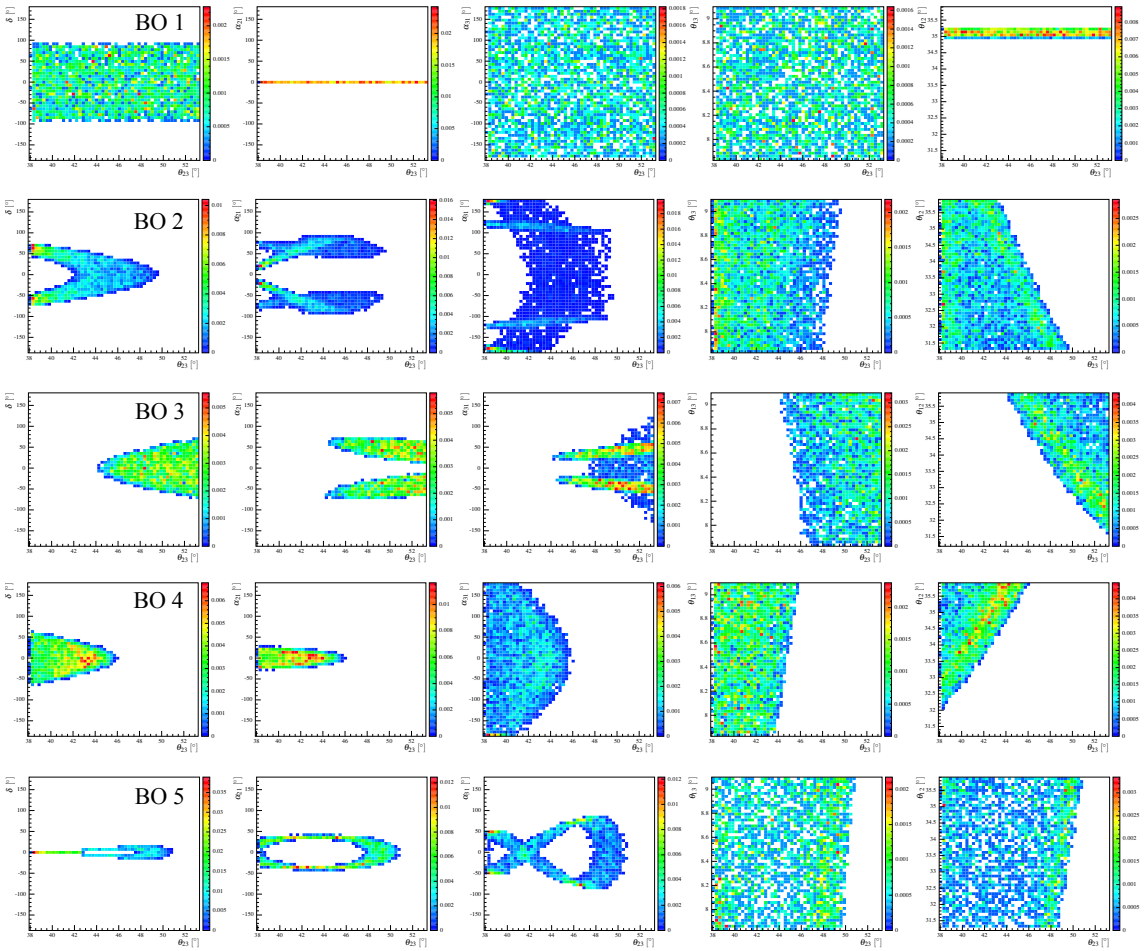

Figure 3.4: Two-dimensional histograms showing the phases and mixing angles as a function of θ_{23} for predictions agree to a 3σ level with global fit data[23]. The colour chart shows relative frequencies of solutions where red (dark blue) represents a higher (lower) frequency. Each prediction is labelled both octant (BO) 1-5.

$38.2° \leq \theta_{23} \leq 45.9°$ respectively.

There is little structure in the δ-θ_{23} correlation of BO 1: δ can attain any value in the range $\pm 90°$ and there is no dependence on θ_{23}. BO 2 has a similar correlation structure to the lower octant predictions: the maximal δ value (73°) is correlated to smaller θ_{23} values and CP-conserving δ spans $42° \leq \theta_{23} \leq 48.2°$. BO 3 and BO 4 have comparable δ-θ_{23} dependence; the maximal δ, 69° and 61° respectively, occurs at the extreme upper and lower 3σ limit of θ_{23}. In comparison with BO 1-4, BO

5 has a highly constrained δ with a maximal value of 14° for $49^\circ \leq \theta_{23} \leq 50^\circ$. In the scenario δ is maximally CP-violating, the only viable prediction of this set is BO 1. Interestingly, in spite of BO 1 lacking predictivity in regards to parameters δ, α_{31} and θ_{13}, its α_{21} and θ_{12} predictions attain very specific values ($\alpha_{21} = 0^\circ$ and $34.8^\circ \leq \theta_{12} \leq 35.2^\circ$). BO 1 would be of particular interest in $0\nu\beta\beta$ decay studies as it has a single α_{21} value and exceptionally narrow θ_{12} range.

The θ_{12}-θ_{23} dependence of BO 3 and BO 4 are similar: for near-maximal θ_{23}, there is a very limited range of θ_{12} values ($\sim 36^\circ$) and for θ_{23} close to the upper or lower 3σ boundary, the possible θ_{12} become less constrained. This appears to be a common theme of many of the predictions: near-maximal θ_{23} have very specific θ_{12} predictions. In the case of BO 2, θ_{12} can attain any value in the 3σ range for $\theta_{23} \leq 43.5^\circ$ and for larger θ_{23}, smaller values of θ_{12} are preferable. There is significant overlap in θ_{12} predictions for BO 2 and BO 5 and only in the scenario, $\theta_{23} \geq 47^\circ$ do their predictions differ. A special feature of BO 5, akin to BO 1, is that certain observables are more constrained than others; for instance predictions of θ_{13} and θ_{12} range widely whereas the leptonic phases are more highly constrained ($|\delta| \leq 14^\circ$, $|\alpha_{21}| \leq 40^\circ$, $|\alpha_{31}| \leq 90^\circ$).

In summary, δ and α_{21} can only attain values $\pm 90^\circ$. Furthermore, there are several examples (BO 1 and BO 5), in which certain observables are highly unconstrained but in balance other parameters can only attain very specific values. Therefore in spite of a lack of predictivity in certain observables, these cases still remain testable by upcoming long and medium base-line experiments. As before, the combinations of matrices used to find these predictions are listed in Table 3.3.

Result	U_{PMNS}
BO 1	$p_1 R_{23} C U_5{}^\dagger \Omega_{12} R_{12} p_4$
BO 2	$p_1 R_{12} C U_6{}^\dagger \Omega_{13} R_{12} p_4$
BO 3	$p_4 R_{23} C U_1{}^\dagger \Omega_{23} R_{12} p_6$
BO 4	$p_4 R_{12} C U_7{}^\dagger \Omega_{23} R_{23} p_1$
BO 5	$p_3 R_{23} C U_5{}^\dagger \Omega_{13} R_{13} p_3$

Table 3.3: PMNS matrices corresponding both octant predictions as shown in Fig. 3.4

3.6 Summary

In this chapter, we studied the correlations of leptonic observables that result from a flavour symmetry, A_5, combined with gCP breaking into residual symmetries $G_\nu = \mathbb{Z}_2 \times \text{CP}$ and $G_\ell = \mathbb{Z}_2$. This combination of residual symmetries introduces three continuous parameters and unsurprisingly, we obtain a wider range of predictions than in studies that use only one input parameter. The flavour symmetry studies that implement one input parameter and are of low order such as A_4[116], S_4[108, 117] and A_5[1, 122, 123] share common predictions such as $|\sin\delta| = 1$, $|\sin\alpha_{21}| = |\sin\alpha_{31}| = 0$ and maximally CP-violating δ associated with maximal θ_{23}. We find the addition of two continuous parameters allows for more possibilities in correlations and predictions of non-trivial leptonic phases differing from 0, $\frac{\pi}{2}$, π and $\frac{3\pi}{2}$. Using a number of example cases we have shown that certain predictions are indistinguishable using oscillation parameters δ, θ_{12} and θ_{23} alone and therefore input from $0\nu\beta\beta$ decay experiments is necessary. We find that, in general, the ability to discriminate between predictions is improved for near-maximal θ_{23} and that even in specific cases in which there is no predictivity for one parameter (e.g. BO 1 and BO 5), other leptonic observables may be highly constrained and provide testable predictions. In spite of a greater number of predictions, all of our cases share the feature of δ and α_{21} phases being bounded by $\pm 90°$, the former of the two which is testable by long base-line oscillation experiments.

In conclusion, we find that relaxing the possible combinations of low-energy residual symmetries permits a wider range of predictions with more complex correlations between leptonic observables which have the potential to be tested at upcoming neutrino oscillation and $0\nu\beta\beta$ experiments.

Chapter 4

Flavour Cosmology: Connecting Flavour Symmetries and the Baryon Asymmetry

In spite of its great success, the SM cannot explain three experimental observations: small but non-zero neutrino masses, the cosmological origin of the matter anti-matter asymmetry and the origin and composition of dark matter (DM). In this chapter, we focus on a possible connection between the baryon asymmetry of the Universe (BAU), low-energy neutrino observables and the flavour structure of the lepton sector as proposed in [3]. This work is not the only attempt to explore the cosmological dynamics associated with flavour models. In [175], the authors explored the possibility that varying Yukawa couplings, whose structure is dictated by the Frogatt-Nielsen mechanism, alter the nature of the electroweak phase transition (EWPT) to be first order such that electroweak baryogenesis can proceed. In the context of high-scale thermal leptogenesis, there have been a number of works [176, 177] that investigate the impact of flavour and generalised CP symmetries on the BAU. In these works, the symmetries constrain the structure of the sterile neutrino Yukawa matrix and therefore the baryon asymmetry produced from the sterile decays. In addition, flavour models with extended Higgs sectors [178] and radiative neutrino mass generation [179] have been examined in the context of leptogenesis. However, [3] introduces a completely new mechanism of leptogenesis and offers

a fresh perspective on the possible connection between flavour models and the BAU.

The outline of this chapter is the following: first, we discuss two methods of measuring the baryon-to-photon ratio in Section 4.1 and then in Section 4.2 we review the necessary conditions any dynamical mechanism are required to fulfil in order to generate the BAU. Second, in order to compare and contrast our mechanism with existing well-established scenarios, we review high-scale thermal leptogenesis and electroweak baryogenesis in Section 4.3.1 and Section 4.3.2 respectively. Finally, in Section 4.4 we motivate and discuss our calculational tool, namely the Closed-Time Path formalism, and in Section 4.5 we introduce our mechanism of leptogenesis.

4.1 Measuring the Baryon Asymmetry

4.1.1 Big Bang Nucleosynthesis

Big Bang Nucleosynthesis (BBN) refers to the synthesis of light nuclei such as deuterium (D), helium (^{3}He, ^{4}He) and lithium (^{7}Li). This process began (ended) several seconds (minutes) after the Big Bang [181] (from $T \sim 1$ MeV - 80 keV). During this epoch, protons and neutrons moved freely of each other as the formation of light nuclei was inhibited by high-energy photons in the thermal plasma. Heavier elements, crucial to create and sustain life, were produced later via stellar synthesis. The nuclear processes of BBN dominantly produced ^{4}He, with a mass fraction $Y_p \sim 0.25$ with respect to hydrogen [182] [1]. While for other nuclei ^{4}He/H $\sim$ D/H $\sim 10^{-5}$ and ^{7}Li/H $\sim 10^{-7}$ as illustrated in Fig. 4.1. The abundance of these light elements is crucially dependent on the baryon-to-photon ratio ($\eta \equiv n_b/n_\gamma \sim 10^{-10}$). From precise measurements of the light elements, in particular deuterium as there are no known astrophysical sources of this element, the baryon-to-photon ratio is [182]

$$5.8 \times 10^{-10} \leq \eta_{BBN} \leq 6.6 \times 10^{-10} \quad (95\%\text{C.L.}). \tag{4.1.1}$$

Fig. 4.1 shows that BBN and CMB measurements are consistent with each other.

[1] For a species X_A with mass and atomic number (A,Z) the mass fraction is defined to be $X_A := \frac{An_A}{n_p+n_N+\sum_i A_i n_i}$ where $\eta_B \propto X_A$.

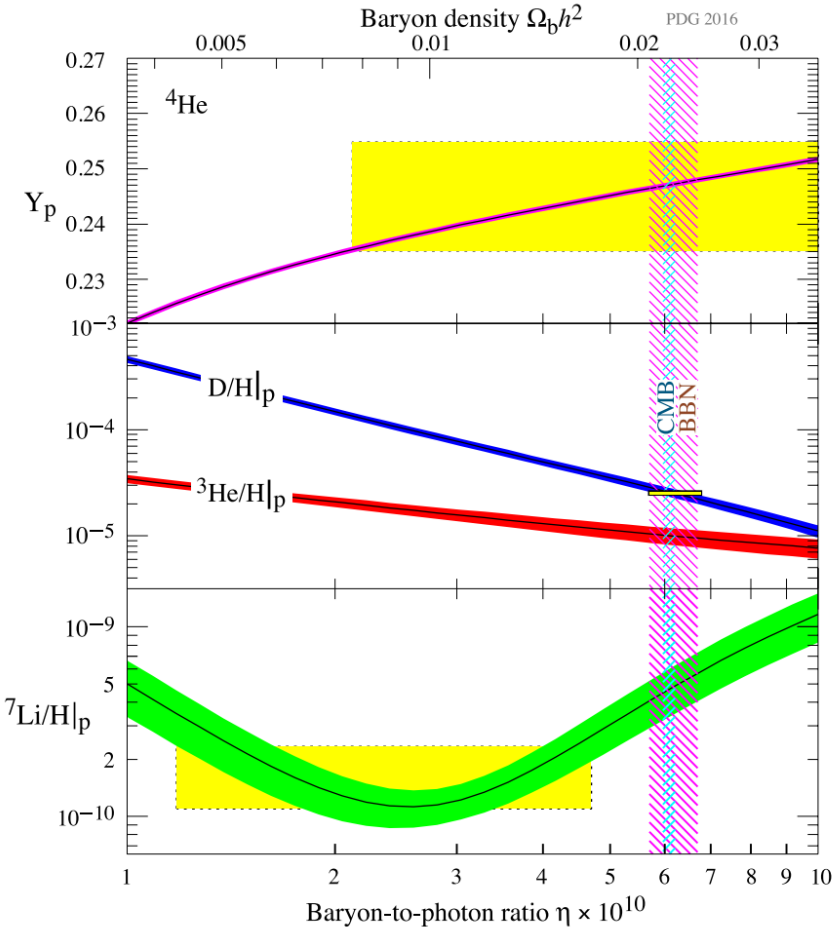

Figure 4.1: The primordial abundances of ^{4}He, D, ^{4}He and ^{7}Li as predicted by the Standard calculations of Big Bang Nucleosynthesis. The thickness of the bands indicate the 95% C.L. range [180]. The vertical pink (blue) band shows the measured cosmic baryon density from BBN (CMB) at 95% C.L.

4.1.2 Cosmic Microwave Background Radiation

There is a second, complementary method of determining the baryon-to-photon ratio using cosmic microwave background (CMB) data. At low temperatures, the usual matter in the Universe was comprised mainly of a neutral hydrogen gas. At earlier times, the temperature was sufficiently high that electrons could move freely of nuclei and the Universe was permeated in a baryon-electron-photon plasma. During this epoch, photons actively scattered off electrons in the plasma. The transition from plasma to neutral gas is known as *recombination* and occurred approximately 370,000 years after the Big Bang ($T \sim 0.3$ eV). During this process, the photons

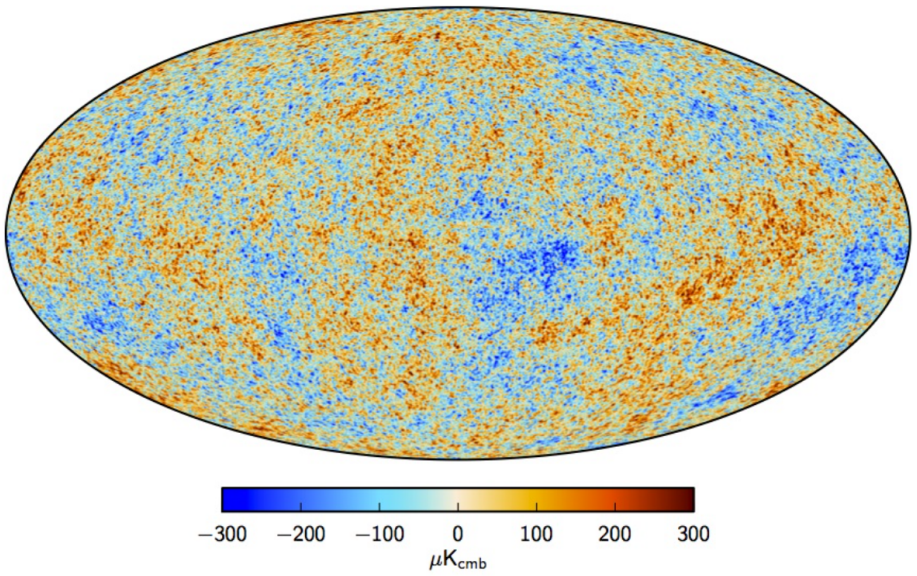

Figure 4.2: A map of the temperature fluctuations over the entire sky as measured by Planck Collaboration [183]. The red (blue) colour indicates the over (under) density.

came out of thermal equilibrium with the plasma and subsequently travelled from the last scattering surface and now constitute the CMB.

An important prediction of the hot big bang model is precisely that the photons were in thermal equilibrium with the electrons in the plasma and therefore the photons should have a blackbody spectrum with a corresponding temperature of $T_\gamma \sim 2.7$ K. This was confirmed with great precision by the COBE satellite in 1992 [185]. They found the CMB to be remarkably uniform and this demonstrates the isotropic and homogeneous nature of the Early Universe on large scales. In spite of the general uniformity of the CMB, there are small temperature fluctuations around T_γ. These anisotrophies occur at a level of 10^{-5} over a wide angular range and these density perturbations are thought to have originated from inflation.

The temperature fluctuations of the CMB ($\Delta T/\overline{T} = (T - \overline{T})/\overline{T}$) form a two-dimensional field, parametrised by angular coordinates θ and ϕ, projected onto the surface of a sphere. For this reason, the temperature distribution of the CMB can

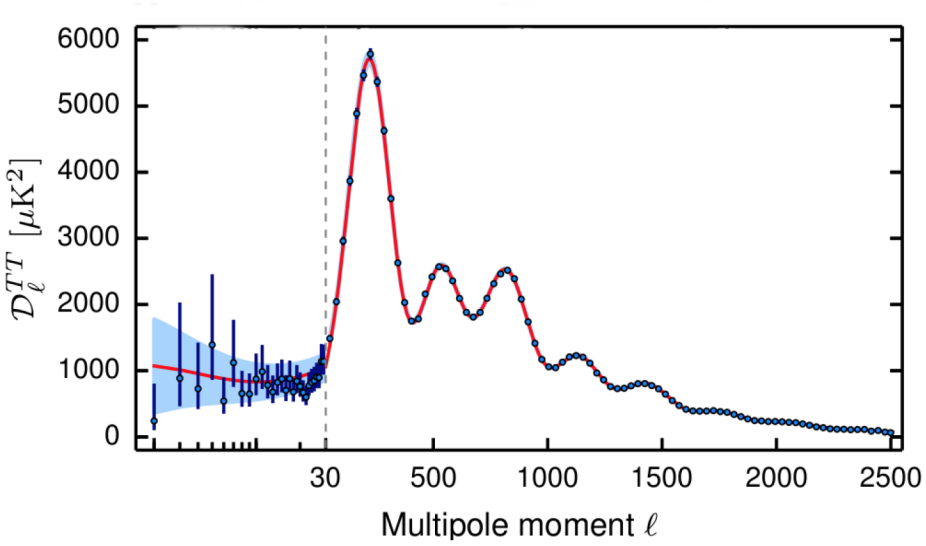

Figure 4.3: The angular power spectrum of the CMB as measured by Planck as shown by the dots (band show $\pm 1\sigma$) error bars [184]. The red line is the best-fit prediction from Λ-CDM and the light-blue shaded region shows the theoretical uncertainty from the cosmic variance.

be characterised by spherical harmonics $Y_{lm}(\theta, \phi)$

$$\frac{\Delta T(\theta,\phi)}{\overline{T}} = \sum_{l=0}^{\infty} \sum_{m=-l}^{l} a_{lm} Y_{lm}(\theta,\phi), \tag{4.1.2}$$

where l is the multipole moment or the total angular wavenumber, m is the azimuthal wavenumber and a_{lm} are the associated amplitudes. The angular size and the multipole moment are related via $\theta \sim \pi/l$. The angular power spectrum is defined to be

$$C_l = \frac{1}{(2l+1)} \sum_{m=-l}^{l} |a_{lm}|^2, \tag{4.1.3}$$

and the power spectrum is related to to the angular power spectrum in the following manner

$$D_l = \left\langle \left(\frac{\Delta T}{\overline{T}} \right)^2 \right\rangle_l = \frac{l(l+1)}{2\pi} C_l. \tag{4.1.4}$$

The power spectrum as a function of the multipole moment is shown in Fig. 4.3. The structure of the acoustic peaks of the power spectrum are affected by the baryonic density and therefore the baryon-to-photon ratio. As illustrated in Fig. 4.4, increasing the baryonic density has the effect of increasing the difference in the amplitude

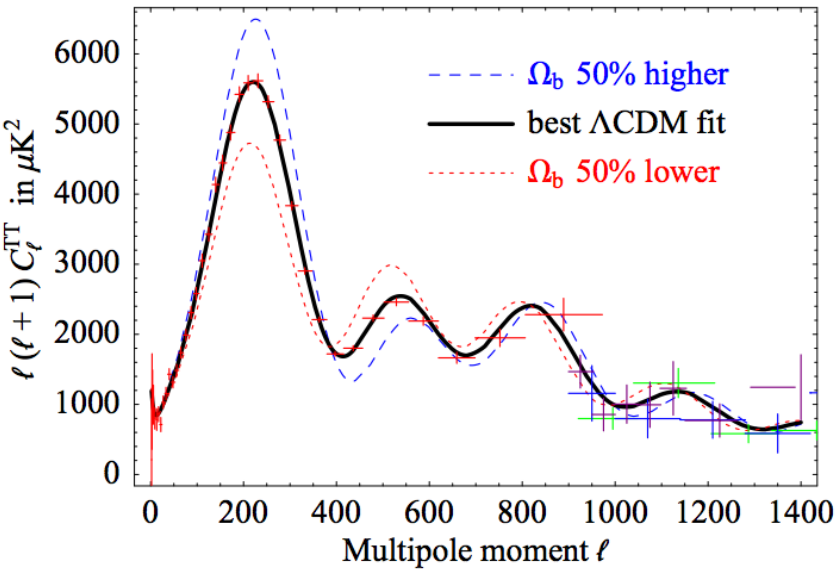

Figure 4.4: The sensitivity of the angular power spectrum to the baryonic density Ω_b, figure taken from [186].

of the first and second acoustic peaks. As a consequence, the accurate measurement CMB power spectrum is used to determine the baryon-to-photon ratio. Using Planck data from 2015 [184], this quantity is measured to be

$$6.0 \times 10^{-10} \leq \eta_{BBN} \leq 6.18 \times 10^{-10} \quad (95\%\text{C.L.}). \tag{4.1.5}$$

4.2 Sakharov's Conditions

In 1967, Andrei Sakharov the prominent physicist and Nobel Peace prize recipient, proposed his three famous conditions [187]. These are the conditions that any dynamical mechanism, with the purpose of generating the observed BAU, must fulfil[2].

- **Baryon Number Violation**: necessary to evolve from a baryo-symmetric to a baryo-asymmetric Universe.

[2]It is important to note Sakharov's Conditions implicitly assume CPT-invariance. It is possible to generate a baryon asymmetry without satisfying these condition if CPT is violated [188].

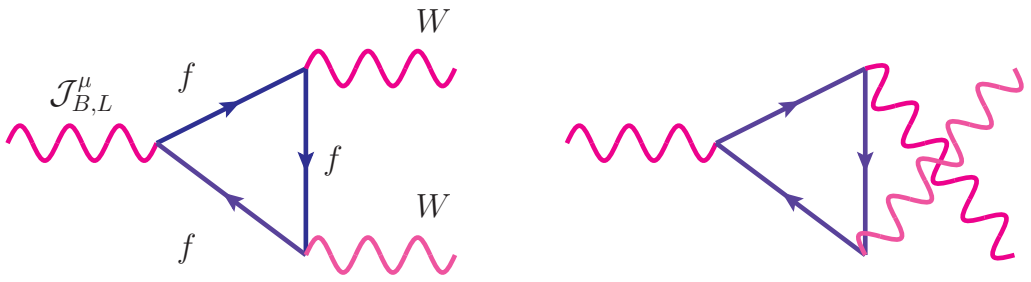

Figure 4.5: The triangle diagrams which give rise to the axial anomaly.

- **C and CP Violation**: if C and CP were conserved then B-number violating processes would proceed at the same rate as anti B-number violating processes with no net excess of baryons generated.

- **Departure from Thermal Equilibrium**: in thermal equilibrium Boltzmann distributions indicate that there should be equal amounts of matter and anti-matter. Therefore, out-of-equilibrium dynamics are essential for generating a baryon asymmetry.

The Standard Model contains the three above ingredients but not in sufficient quantities. We shall further elucidate this point in Sections. (4.2.1), (4.2.2) and (4.2.3)

4.2.1 B-Number Violation

Baryon (B) and lepton (L) number are *accidental* symmetries of the SM. This means they are conserved to all orders in perturbation theory but are violated via *non-perturbative* processes. We may defined B and L number by their charges in the conventional manner

$$Q_B = \int d^3x \mathcal{J}^0_B \quad \text{and} \quad Q_L = \int d^3x \mathcal{J}^0_L, \tag{4.2.6}$$

where

$$\mathcal{J}^{\mu}_B = \frac{1}{3}\left(\overline{q}\gamma^{\mu}q + \overline{u}_R\gamma^{\mu}u_R + \overline{d}_R\gamma^{\mu}d_R\right) \quad \text{and} \quad \mathcal{J}^{\mu}_L = \ell\gamma^{\mu}\ell + e_R\gamma^{\mu}e_R, \tag{4.2.7}$$

and

$$q = \begin{pmatrix} u_L \\ d_L \end{pmatrix} \quad \text{and} \quad \ell = \begin{pmatrix} \nu_L \\ e_L \end{pmatrix}. \tag{4.2.8}$$

As mentioned before, Q_B and Q_L are conserved in any Feynman diagram. However, chiral processes involving the W-boson allow for the possibility of the axial anomaly shown in Fig. 4.5 and manifest in the non-conservation of the baryonic and leptonic current

$$\partial_\mu \mathcal{J}^\mu_{B/L} = \frac{g^2}{32\pi^2} F^i_{\mu\nu} \tilde{F_i^{\mu\nu}}, \quad \text{where} \quad F^i_{\mu\nu} = \partial_\mu W^i_\nu - \partial_\nu W^i_\mu + g\epsilon^{ijk} W^j_\mu W^k_\nu, \tag{4.2.9}$$

where g is the $\mathrm{SU}(2)_W$ gauge coupling and the dual of the field strength tensor is $\widetilde{F_i^{\mu\nu}} = 1/2\epsilon^{\mu\nu\lambda\rho} F_{\lambda\rho i}$. Simplifying notation, we may write $\partial_\mu G^\mu = F^i_{\mu\nu} \widetilde{F_i^{\mu\nu}}$ and thus the baryonic and leptonic currents are given by [3]

$$\partial_\mu \mathcal{J}^\mu_L = \partial_\mu \mathcal{J}^\mu_B = \frac{g^2}{32\pi^2} \partial_\mu G^\mu, \tag{4.2.10}$$

and are non-vanishing thereby implying the violation of B and L number. To investigate how the baryonic and leptonic charges change in time, Eq. (4.2.10) may be integrated over such that

$$\Delta Q_L = \Delta Q_B = \frac{g^2}{32\pi^2} \int d^4x F^i_{\mu\nu} \widetilde{F_i^{\mu\nu}}, \quad F_{\mu\nu} = \frac{g^2}{32\pi^2} \int d^4x \partial_\nu K^\nu = \Delta K, \tag{4.2.11}$$

where K^ν is the Chern-Simons (CS) current which has been discussed in the Appendix. It is important to note, in perturbation theory the integration over the divergence of the current vanishes and therefore baryon and lepton number are conserved symmetries. However, if the gauge-field fluctuations are sizeable $\sim 1/g$ (i.e. non-perturbative) then the integration does not necessarily yield zero.

Instantons

Instanton solutions interpolate between the topologically disconnected vacua of the Yang-Mills (YM) theory [191, 192] (see Fig. 4.6) and in this example will correspond to B or L-number violating processes. Tunnelling between these vacua (the

[3] This is a standard calculation and is shown explicitly in [189, 190]. In general the anomaly may be calculated perturbatively by evaluating the diagram in Fig. 4.5 or via the path integral formalism. Using the latter approach (otherwise known as the Fujikawa method), the anomaly, or non-vanishing divergence of the current, arises from the path-integral measure transforming differently than the integrand itself.

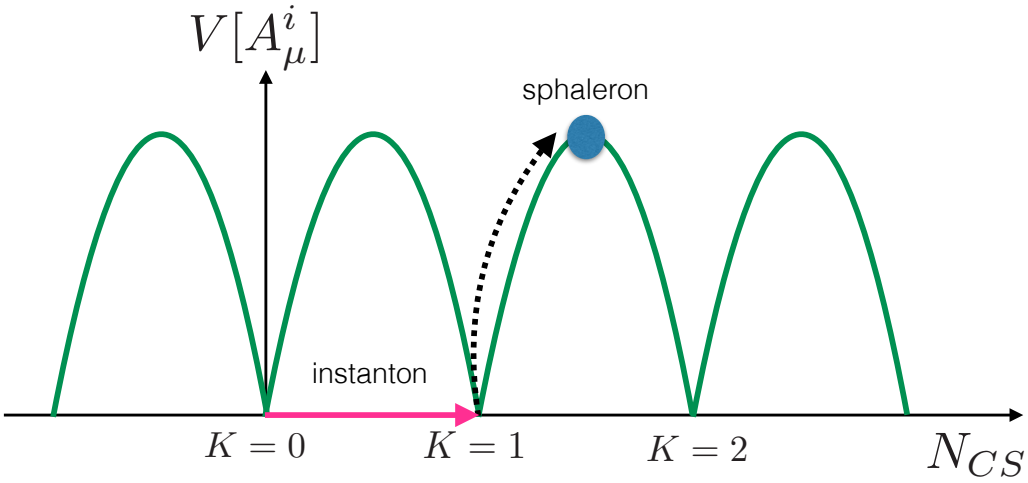

Figure 4.6: Schematic diagram of $V[A^i_\mu]$ as a function of the Chern-Simons number, N_{CS}.

instanton solution) is suppressed by the instanton suppression factor [193]

$$\mathcal{A}_{\not{\varnothing}} \propto \exp\left[-\frac{2\pi}{\alpha_2(v)}\right] \tag{4.2.12}$$

where $\alpha_2(v)$ associated to the weak force is experimentally determined to be

$$\alpha_2 = \frac{g^2}{4\pi} \sim \frac{1}{31}. \tag{4.2.13}$$

As g is small, the rate of tunnelling is heavily suppressed due to the high barrier between the vacua and is approximated as

$$\Gamma_{\not{\varnothing}} \propto \exp\left[-\frac{4\pi}{\alpha_2(v)}\right] \sim 10^{-170}. \tag{4.2.14}$$

Sphalerons

It is possible thermal effects may reduce the large suppression factor. In the Early Universe, the temperatures are sufficiently high such that thermal fluctuations are of the same order as the height of the barrier in Fig. 4.6. The top of the barrier or potential is also an extremum of the YM-field and such a field configuration corresponds to a static solution to the classical equations of motion. Moreover, these solutions are unstable, have non-integer winding number (indeed they have half-integer winding number) and are referred to as *sphalerons*. Sphalerons are thermally

produced and correspond to the movement of the system from one vacua to another via the saddle point between the two vacua. The sphaleron rates are computed using statistical mechanics and their rates are proportional to a Boltzmann factor [4]

$$\Gamma_{\not{B}} \propto \exp\left[-\frac{M_{\rm sph}}{T}\right], \tag{4.2.15}$$

where $M_{\rm sph}$ is the mass of the sphalerons and may be written as [193]

$$M_{\rm sph} = \pi\frac{M_W}{\alpha_2} = 2\pi^2\sqrt{2}\frac{v_H}{g}, \tag{4.2.16}$$

and v_H is the Higgs VEV. Therefore *before* the EWPT the rates of B and L-number-violating sphalerons may proceed unsuppressed whilst *after* these sphaleron processes are heavily suppressed.

4.2.2 C and CP-Violation

The weak interactions maximally violate C-symmetry. In addition, the SM has a CP-violating complex phase associated to the CKM matrix [21]. However, it has been known for some time that the CP-violation from this phase is not sufficient to produce the BAU [195, 196].

4.2.3 Departure from Thermal Equilibrium

In principle, the electroweak phase transition could provide a departure from thermal equilibrium. However, from lattice calculations the phase transition is not sufficiently strongly first order for successful baryogenesis [197].

In summary, any mechanism constructed to explain the BAU dynamically must contain new sources of CP-violation and provide a departure from thermal equilibrium either by introducing new dynamics or alternating the existing EWPT such that it is first order. For the last three decades, baryogenesis has been a very active field of research and some of the proposed mechanisms are described below.

[4] To compute the height of the barrier involves finding the saddle-point solutions to the potential $V[A^i_\mu]$ and a worked example for the SM may be found in [194].

- **GUT Baryogenesis** The purpose of Grand Unified Theories (GUTs) is to unify the three forces of the SM at sufficient high energies. From renormalisation group running, the SM constants unify around $10^{15} - 10^{16}$ GeV. Various GUT models, based on gauge groups such as $SU(5)$ and $SO(10)$, contain gauge bosons which have B and CP-violating couplings to leptons and baryons. Subsequently, the out-of-equilibrium decay of these gauge bosons satisfies Sakharov's Conditions and produces a baryon asymmetry [38, 198–200]. GUT baryogenesis is currently out of favour because a generic feature of GUTs is magnetic monopole or gravitino production, which would over close the Universe. This problem can be avoided if inflation occurs after GUT symmetry-breaking thereby diluting the monopoles. However, such a scenario would also dilute the baryon asymmetry.

- **High-Scale Thermal Leptogenesis** As discussed in Section 1.5 there are three ways to generate the Weinberg operator at tree level: the introduction of a fermionic singlet, a scalar triplet or a fermionic triplet. These are known as type-I, II and III see-saws respectively. The coupling of these heavy new degrees of freedom breaks lepton number and, similarly to GUT baryogenesis, their decays can produce a lepton asymmetry which is converted to a baryon asymmetry via electroweak sphaleron processes. We will focus on thermal leptogenesis in the context of a type-I see-saw mechanism in Section 4.3.1 but leptogenesis is also possible in type-II [43–48] and type-III [49–52] scenarios.

- **Dirac Leptogenesis** The vast majority of leptogenesis scenarios assume that neutrinos are Majorana particles. However, in Dirac leptogenesis this need not be the case [201–205]. The basic idea is the following: symmetries can be implemented so that tree-level Dirac and Majorana neutrino mass terms (i.e. NLH and MNN respectively) are forbidden. Additionally, heavy vector-like fields are introduced which have non-trivial and CP-violating coupling to SM fields. These vector-like fields will play a similar role to sterile neutrinos in conventional type-I leptogenesis and they will decay to left and right-handed leptons in such a manner that conserves total lepton number ($L_{tot} = L_\ell + L_{\nu_R}$).

The small loop-suppressed coupling between the SM Higgs and the left and right-handed neutrinos prevents the asymmetries in the neutrino sector from equilibrating until late times. Electroweak sphaleron processes convert L_ℓ into a baryon asymmetry before L_ℓ and L_{ν_R} have equilibrated.

4.3 Popular Mechanisms of Baryogenesis

4.3.1 High-Scale Leptogenesis

As we discussed in Section 1.5.1, the type-I see-saw mechanism minimally adds two Majorana-type fermions or sterile neutrinos to the SM particle spectrum. These particles are singlets of the SM gauge group but couple to leptons and SM Higgs via a Yukawa term. In the mass basis, the following gauge invariant terms are added to the SM Lagrangian

$$\mathcal{L} = \mathcal{L}_{SM} \quad -i\sum_{i=1}^{3}\overline{N_{iR}}\partial^\mu N_{iR} - \sum_\alpha y_\alpha^D \overline{\ell_{\alpha L}}\ell_{\alpha R}\phi - \sum_{\alpha,i} h_{\alpha i}\overline{\ell_{\alpha L}}N_{iR}\tilde{\phi} - \frac{1}{2}\sum_i \overline{N_{iR}^C}M_{ii}^D N_{iR} + \text{h.c.} \tag{4.3.17}$$

where M_{ii} is the Majorana mass matrix of the sterile neutrinos, ℓ leptonic doublets and $\phi = (\phi^+, \phi^0)$ is the Higgs doublet[5]. If we consider three sterile neutrinos, it is clear the implementation of the type-I see-saw has introduced 18 new parameters to the SM: three sterile neutrino masses and 15 entries of the Yukawa matrix h (nine entries and six phases). As N_i are SM-singlets their mass scale can be much higher than the electroweak scale, $M_i \gg \langle\phi\rangle = 174$ GeV. After electroweak symmetry breaking, the mass matrix of the active neutrinos is given by the well-known see-saw relation

$$m_\nu \simeq v_H^2 \frac{hh^T}{M}. \tag{4.3.18}$$

If we assume $h \sim \mathcal{O}(1)$ and $m_\nu \sim \sqrt{\Delta m_{atm}} \sim 0.05$ eV this implies $M \sim 10^{15}$ GeV, which is close to the GUT scale. In addition to providing an elegant solution to

[5]Note that we have changed notation slightly from Section 1.5.1, where the ν_R was the sterile neutrino in the mass basis. We have made this modification, at this point in the thesis, as it is consistent with much of the leptogenesis literature.

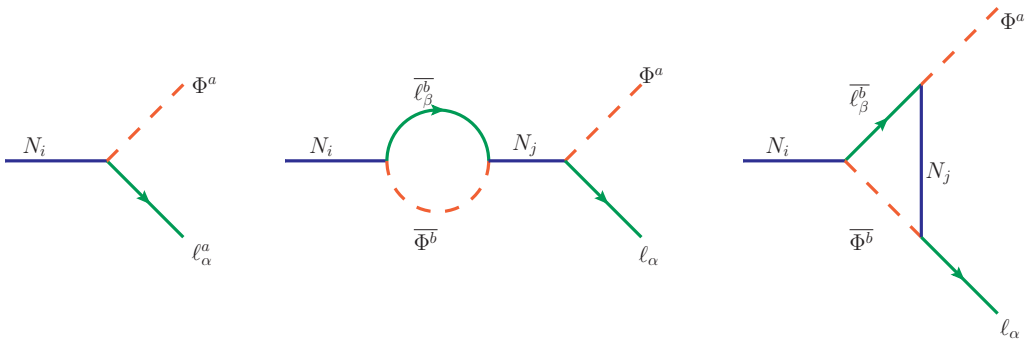

Figure 4.7: The CP-asymmetry arises from the interference between tree and loop level diagrams.

small but non-zero neutrino masses, the see-saw mechanism qualitatively satisfies Sakharov's conditions: the Majorana neutrino mass matrix break lepton number, the entries of the Yukawa matrix, h, can be complex and therefore CP-violating and finally the sterile neutrino is a good candidate to decay out of thermal equilibrium because its decay rate (Γ_{N_i}) can easily fall below the Hubble expansion rate (H)

$$\Gamma_{N_i} = \frac{\left(h^\dagger h\right)_{ii} M_i}{8\pi} \quad \text{and} \qquad H(T) = \frac{2}{3}\sqrt{\frac{g*\pi^3}{5}}\frac{T^2}{M_{PL}}, \tag{4.3.19}$$

where $g*$ is the effective number of degrees of freedom ($g* = 106.75$ for the SM excluding sterile neutrinos) and $M_{PL} = 1.22 \times 10^{19}$ GeV is the Planck mass. In thermal leptogenesis, the out-of-equilibrium condition is provided by the expansion of the Universe. A particle species may maintain thermal equilibrium with the thermal bath only if its interaction rates are faster than the expansion rate of the Universe i.e. $\Gamma > H$. If the interaction rates drop below the Hubble expansion rate then the particular particle species comes out of thermal equilibrium and freeze-in occurs. In the context of leptogenesis using a type-I see-saw, the non-equilibrium dynamics of the sterile neutrino can be encapsulated by the decay parameter

$$K_i = \frac{\Gamma_{N_I}}{H(M_i)} = \frac{\tilde{m}_i}{m_*}, \tag{4.3.20}$$

where the effective and equilibrium neutrino masses are defined as [206]

$$m_* = \frac{16\pi^{\frac{5}{2}}\sqrt{g*}}{3\sqrt{5}}\frac{v_H^2}{M_{PL}} \sim 1.08 \times 10^{-3}\text{eV} \quad \text{and} \quad \tilde{m}_i = \frac{\left(h^\dagger h\right)_{ii} v_H^2}{M_i}. \tag{4.3.21}$$

There are three regimes of interest: $K_i \gg 1$, $K \sim 1$ and $K < 1$ and imply strong, intermediate and weak washout respectively. The phenomenological consequences

of these regimes will be discussed in Section 4.3.1.

CP-Asymmetries

Sterile neutrinos are Majorana particles and therefore can decay to leptons and Higgs or via the CP-conjugate decay

$$N_i \to \ell_\alpha^a + \phi^a \quad \text{and} \quad N_i \to \overline{\ell_\alpha^a} + \overline{\phi^a}, \tag{4.3.22}$$

where $a = 1, 2$ is the $SU(2)_L$ index and $\alpha = e, \mu, \tau$. The first leptogenesis calculations were completed in the one-flavoured regime. In such a regime, the leptons and anti-leptons which couple to the sterile neutrinos maintain their coherence during the leptogenesis era and therefore are characterised as a linear combination of the flavour states

$$\ell_1 = \sum_\alpha c_{\alpha 1} \ell_\alpha \quad \text{and} \quad \overline{\ell_1} = \sum_\alpha {c'_{\alpha 1}}^* \overline{\ell_\alpha}, \tag{4.3.23}$$

where $c_{\alpha 1}$ and ${c'_{\alpha 1}}^*$ are functions of Yukawa coupling, h. The one-flavoured regime is a valid assumption only if leptogenesis occurs at sufficiently high temperatures ($T > 10^{12}$ GeV) when all leptons are out of thermal equilibrium, i.e. $\Gamma_\alpha < H$. At lower temperatures, charged lepton interactions mediated by SM Yukawa coupling, y, cause the charged leptons to equilibrate. At this time, the Universe can distinguish different charged lepton flavours and application of the one-flavoured regime fails [6].

Accounting for flavour effects, the preferential decays of the sterile neutrinos is quantified via the CP-asymmetry

$$\epsilon_{i\alpha} = \frac{\Gamma(N_i \to \ell_\alpha \phi) - \Gamma(N_i \to \overline{\ell_\alpha} \phi^*)}{\Gamma(N_i \to \ell_\alpha \phi) + \Gamma(N_i \to \overline{\ell_\alpha} \phi^*)}, \tag{4.3.24}$$

where Γ are thermally averaged decay rates and i the sterile neutrino mass eigenstate. In the one-flavoured regime, the flavour index α, may be summed over such that the CP-asymmetry takes the following form

$$\epsilon_i = \sum_{\alpha = e, \mu, \tau} \epsilon_{i\alpha}. \tag{4.3.25}$$

[6] The charged lepton interaction rate is approximated as [207, 208] $\Gamma_\alpha(T) \sim 8 \times 10^{-3} y_\alpha^2 T$ which implies that $\Gamma_\alpha(T) > H(T)$ for $T_e \sim 10^4$ GeV, $T_\mu \sim 10^9$ GeV and $T_\tau \sim 10^{12}$ GeV.

Such CP-asymmetries occur from the interference between tree and loop decay diagrams as shown in Fig. 4.7. Using a hierarchical sterile neutrino mass spectrum, the calculation of the CP-asymmetry at leading order yields [209, 210]

$$\epsilon_{i\alpha} = \frac{3}{16\pi \left(h^\dagger h\right)_{ii}} \sum_{i \neq j} \left[\mathrm{Im}\left[h^*_{\alpha i} h_{\alpha j} \left(h^\dagger h\right)_{ij}\right] \xi\left(\frac{M_j^2}{M_i^2}\right) + \mathrm{Im}\left[h^*_{\alpha i} h_{\alpha j} \left(h^\dagger h\right)_{ji}\right] \frac{2}{3\left(x_j/x_i - 1\right)} \right], \tag{4.3.26}$$

where M_i is the mass of N_i, $x_i = M_i^2/M_1^2$ and

$$\xi\left(x\right) = \frac{2}{3} x \Big[\left(1+x\right) \log\left(\frac{1+x}{x}\right) - \frac{2-x}{1-x} \Big]. \tag{4.3.27}$$

Note that if the Yukawa coupling between the sterile neutrino, leptons and Higgs were real then the CP-asymmetry would vanish, as expected. The first (second) term of (4.3.26) corresponds to the vertex (bubble) diagram of Fig. 4.7. Also, for small mass squared splittings, $M_i \sim M_j$, the contribution from the bubble diagram can be resonantly enhanced and therefore the scale of leptogenesis may be significantly lowered [211].

Semi-Classical Boltzmann Equations for Minimal Thermal Leptogenesis

The ultimate aim for theories of leptogenesis will be to derive kinetic equations that track the lepton and anti-lepton number density in time. As an example, we will consider one-flavoured N_1-leptogenesis scenario. In such a scenario, the lepton asymmetry is generated entirely by the decays of the lightest sterile neutrino, N_1, and the contribution of N_2 and N_3 are neglected. Such a scenario may be realised if the masses of N_2 and N_3 are greater than the reheating temperature and therefore not produced in the Early Universe.

The most basic form of these kinetic equations, based on semi-classical Boltzmann equations, account for the decay and washout in the one-flavoured regime (excluding $\Delta L = 1$ scattering [212] and $\Delta L = 2$ [206, 212–216] washout processes). The decay term parametrises the lepton asymmetry produced from the sterile neutrino decays while the washout term quantifies the processes in the thermal plasma which compete and reduce the overall lepton asymmetry. As discussed in Section 4.3.1,

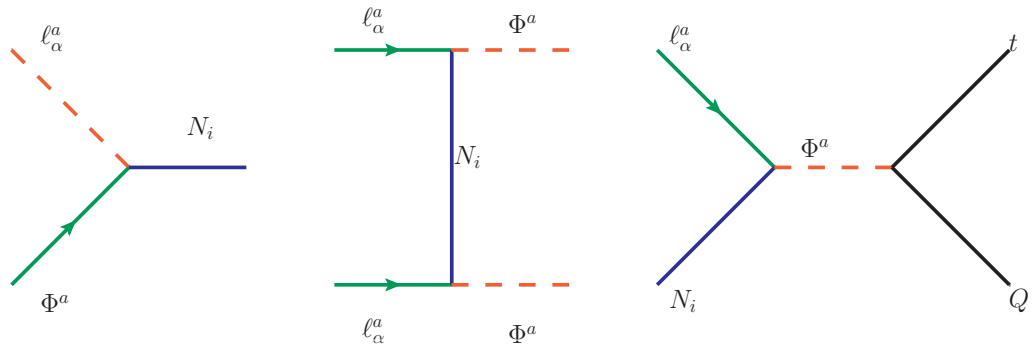

Figure 4.8: Decay, $\Delta L = 1$ and $\Delta L = 2$ washout processes from left to right.

this regime is only realised at very high temperatures when the rates of processes mediated by the charged lepton Yukawa couplings are out of thermal equilibrium and therefore there is a single charged lepton flavour state, ℓ_1. At lower temperatures, when flavour effects may no longer be neglected, a density matrix formalism [214, 217–220] allows for a more general description than semi-classical Boltzmann equations, since it is possible to calculate the asymmetry in intermediate regimes where the one and two-flavoured treatments are inadequate. There are additional effects which can be included to improve the accuracy of the leptogenesis calculations. Such effects include spectator processes [221–223], thermal corrections [216, 224] and quantum kinetic effects [225–228]. Spectator processes cause the redistribution of the asymmetry generated in the leptonic doublets amongst other particle species in the thermal bath. These processes typically protect the lepton asymmetry from washout and therefore increase the efficiency of leptogenesis. However, for the present discussion we will ignore these sub-leading effects. The decay and washout terms of the semi-classical Boltzmann equations are given by [229]

$$D_1(z) = K_1 z \frac{\mathscr{K}_1(z)}{\mathscr{K}_2(z)} \quad \text{and} \quad W_1(z) = \frac{1}{4} K_1 \mathscr{K}_1(z) z^3, \tag{4.3.28}$$

where $z = M_1/T$ and $\mathscr{K}$ are modified Bessel functions.

One-Flavoured Boltzmann Equation

The one-flavoured Boltzmann equation used to calculate the lepton asymmetry produced from the decay of the lightest sterile neutrino, N_i, may be written as [206,

212–216]

$$\begin{aligned}\frac{dN_{N_i}}{dz} &= -D_1(z)\left(N_{N_i}(z) - N_{N_i}^{\rm eq}(z)\right)\\ \frac{dN_{B-L}}{dz} &= \epsilon_i D_1(z)\left(N_{N_i}(z) - N_{N_i}^{\rm eq}(z)\right) - W_1 N_{B-L}(z),\end{aligned} \tag{4.3.29}$$

where ϵ is the CP asymmetry and N are number densities calculated in a co-moving volume. We have adopted a similar notation and normalisation as applied in [220] where $N_N^{\rm eq}(z=0)=1$ i.e. one ultra-relativistic sterile neutrino per co-moving volume and the equilibrium abundance of the sterile neutrinos is given by

$$N_{eq}(z) = \frac{1}{2}z^2 K_2(z). \tag{4.3.30}$$

The second term of (4.3.29) displays explicitly how N_1-leptogenesis satisfies Sakharov's conditions: ϵ_i quantifies the CP-violation, D_1 is a $B-L$ violating decay term and finally $N_{N_i}(z) \neq N_{N_i}^{\rm eq}(z)$ implies a departure from thermal equilibrium. In the scenario, $N_{N_1} > N_{eq}$ there is an over-abundance of sterile neutrinos and the N_{B-L} asymmetry increases from their decays. On the other hand, if $N_{N_1} < N_{eq}$, the N_{B-L} asymmetry receives a negative contribution from inverse decays which use lepton and anti-leptons to increase the sterile neutrino abundance. The factor that converts N_{N_1} to N_{B-L} is the CP-asymmetry while the washout term W accounts for the competing inverse decays (examples of which are shown in Fig. 4.8) which inhibits N_{B-L} production. The final value of N_{B-L} must be compared with the baryon-to-photon ratio [215]. These two quantities are related in the following way

$$\eta_B = a_{\rm sph}\frac{N_{B-L}^f}{N_\gamma^{\rm rec}} \sim 9.5\times 10^{-3} N_{B-L}^f, \tag{4.3.31}$$

where $N_\gamma^{\rm rec} \sim 37$, N_{B-L}^f is the final $B-L$ asymmetry and $a_{\rm sph} = 28/79$ is the sphaleron conversion factor which accounts for the partial conversion of the $B-L$ asymmetry into a B asymmetry by the electroweak sphalerons. The numerical solution to (4.3.29) has been plotted for N_{N_1}, N_{B-L} and N_{eq} as a function of $z = M_1/T$. The left (right) plot of Fig. 4.9 shows the result for strong (weak) washout where a vanishing initial abundance of sterile neutrinos has been applied. In this scenario, the sterile neutrinos are thermally produced via inverse-decays and scatterings present in the thermal plasma (hence the name *thermal* leptogenesis). This can be seen

in the left plot which shows the result for strong washout. The inverse decays are sufficient to increase the sterile neutrino abundance to thermal abundance prior to the decays which produce the B-L asymmetry. This asymmetry is then washed out so that the particular details of the sterile production or initial abundance do not greatly affect the final B-L asymmetry [215, 230]. This has the effect of greatly reducing theoretical error. In the case of weak washout, shown in the right plot of Fig. 4.9, it takes longer for the inverse-decays to build a sizeable abundance of sterile neutrinos and therefore the final B-L asymmetry is sensitive to the initial conditions.

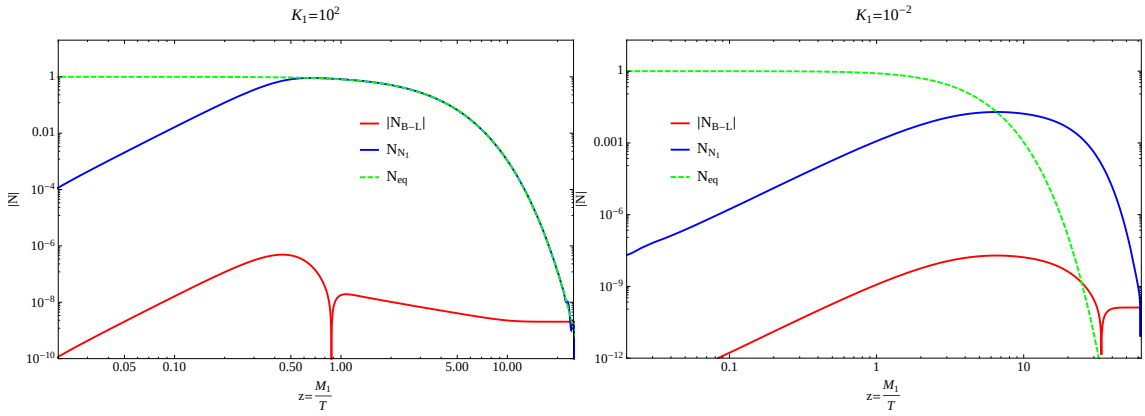

Figure 4.9: The number density of N_1, $|N_{B-L}|$ and N_{eq} as a function of z. A zero initial condition is applied with strong (weak) washout regime shown on the left (right) where $\epsilon_1 = 10^{-6}$.

An appealing feature of N_i-leptogenesis is its connection with neutrino physics. Assuming three sterile neutrinos, the Casas-Ibarra parametrisation [231] allows the Yukawa matrix to be decomposed into high and low-energy components

$$h = \frac{1}{v_H}\sqrt{M_N}R\sqrt{m_\nu}U^\dagger_{\rm PMNS}, \tag{4.3.32}$$

where M_N (m_ν) is the diagonal sterile (active) neutrino mass matrix, R is a complex orthogonal matrix and $U_{\rm PMNS}$ is the PMNS matrix. In the scenario leptogenesis occurs in the one-flavoured regime, the CP-asymmetry depends on the sum over three flavours (as illustrated in (4.3.25)) and may be written as

$$\epsilon_1 = \frac{3}{16\pi}\frac{M_1}{v_H^2}\frac{\sum_i m_{\nu_i}{\rm Im}\left(R_{1i}^2\right)}{\sum_i m_{\nu_i}\left|R_{1i}^2\right|}. \tag{4.3.33}$$

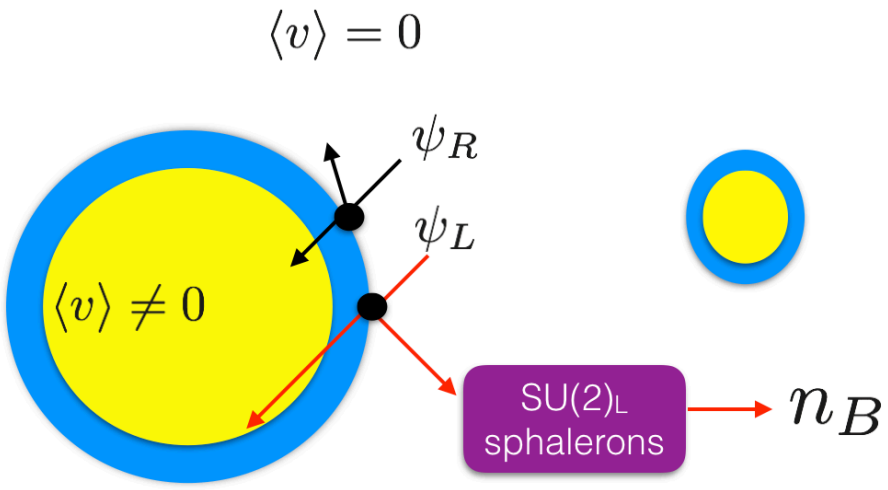

Figure 4.10: Schematic diagram of electroweak baryogenesis.

From (4.3.33) it is clearly seen ϵ_1 is not a function of the PMNS matrix and therefore is insensitive to low-energy CP-violation and leptonic mixing angles. However, in flavoured leptogenesis, there are now at least two CP-asymmetries (one for each lepton flavour and also for flavour correlations between differing lepton flavours) and they are a function of the PMNS matrix which enables a connection between high-scale leptogenesis and low-scale leptonic observables. Using such a set-up, it has been demonstrated that non-zero values of $\delta_{\rm CP}$ can produce the BAU [232, 233]. In addition, the application of flavour effects allows the scale of thermal leptogenesis (i.e. mass of sterile neutrino) to be lowered several orders of magnitude and still produce a baryon asymmetry consistent with observation.

4.3.2 Electroweak Baryogenesis

One possible alternative to leptogenesis is electroweak-baryogenesis (EWBG). This mechanism operates during the EWPT when the Higgs field acquires a non-zero VEV which leads to the breaking of electroweak symmetry to its $U(1)_{\rm EM}$ subgroup. A requirement of EWBG is a first order EWPT. The difference between first and second order phase transitions can be determined from the Higgs potential at finite temperature as shown in Fig. 4.11. Above the critical temperature (T_C) the potential is in the symmetric phase, where the only vacua is located at the origin. As the

temperature lowers, $T < T_C$, a second, deeper vacua may develop. If there is a *bump* separating the two vacua, the transition from the false to true vacua proceeds via thermal tunnelling and is classified as a first order phase transition. This corresponds to a discrete change in the VEV and subsequently a finite-sized bubble is nucleated. Conversely, if the field value can simply "roll down the hill", a smooth crossover transition occurs. For such a transition, the field value changes continuously in space and therefore bubbles cannot form. In the case of EWBG, bubble nucleation

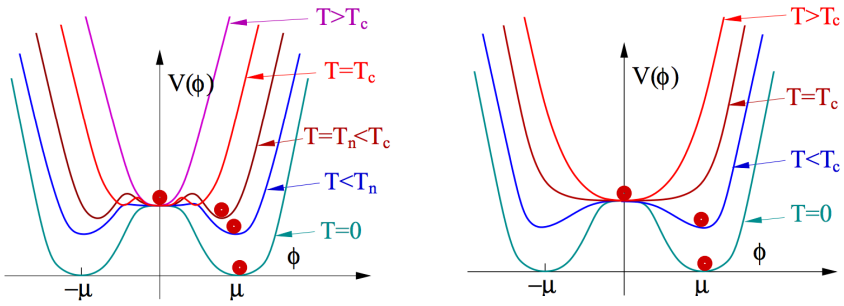

Figure 4.11: The left (right) diagram shows a first order (smooth crossover) phase transition [234].

occurs and the baryon asymmetry is created in the vicinity of the bubble walls. Particles in the thermal bath can scatter off or diffuse through the bubble wall depending on their transmission and reflection coefficients. If the EWBG theory contains sources of CP-violation then this scattering can produce a chiral charge asymmetry in the particle number density in front of the bubble wall [235, 236].

In the symmetric phase, non-perturbative $SU(2)_L$ processes occur at unsuppressed rates and from scaling arguments proceed at $\Gamma_{\text{sph}} \propto \alpha_W^5 T^4$ [237]. These sphalerons convert the chiral asymmetry in the particle number densities (in front of the bubble wall) into a baryon asymmetry. Subsequently, some of the baryon asymmetry will diffuse into the bubble, where the sphaleron transitions are Boltzmann-suppressed, and the baryon asymmetry remains stable in time.

EWBG fails in the SM due to insufficient CP-violation and the smooth crossover of the EWPT [197]. However, New Physics which modifies the Higgs potential and introduces new CP-violating couplings remedies both problems. Such examples,

amongst others, include the MSSM [238–240], two Higgs doublet [241, 242] and inert Higgs doublet models [243–245]. As a consequence, this makes EWBG a very predictive theory as the new particles must couple to the Higgs. In addition, such particles should be abundant in the thermal plasma around the EW scale and are generically not very heavy. In addition to being predictive, this feature makes EWBG a falsifiable theory.

4.4 Calculational Tools

4.4.1 Semi-Classical Boltzmann Equation

In Section 4.3.1, the N_1-leptogenesis scenario was presented using semi-classical Boltzmann equations. Such equations are derived from *Liouville's* equation which states that the probability distribution function (f) of a system of particles does not change along any trajectory in phase space

$$\frac{df}{dt} = \frac{\partial f}{\partial t} + \sum_i^N \left(\frac{\partial f}{\partial \vec{r}_i} . \dot{\vec{\boldsymbol{r}}_i} + \frac{\partial f}{\partial \vec{p}_i} . \dot{\vec{\boldsymbol{p}}_i} \right) = 0, \tag{4.4.34}$$

where $\vec{r}$ and $\vec{p}$ are position and momentum respectively. (4.4.34) details the evolution of an N-particle system and hence the probability distribution function in 6N dimensional phase space (three position and three momentum coordinates are needed to describe each particle). Using the Poisson bracket, (4.4.34) may be rewritten in the following manner

$$\frac{\partial f}{\partial t} = \{H, f\} \quad \text{where} \quad \{A, B\} = \frac{\partial A}{\partial \vec{r}_i} . \frac{\partial B}{\partial \vec{p}_i} - \frac{\partial A}{\partial \vec{p}_i} . \frac{\partial B}{\partial \vec{r}_i}, \tag{4.4.35}$$

where H is the Hamiltonian of the system. For typical systems, the distribution function is dependent on a very large number of variables ($\sim 10^{23}$) and solving (4.4.35) quickly becomes intractable. The first step in simplifying these equations is to apply the Bogoliubov-Born-Green-Kirkwood-Yvon (BBGKY) hierarchy which allows the N-distribution function to be written as a function of the N+1 distribution function (essentially $f_1 = \mathcal{F}(f_2), f_2 = \mathcal{F}(f_3), ...$). These sets of recursive equations are just as difficult as Eq. (4.4.35) to solve. However, if the system of particles is a

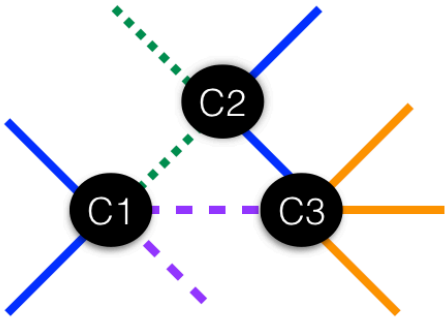

Figure 4.12: The coloured lines represent propagating particles and the black circles their successive collisions.

dilute gas [7] then these equations can be truncated such that the time evolution of the system is represented by the one-particle distribution function (f_1)

$$\frac{\partial f_1}{\partial t} = \{H_1, f_1\} + \left(\frac{\partial f_1}{\partial t}\right)_{\text{coll}}, \tag{4.4.36}$$

where the third term of (4.4.36) is the collision integral and accounts for scattering between particles[8]. Such scatterings are calculated using S-matrix elements in the usual *in-out* formalism (QFT at zero temperature). From the Lehmann-Symanzik-Zimmermann (LSZ) formula S-matrix elements are expressed in terms of correlation functions of fields which are asymptotically free of each other; in a dilute gas this approximation is reasonable given that the timescale of collisions between particles is significantly shorter than the timescale of particle propagation and thus the in-going and out-going are asymptotically free. This has the consequence that the system is essentially *memoryless* i.e. from Fig. 4.12 the collision C_2 has no effect on C_3.

However, in the Early Universe the environment (i.e. thermal plasma) is extremely hot and of finite density. Therefore, representing the system as a dilute gas may not be fully descriptive given that the timescale of particle propagation may

[7] See Fig. 4.12. In the dilute gas approximation the timescale of the collisions (t_{C_i}) is much smaller than the timescale of the particles propagating between collisions (t_{prop}) i.e. $t_{C_i} \ll t_{prop}$

[8] The semi-classical Boltzmann equation of (4.4.36) is a standard result of kinetic theory and some steps have been skipped. For the interested reader see [246].

not be significantly different than the timescale of the collisions; in such a scenario C_2 will affect C_3 and therefore the system becomes non-Markovian. To capture such memory effects amounts to going beyond the *in-out* formalism to using *in-in* formalism. This formalism may also be known as the Real-Time, Closed-Time Path (CTP) and Schwinger-Keldysh formalism. Regardless of the nomenclature, the benefit of using such an approach allows the assumption of asymptotically free states to be removed.

4.4.2 The Closed-Time Path Formalism

In the preceding section, we discussed the general motivation for using the Closed-Time Path (CTP) formalism for Early Universe calculations. In this section we discuss some basic results of this formalism which will be necessary for our calculation in Section 4.5.2: these include defining the CTP propagators and the equation of motion. This short discussion shall not do justice to what is a rich field of study with many possible physical applications however, some select references include [247–251].

To begin, we first define the Closed-Time Path contour by considering an ingoing state at an initial time t_i as $\phi_{\rm IN}\left(t_i + i\epsilon/2\right)$. We evolve this state forwards in time, via an external source J_+, to a state in the future at time $t_f + i\epsilon/2$, which will be a sum over all possible future states. This summation over all future states can be evolved back to the initial state via the source term J_-. This evolution of states is defined on a Closed-Time contour, $\mathcal{C} = \mathcal{C}^+ \cup \mathcal{C}^-$, in the complex plane. This time contour, as shown in Fig. 4.13, starts at time $t_i + i\epsilon/2$ and continues to time $t_f + i\epsilon/2$ and loops back to $t_i - i\epsilon/2$ where ϵ is an infinitesimal parameter. The generating functional, defined on this time path [251], may be written as

$$Z_{\mathcal{C}}[J] = \mathrm{Tr}\left(T_C \mathrm{exp}\left(i\int d^4x J(x)\phi(x)\right)\rho\right), \tag{4.4.37}$$

where T_C is time-ordering on the complex time plane and ρ is the density matrix characterising the initial conditions of the system. At zero temperatures, the density matrix is given by $\rho = |\Psi_0\rangle\langle\Psi_0|$ where $|\Psi_0\rangle$ is the ground state of the full interacting

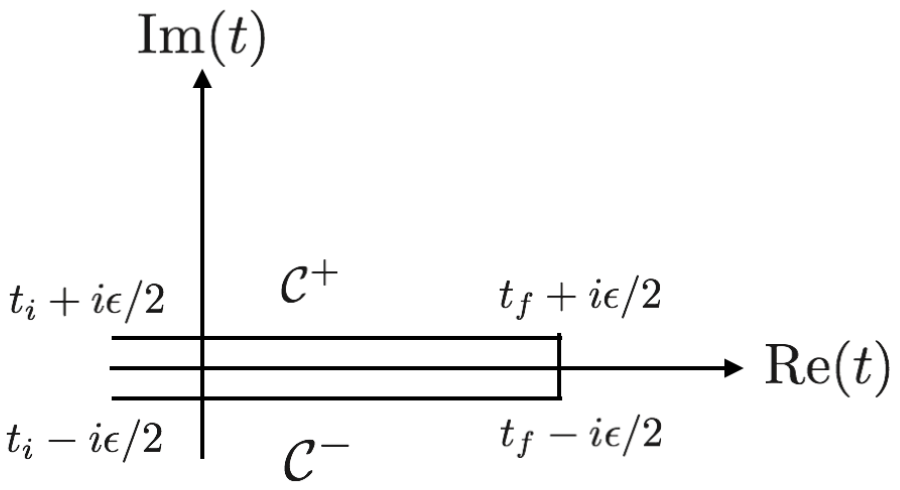

Figure 4.13: The Closed-Time Path: $\mathcal{C} = \mathcal{C}^+ \cup \mathcal{C}^-$.

theory. At finite temperatures, $\rho = e^{\beta(-H+\mu_i Q_i)}/\mathrm{Tr}\left((-H+\mu_i Q_i)\right)$ where $\beta = 1/T$, H is the Hamiltonian, Q_i are conserved charges and μ_i are the corresponding chemical potentials[9]. Much like the zero-temperature case, derivatives with respect to the variational current yield path-ordered products

$$\langle\phi(x_1)....\phi(x_N)\rangle = \frac{1}{Z[J]}\frac{\delta^N}{i\delta J(x)....\delta J(x_N)}Z[J]\bigg|_{J=0}. \tag{4.4.38}$$

For a two-point function, we find there are four possible ways to order the two times on the Closed-Time path which result in four propagators as shown in Fig. 4.14. The generating functional of (4.4.37) has a path integral representation

$$\mathcal{Z}_{\mathcal{C}}[J] = \int \mathcal{D}\phi_+\mathcal{D}\phi_+\langle\phi_-|\rho|\phi_+\rangle\langle\phi_-|T_C\left(\exp\left(i\int d^4x\left(\mathcal{L}(x)+J(x)\phi(x)\right)\right)\right)|\phi_+\rangle, \tag{4.4.39}$$

where $\phi_+ \equiv \phi_{\mathrm{IN}}(t_i + i\epsilon/2)$, $\phi_- \equiv \phi_{\mathrm{IN}}(t_i - i\epsilon/2)$ and in the infinitesimal limit ($\epsilon \to 0$) (4.4.39) reduces to

$$\mathcal{Z}_{\mathcal{C}}[J] = \int \mathcal{D}\phi_+\mathcal{D}\phi_-\langle\phi_-|\rho|\phi_+\rangle\int \mathcal{D}\phi T_C\left[\exp\left(i\int d^4x\left(\mathcal{L}(x)+J(x)\phi(x)\right)\right)\right]. \tag{4.4.40}$$

[9]In this work we set all chemical potentials to zero.

The ensemble average over the initial conditions is described by $\mathcal{D}\phi_+\mathcal{D}\phi_-\langle\phi_-|\rho|\phi_+\rangle$. In principle, the calculation of ρ typically involves all n-point functions. In practice, typically only the one and two-point functions are considered and the higher order n-point functions are assumed to be functions of the lower order n-point functions. Such an assumption of *Gaussian* initial conditions is useful, as a convenient redefinition can be made such that the source term absorbs the initial conditions. This has the consequence that the initial conditions disappear from the calculations. Applying this assumption, the generating functional for the free theory is [251]

$$Z_{\mathcal{C}}^{\text{free}} = \mathcal{R}\text{exp}\left(-\frac{1}{2}\int_{\mathcal{C}} d^4x d^4y J(x)\Delta_{\mathcal{C}}^{\text{free}}(x,y)J(y)\right), \tag{4.4.41}$$

where $\mathcal{R}$ is a normalisation factor and $\Delta_{\mathcal{C}}^{\text{free}}(x,y)$ is the free generating functional in the absence of sources and is given by

$$\left(\Box_1 + m^2\right)\Delta_{\mathcal{C}}^{\text{free}}(x,y) = -i\delta^{(4)}{}_{\mathcal{C}}\left(x-y\right). \tag{4.4.42}$$

The generating functional of the full theory (4.4.40) is related to the generating functional of the free theory (4.4.41) by

$$Z_{\mathcal{C}}[J] = \text{exp}\left\{-i\int_{\mathcal{C}} d^4x V\left[\frac{\delta}{i\delta J(x)}\right]\right\} Z_{\mathcal{C}}^{\text{free}}[J(x)], \tag{4.4.43}$$

From here the Schwinger-Dyson equation can be found

$$(\Box + m^2)\Delta_{\mathcal{C}}(x_1,x_2) + \int_C d^4\overline{x}\Pi_{\mathcal{C}}(x,\overline{x})\Delta_{\mathcal{C}}(\overline{x},y) = -i\delta_{\mathcal{C}}(x-y), \tag{4.4.44}$$

where $\Delta_{\mathcal{C}}$ ($\Pi_{\mathcal{C}}$) is the full propagator (self-energy correction). As mentioned previously, the time coordinates of the Δ and Π can live on the upper or lower time-contour as illustrated in Fig. 4.14. For t_1 and t_2 on the positive branch, $\mathcal{C}^+$, this path-ordering corresponds to time-ordering and the propagator (Δ_{++}) is the usual Feynman propagator, Δ^F. Conversely, if t_1 and t_2 live on the negative branch, the path-ordering is anti-time ordering and the corresponding propagator (Δ_{--}) is the Dyson propagator, Δ^D. Finally, if t_1 and t_2 live on differing branches, the Wightman propagators ($\Delta_<$ and $\Delta_>$) are obtained. As the Closed-Time path involves the use of time and anti-time ordering, this gives rise to a doubling in the degrees of freedom (d.o.f.). This increase in the d.o.f. has the consequence that the propagators and

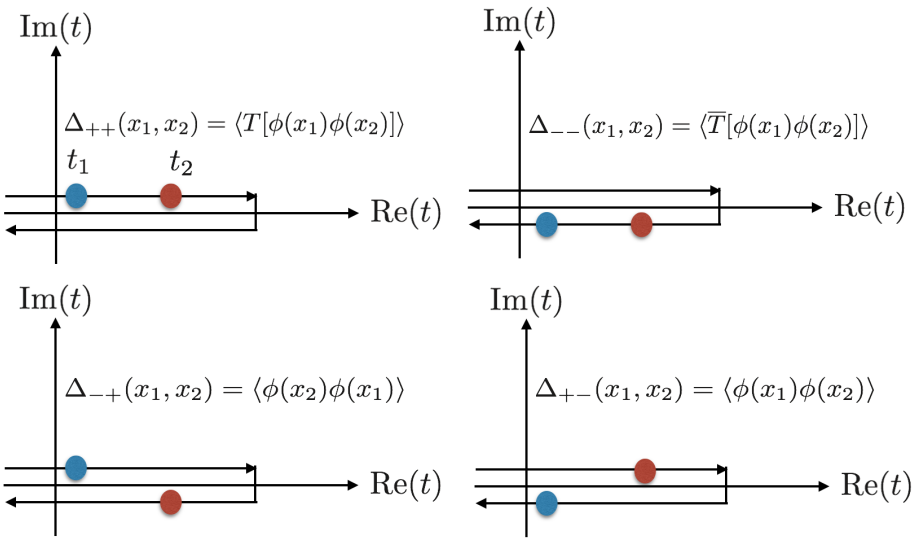

Figure 4.14: The blue (red) circle represents t_1 (t_2) and there are four possible ways of ordering two times on the Closed-Time Path.

self-energies can be expressed as 2×2 matrices

$$\Delta^{ab}(x_1, x_2) \equiv \begin{pmatrix} \Delta^F(x_1, x_2) & \Delta^<(x_1, x_2) \\ \Delta^>(x_1, x_2) & \Delta^D(x_1, x_2) \end{pmatrix} \quad \text{and} \quad \Pi^{ab}(x_1, x_2) \equiv \begin{pmatrix} \Pi^F(x_1, x_2) & \Pi^<(x_1, x_2) \\ \Pi^>(x_1, x_2) & \Pi^D(x_1, x_2) \end{pmatrix}, \tag{4.4.45}$$

where $a, b \equiv \pm$. Consequently, for a given process the number of diagrams to be evaluated is larger than in the zero-temperature, vacuum theory.

In the proceeding work, we will be interested in calculating the lepton asymmetry and therefore will solve kinetic equations. Using the CTP-formalism, the kinetic equations are derived from the Schwinger-Dyson equations and are the *Kadanoff-Baym* equations

$$\begin{aligned} (\Box + m^2)\Delta^>(x_1, x_2) &= -\int d^4\overline{x} \left[\Pi^>(x_1, \overline{x})\Delta^A(\overline{x}, x_2) + \Pi^R(x_1, \overline{x})\Delta^>(\overline{x}, x_2)\right], \\ (\Box + m^2)\Delta^<(x_1, x_2) &= -\int d^4\overline{x} \left[\Pi^<(x_1, \overline{x})\Delta^A(\overline{x}, x_2) + \Pi^R(x_1, \overline{x})\Delta^<(\overline{x}, x_2)\right], \end{aligned} \tag{4.4.46}$$

where the advanced and retarded propagators and self-energies are

$$\begin{aligned}
\Delta^R(x_1,x_2) &= \Delta_{++}(x_1,x_2) - \Delta_{+-}(x_1,x_2) = \Delta_{-+}(x_1,x_2) - \Delta_{--}(x_1,x_2),\\
\Delta^A(x_1,x_2) &= \Delta_{++}(x_1,x_2) - \Delta_{-+}(x_1,x_2) = \Delta_{+-}(x_1,x_2) - \Delta_{--}(x_1,x_2),\\
\Pi^R(x_1,x_2) &= \Pi_{++}(x_1,x_2) - \Pi_{+-}(x_1,x_2) = \Pi_{-+}(x_1,x_2) - \Pi_{--}(x_1,x_2),\\
\Pi^A(x_1,x_2) &= \Pi_{++}(x_1,x_2) - \Delta_{-+}(x_1,x_2) = \Pi_{+-}(x_1,x_2) - \Pi_{--}(x_1,x_2).
\end{aligned} \tag{4.4.47}$$

4.5 Creation of the BAU from Lepto-Bubbles

4.5.1 Basic Mechanism

Our principal assumption is similar to that of Chapter 2, that neutrinos are Majorana in nature and therefore, to leading order, their mass model reduces to the lepton number violating Weinberg operator

$$\mathcal{L}_W = \frac{\lambda_{\alpha\beta}}{\Lambda}\left(\overline{L_{\alpha L}}\widetilde{\phi}\right)\left(\phi^\dagger\widetilde{L_{\beta R}}\right), \tag{4.5.48}$$

where $\lambda_{\alpha\beta} = \lambda_{\beta\alpha}$ is a model-dependent coupling and Λ the scale of new physics. As has been discussed at length, the Weinberg operator may be UV-completed in a number of ways ranging from loop effects to the introduction of heavy new degrees of freedom. However, unlike typical scenarios of leptogenesis, the details of the UV-completion of the dimension five operator need not be specified in this mechanism. This has the interesting consequence that the scale of neutrino mass generation is higher than the scale of CP-violation, unlike in all other scenarios of leptogenesis. A second key postulate is the coupling of the Weinberg operator is functionally dependent upon a SM-singlet scalar, ϕ, such that $\lambda_{\alpha\beta} = \lambda^0_{\alpha\beta} + \lambda^1_{\alpha\beta}\langle\phi\rangle/v_\phi$[10]. Associated to ϕ is a finite temperature scalar potential, which is symmetric under a leptonic flavour symmetry at sufficiently high temperatures. As the temperature of the Universe lowers, the minima at the origin of this potential becomes metastable and a phase transition occurs. As a result, the minima changes from the vacua at

[10]Using this form of the coupling implies that a dimension-six operator accompanies the dimension-five operator. However, if we assume the mass of the flavon is sufficiently heavy, the effects of a dimension-six operator are negligible.

the origin to a deeper, true vacua which is stable and non-zero, $\langle\phi\rangle$. The ensemble expectation value (EEV) of ϕ spontaneously breaks the high-scale flavour symmetry and results in the observed pattern of leptonic masses and mixing. Assuming a first order phase transition, (lepto) bubbles of the leptonically CP-violating broken phase nucleate. To further clarify, from Fig. 4.15, it can be seen that the EEV deep inside the bubble has a non-zero and constant value as a function of spacetime. While outside the bubble, the EEV is zero-valued. Inside the bubble wall, the EEV varies with spacetime and therefore the coupling of the Weinberg operator, $\lambda_{\alpha\beta}$, must also vary with spacetime. This has the effect that interference of the Weinberg operator, at different times, produces a lepton asymmetry[11].

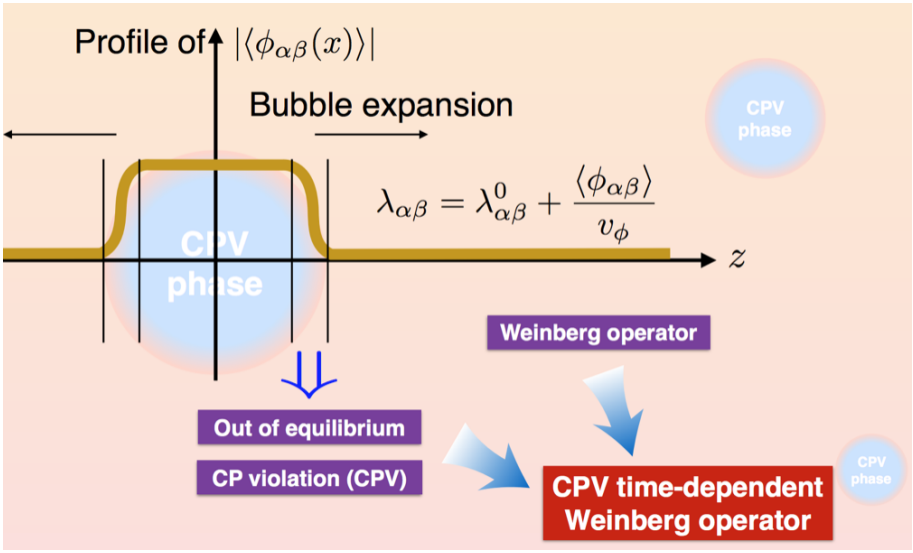

Figure 4.15: Schematic representation of a lepto-bubble. The brown line represents the EEV as a function of z (the direction of bubble expansion). With thanks to Ye-Ling Zhou for the figure.

4.5.2 Calculating the Lepton Asymmetry

We follow the techniques developed for thermal leptogenesis as presented in [227] and calculate the lepton asymmetry to leading order in a time-independent flavour

[11] One point to bear in mind is that if neutrinos are Dirac particles then this mechanism is no longer feasible.

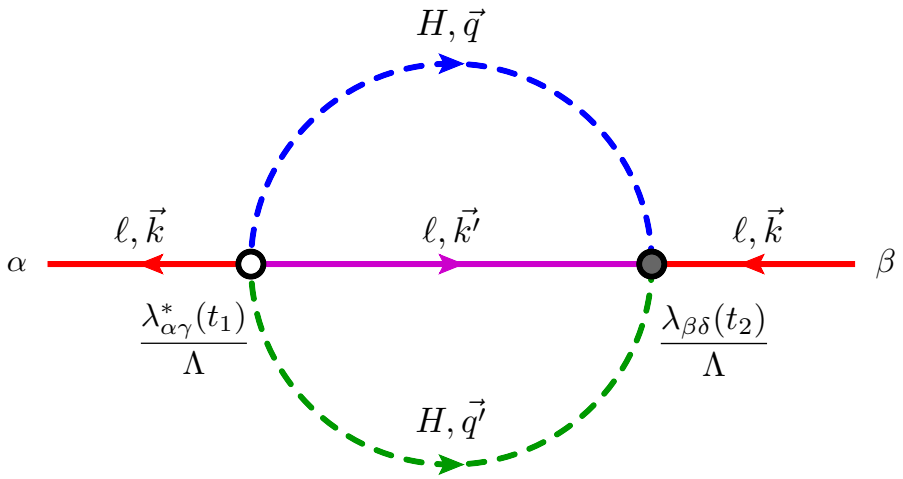

Figure 4.16: The two-loop lepton-number-violating contribution of the CP-violating and time-dependent Weinberg operator to the lepton self energy.

basis. In order to derive the lepton asymmetry, the Green functions for the Higgs and leptons are Fourier-transformed

$$\Delta_{\vec{q}}(t_1,t_2)=\int d^3r e^{i\vec{q}\cdot\vec{r}}\Delta(x_1,x_2),\quad S_{\vec{k}}(t_1,t_2)\ =\int d^3r e^{i\vec{k}\cdot\vec{r}}S(x_1,x_2)\,, \tag{4.5.49}$$

where $r\equiv x_1-x_2$, $t_1\equiv x_1^0$ and $t_2\equiv x_2^0$. Subsequently, the lepton asymmetry at a fixed space point in the bubble wall may be written as $n_L(x)=\int\frac{d^3k}{(2\pi)^2}L_{\vec{k}}$ with

$$\begin{aligned}L_{\vec{k}}&\equiv f_{\ell\vec{k}}-f_{\bar{\ell}\vec{k}}\\&=-\int_{t_i}^{t_f}dt_1\partial_{t_1}\mathrm{tr}[\gamma_0 S^<_{\vec{k}}(t_1,t_1)+\gamma_0 S^>_{\vec{k}}(t_1,t_1)]\\&=-\int_{t_i}^{t_f}dt_1\int_{t_i}^{t_f}dt_2\mathrm{tr}\left[\Sigma^>_{\vec{k}}(t_1,t_2)S^<_{\vec{k}}(t_2,t_1)-\Sigma^<_{\vec{k}}(t_1,t_2)S^>_{\vec{k}}(t_2,t_1)\right],\end{aligned} \tag{4.5.50}$$

where t_i (t_f) is the initial (final) time, $\Sigma_{\vec{k}}(t_1,t_2)$ is the self-energy contribution and the step from the second to third line of Eq. (4.5.50) comes from applying the Kadanoff-Baym equation[12]. The leading CP-violating contribution to $\Sigma_{\vec{k}}(t_1,t_2)$ is a two-loop diagram as shown in Fig. 4.16. The memory effect is reflected in the *memory-integral* over time variables, t_1 and t_2, which involves the time-dependent

[12]The lepton asymmetry comes from zeroth component of the lepton current, $L(t,t')=-\mathrm{tr}\left[\gamma^0 S^+(t,t')\right]$. The explicit derivation from the lepton current to Eq. (4.5.50) may be found in [227].

couplings shown in Fig. 4.16. Using Eq. (4.5.48), the lepton asymmetry may be re-expressed as

$$L_{\vec{k}\alpha\beta} = \sum_{\gamma\delta} \frac{12}{\Lambda^2} \int_{t_i}^{t_f} dt_1 \int_{t_i}^{t_f} dt_2 \mathrm{Im}\big\{\lambda^*_{\alpha\gamma}(t_1)\lambda_{\beta\delta}(t_2)\big\} \int_{q,q'} M_{\alpha\beta\gamma\delta}(t_1, t_2, k, k', q, q')\,, \tag{4.5.51}$$

where $\int_{q,q'} = \int \frac{d^3q}{(2\pi)^3} \frac{d^3q'}{(2\pi)^3}$. $M_{\alpha\beta\gamma\delta}(t_1, t_2, k, k', q, q')$ is the finite temperature matrix element. It is worth-noting, the lepton asymmetry has factorised into a part which is dependent upon the Weinberg operator coefficient and another which is the finite temperature matrix element, $M_{\alpha\beta\gamma\delta}(t_1, t_2, k, k', q, q')$. The derivation of this factorisation may be found in Section C.1.

For the present calculation, and indeed for simplicity, we have ignored the differing thermal widths of the lepton propagators (i.e. flavour effects). As discussed in Section 4.3.1, the inclusion of flavour effects, generally allows for a wider range of temperatures in which leptogenesis is feasible. Additionally, we set $t_i \to -\infty$, $t_f \to +\infty$ and the total lepton asymmetry $L_{\vec{k}} \equiv \sum_\alpha L_{\vec{k}\alpha\alpha}$ may be written as

$$L_{\vec{k}} = \frac{12}{\Lambda^2} \int_{-\infty}^{+\infty} dt_1 \int_{-\infty}^{+\infty} dt_2 \mathrm{Im}\big\{\mathrm{tr}\left[\lambda^*(t_1)\lambda(t_2)\right]\big\} \int_{q,q'} M\,, \tag{4.5.52}$$

where the finite temperature matrix element, decomposed in terms of the lepton and Higgs propagators, is expressed as

$$M = \mathrm{Im}\big\{\Delta^<_{\vec{q}}(t_1, t_2)\Delta^<_{\vec{q}'}(t_1, t_2)\mathrm{tr}\big[S^<_{\vec{k}}(t_1, t_2)S^<_{\vec{k}'}(t_1, t_2)P_L\big]\big\}\,.$$

A key assumption in the derivation of Eq. (4.5.50) is a homogeneous system [227]. However, this is clearly not the case for this mechanism as the lepto-bubble expansion provides a special direction perpendicular to the bubble wall which results in the transport of the lepton asymmetry along this particular direction. We anticipate the directional dependence of the asymmetry will be small and therefore ignore its impact at this stage[13]. As the temperature at which lepto-bubble nucleation occurs is significantly higher than the electroweak scale, both leptons and the Higgs are almost

[13]The spatial dependence of the lepton-asymmetry will be further elucidated upon in future works.

in thermal equilibrium and we apply this approximation throughout. The time-dependent flavon EEV, $\langle\phi\rangle$, plays an important role in this mechanism. Without loss of generality, one may assume $\langle\phi\rangle = v_\phi f(t)$ where $f(t)$ varies continuously from 0 to 1. The coupling coefficient, λ, takes the form

$$\lambda(t) = \lambda^0 + \lambda^1 f(t)\,. \tag{4.5.53}$$

where λ^0 is the coupling before the phase transition. The lepton asymmetry should not be sensitive to the precise functional form of $f(x)$. The simplest example of $f(t)$ is a step function, $f(t) = \vartheta(v_w t - z)$, where v_w is the velocity of the bubble wall and z a certain point along the direction of bubble expansion. Another example is a tanh function $f(t) = \frac{1}{2}\Big[1 + \tanh\Big(\frac{v_w t - z}{L_w}\Big)\Big]$ where L_w the width of the wall. The latter case is analogous to the Higgs EEV profile studied in the electroweak strong first-order phase transition, which has been numerically checked [252–256]. In the limit $L_w \to 0$, the second example reduces to the first. Both cases yield the same result, shown in Eq. (4.5.55), as expected.

After an exchange of integration variables from t_1 (t_2) to $\tilde{t} = (t_1 + t_2)/2$ ($y = t_1 - t_2$) and using

$$\int_{-\infty}^{+\infty} d\tilde{t}[f(\tilde{t} + y/2) - f(\tilde{t} - y/2)] = y\,, \tag{4.5.54}$$

we find[14]

$$\int_{-\infty}^{+\infty} d\tilde{t}\,\mathrm{Im}\big\{\mathrm{tr}\,[\lambda^*(t_1)\lambda(t_2)]\,\big\} = \mathrm{Im}\big\{\mathrm{tr}\,\big[\lambda^0\lambda^*\big]\,\big\}y\,. \tag{4.5.55}$$

Therefore, the lepton asymmetry can be written as

$$L_{\vec{k}} = -\frac{12}{v_H^4}\mathrm{Im}\{\mathrm{tr}[m_\nu^0 m_\nu^*]\}\int_{-\infty}^{+\infty} dyy\int_{q,q'} M\,, \tag{4.5.56}$$

where we have reparametrised the effective neutrino mass matrices as $m_\nu^0 \equiv \lambda^0 v_H^2/\Lambda$ and $m_\nu \equiv (\lambda^0 + \lambda^1)v_H^2/\Lambda$. It is worth stressing that the parameters associated to the bubble, v_w and L_w, do not affect the lepton asymmetry Eq. (4.5.56). This is because we have assumed a fast-bubble wall expansion. Such an assumption is reasonable because the flavon couples only to leptons and Higgs in the thermal

[14]For a proof see the Appendix.

bath and therefore the plasma will not exert too much friction on the lepto-bubble wall. In the remainder of this work, we shall continue to assume that the bubble is expanding significantly faster than the Universe. As the bubble wall sweeps over a certain region, the temperature, $T = 1/\beta$, changes slightly. To evaluate Eq. (4.5.56), first we calculate M using the lepton and Higgs propagators. In the massless limit, the lepton and Higgs propagators are written as

$$\begin{aligned} \Delta^{<}_{\vec{q}}(t_1, t_2) &= \frac{\mathrm{c}_q}{2q\,\mathrm{sh}_q} e^{-\gamma_H |y|}, \\ S^{<}_{\vec{k}}(t_1, t_2) &= \frac{\gamma^0 \mathrm{c}_k + i\vec{\gamma}\cdot\hat{k}\,\mathrm{s}_k}{2\,\mathrm{ch}_k} e^{-\gamma_\ell |y|}, \end{aligned} \tag{4.5.57}$$

where $k = |\vec{k}|$, $q = |\vec{q}|$, $\mathrm{c}_k = \cos(ky^-)$, $\mathrm{s}_k = \sin(ky^-)$, $\mathrm{ch}_k = \cosh(k\beta/2)$, $\mathrm{sh}_k = \sinh(k\beta/2)$, $y^- = y - i\beta/2$, $\hat{k} = \vec{k}/k$ and γ_H, γ_ℓ are the thermal damping rates of the Higgs and the leptonic doublets respectively [227]. Substituting Eq. (4.5.57) into Eq. (4.5.53), M becomes

$$M = \frac{\mathrm{Im}\left\{\mathrm{c}_q \mathrm{c}_{q'} [\mathrm{c}_k \mathrm{c}_{k'} + \hat{k}\cdot\hat{k}' \mathrm{s}_k \mathrm{s}_{k'}]\right\}}{8qq' \mathrm{sh}_q \mathrm{sh}_{q'} \mathrm{ch}_k \mathrm{ch}_{k'}} e^{-2\gamma|y|}\,, \tag{4.5.58}$$

where $\gamma = \gamma_\ell + \gamma_H$. To calculate the lepton asymmetry of Eq. (4.5.56), we must complete the time (y) and momentum integration. The y integration may be performed by applying the oddness of M

$$\int_{-\infty}^{+\infty} dy y M = 2\int_0^{\infty} dy y M = -\sum_{\eta_2,\eta_3,\eta_4=\pm 1} \frac{K_{\eta_2\eta_3\eta_4}\gamma \sin(\beta K/2)\,[1 - \eta_2 \hat{k}\cdot\hat{k}']}{16qq' \left(K^2_{\eta_2\eta_3\eta_4} + 4\gamma^2\right)^2 \mathrm{sh}_q \mathrm{sh}_{q'} \mathrm{ch}_k \mathrm{ch}_{k'}}\,,$$

where $K_{\eta_2\eta_3\eta_4} = k + \eta_2 k' + \eta_3 q + \eta_4 q'$. The evaluation of the momentum integration closely follows that of [227]. We abstain from re-deriving the details of this calculation and instead refer the reader to the reference. However we will present the simplified form of the momentum integration

$$\int_{q,q'} = \frac{1}{(2\pi)^4} \int_0^{\infty} dp \int_0^{\infty} k' dk' \int_{|k-p|}^{|k+p|} q dq \int_{|k'-p|}^{|k'+p|} q' dq'\,, \tag{4.5.59}$$

where $p = k - q = k' - q'$, $q^2 = k^2 + p^2 - 2pk\cos\theta$ and $q'^2 = k'^2 + p^2 - 2pk'\cos\theta$ have been applied. Using Eq. (4.5.59) with Eq. (4.5.59), the final result is written as

$$L_{\vec{k}} = \frac{3\,\mathrm{Im}\left\{\mathrm{tr}\left[m^0_\nu m^*_\nu\right]\right\} T^2}{(2\pi)^4 v_H^4} F(x_1, x_\gamma)\,. \tag{4.5.60}$$

$F\left(x_1, x_\gamma\right)$ is a loop factor given by

$$F\left(x_1, x_\gamma\right) = \frac{1}{x_1}\int_0^{+\infty} dx \int_0^{+\infty} x_2 dx_2 \int_{|x_1-x|}^{|x_1+x|} dx_3 \int_{|x_2-x|}^{|x_2+x|} dx_4 \sum_{\eta_2,\eta_3,\eta_4=\pm 1}\left[1 - \frac{\left(x_1^2+x^2-x_3^2\right)\left(x_2^2+x^2-x_4^2\right)}{4\eta_2 x_1 x_2 x^2}\right] \times \frac{X_{\eta_2\eta_3\eta_4} x_\gamma \sinh X_{\eta_2\eta_3\eta_4}}{\left(X_{\eta_2\eta_3\eta_4}^2 + x_\gamma^2\right)^2 \cosh x_1 \cosh x_2 \sinh x_3 \sinh x_4},$$

where $x_1 = k\beta/2$, $x_2 = k'\beta/2$, $x_3 = q\beta/2$, $x_4 = q'\beta/2$, $x = p\beta/2$ and $X_{\eta_2\eta_3\eta_4} = x_1+\eta_2 x_2+\eta_3 x_3+\eta_4 x_4$. The loop factor depends on the lepton energy and the thermal width normalised by the temperature, i.e. x_1 and x_γ. A key difference between this mechanism and conventional scenarios of leptogenesis is that as once the lepton asymmetry is produced, it will not be washed out. This is because the lepton-antilepton transition rate proceeds via the Weinberg operator and is proportional to $(\lambda/\Lambda)^2 T^3$ which is much smaller than the Hubble expansion rate. Thus, the washout processes via the Weinberg operator are negligible. The lepton asymmetry is partially converted into the baryon asymmetry via electroweak sphaleron processes which are active above the electroweak scale. However, $n_{B-L} \equiv -n_L(T = T_{\rm PT})$ is conserved, where $T_{\rm PT}$ is the phase transition temperature. The final baryon symmetry is approximately given by $n_B \approx \frac{1}{3} n_{B-L}$. The baryon-to-photon ratio η_B is defined as

$$\eta_B \equiv \frac{n_B}{n_\gamma} \approx -\frac{{\rm Im}\{{\rm tr}[m_\nu^0 m_\nu^*]\} T^2}{8\pi^4 \zeta(3) v_H^4} F(x_\gamma)\,, \tag{4.5.61}$$

where $F(x_\gamma) = \int_0^{+\infty} x_1 dx_1 F(x_1, x_\gamma)$, $n_\gamma = 2\zeta(3)T^3/\pi^2$ and $\zeta(3) = 1.202$[15]. In order to produce a positive baryon asymmetry, ${\rm Im}\{{\rm tr}[m_\nu^0 m_\nu^*]\}$ should take a minus sign.

4.5.3 Discussion

The lepton asymmetry, shown in Eq. (4.5.50), depends upon three factors: the loop function $F(x_1, x_\gamma)$ derived from the self-energy correction to the lepton propagator; the effective neutrino mass matrices m_ν^0, m_ν and the temperature, T, of the phase transition. In Fig. 4.17, we allow x_γ to take several values and display the

[15] Although the baryon-to-photon ratio of Eq. (4.5.61) appears to be dependent upon the VEV of the Higgs $\propto 1/v_H^4$ it is not. This is because $m_\nu^0, m_\nu \propto v_H^2$.

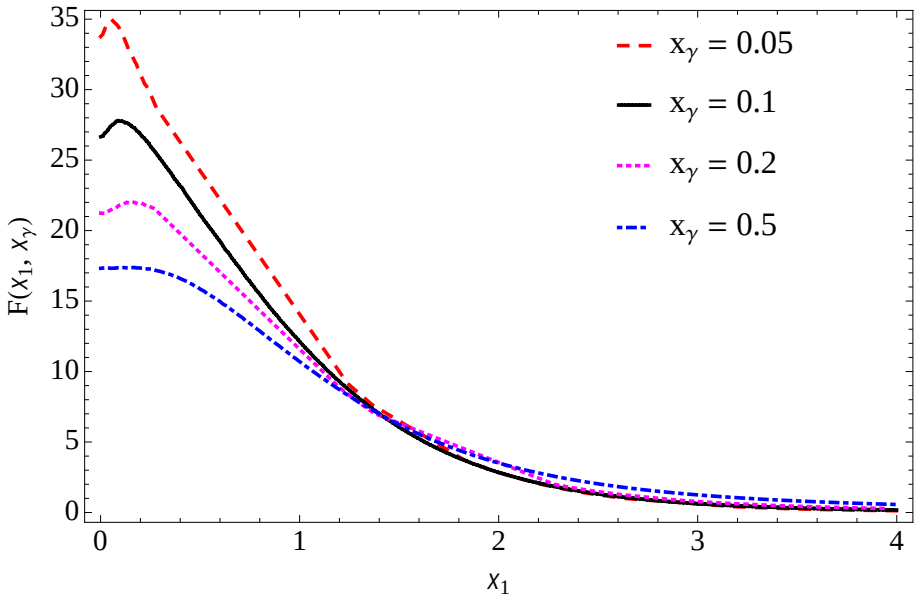

Figure 4.17: The loop factor $F(x_1, x_\gamma)$ as a function of the lepton energy k and the thermal width γ, where $x_1 = k\beta/2$ and $x_\gamma = \gamma\beta$.

numerical results of the loop factor $F(x_1, x_\gamma)$ as a function of x_1. The Standard Model value, $x_\gamma \approx 0.1$, comes from electroweak gauge couplings [247]. However, it is possible this value may be enhanced due to new physics contributions at high-energy scales. For $x_1 \sim 1$, we observe that the loop factor provides a factor $\mathcal{O}(10)$ enhancement to the lepton asymmetry. There are two effective neutrino mass matrices m_ν^0 and m_ν. The structure of m_ν^0 is dependent on the coupling of the flavons to the Weinberg operator and is determined by the details of particular flavour models and will be studied in the future. After the phase transtion, the coefficients of the Weinberg operator are fixed and m_ν is identified to the measurable low-energy neutrino mass matrix[16]. This mass matrix is diagonalised by the PMNS matrix, i.e. $U_{\rm PMNS}^T m_\nu U_{\rm PMNS}^* = {\rm diag}\{m_1, m_2, m_3\}$, and therefore allows for a connection between lepton asymmetry and low-energy leptonic observables. To estimate the phase transition temperature, we assume ${\rm Im}\{{\rm tr}[m_\nu^0 m_\nu^*]\}$ is the same order as $m_\nu^2 \sim (0.1\ {\rm eV})^2$. Numerically, we have checked that $F(x_\gamma)$ provides an $\mathcal{O}(10^2)$ factor enhancement for $x_\gamma \sim 0.1$. Therefore, the temperature for successful leptogenesis

[16]Ignoring RG running effects which merit discussion in future works.

via lepto-bubbles is

$$T \sim \sqrt{\eta_B}\,\frac{v_H^2}{m_\nu}\,. \tag{4.5.62}$$

Using the observed ratio of baryon-to-photon, $\eta_B = (6.19 \pm 0.15) \times 10^{-10}$ [21], we conclude $T \sim 10^{11}$ GeV. This is an estimation and a more detailed calculation, involving more generic bubble properties and inclusion of effects such as differing thermal width of charged leptons, may indeed lower this scale. Note that, this mechanism relies upon the UV-completion scale Λ being higher than the temperature of phase transition T. If $\Lambda \lesssim T$, new lepton-number-violating particles, e.g. right-handed neutrinos in type-I see-saw, may be present in the thermal bath during the phase transition, and the phase transition may influence the leptogenesis via the decays of these particles [257]. In the above, we have calculated the lepton asymmetry generated by the time-dependent coupling of the Weinberg operator. However, during the lepto-bubble expansion, this coupling is also space-dependent. Including the space-dependent calculation would not produce any additional lepton asymmetry because we assume thermal equilibrium form of the lepton and Higgs propagators as seen in Eq. (4.5.57). In equilibrium, the momentum distributions of the Higgs and leptons are spatially isotropic. As a consequence, there is no preferred direction for the Higgs and lepton propagators. Therefore, combining these propagators with the space-dependent coupling, which specifies the z direction, cannot generate any lepton asymmetry. However, it is in principle possible that a deviation from the equilibrium may result in additional lepton asymmetry. Nonetheless, this contribution may be safely ignored for temperatures far above the electroweak scale as the deviation is very small and the generated lepton asymmetry would be negligible.

4.6 Summary

Leptogenesis via lepto-bubbles is a completely new and novel mechanism that provides a connection between the BAU and the flavour structure of the lepton sector. Unlike conventional scenarios of leptogenesis, which specify a particular way to generate neutrino masses, this mechanism allows for relative model independence as the new physics responsible for neutrino masses has already been integrated out before

the CP-violating phase transition occurs. This has the effect that the CP-violating scale, and in turn the flavour-breaking scale, lies below the scale of neutrino mass generation. There are several interesting aspects of our mechanism that could be further explored. These include:

- Investigating the impact of more generic bubble properties, such as thick-wall and slow expansion.
- Accounting for differing thermal widths of the charged leptons. This may lower the scale of the phase transition by several orders of magnitude.
- Investigate the effect of specific flavour models and the impact this has on the BAU.
- If the scale of this mechanism could be lowered sufficiently, it would be of interest to calculate the gravitational wave spectra given a particular flavour symmetric potential.
- At present the lepton asymmetry is calculated numerically in the context of the Closed-Time Path formalism. It would be of interest to calculate the lepton asymmetry using more conventional methods and investigate the quantitative difference between the two approaches. Moreover, finding analytic formulae would allow others to apply this mechanism more easily.
- This mechanism could be applied in conjunction with existing leptogenesis. Thermal leptogenesis (with flavour effects) could occur at relatively low scales ($10^4 - 10^6$ GeV) and partially produce a lepton asymmetry. If lepto-bubble nucleation occurred as a secondary process, it would enhance the existing lepton asymmetry to be consistent with observation. This two-stage leptegenesis scenario, could allow for successful leptogenesis at significantly lower temperatures than previously thought possible.

Chapter 5

Summary and Outlook

Measuring the fine structure of leptonic mixing is one of the foremost challenges in experimental neutrino physics. In conjunction, understanding the origin of the pattern of mixing is of great interest from a theoretical perspective. In this thesis, we reviewed one possible method of approaching this *flavour* problem which avoids the difficulties of flavour model building by focussing purely on symmetry constraints. In Chapter 2 we applied an A_5 flavour and gCP symmetry to constrain the PMNS matrix and thereby predict three mixing angles and three phases. Given the choice of high and low-scale residual symmetries, these leptonic observables were a function of one internal parameter which could be eliminated in order to determine *sum rules*. The testability of these sum rules for currently running and future planned facilities was discussed at length in Chapter 2.

In Chapter 3, we considered a slightly less constrained combination of Abelian residual symmetries than in Chapter 2 and this had the consequence of providing a greater range of predictions with more complex correlations between observables. If nature is governed by a flavour symmetric principle and chooses to break her symmetries in such a relaxed manner it would be more challenging to determine this from oscillation experiments and indeed information from neutrinoless double-beta decay would be necessary.

In these discussions, we have only touched on a very specific application of flavour

symmetries in the lepton sector. The flavour problem has been scrutinised in many ways and includes developments in flavour model building, exploring predictions using groups of very large order, flavour anomalies and RG-running effects on flavour sum-rules amongst many others. However, in order to determine if indeed nature is governed by a symmetric principle, we shall need to be patient and await experimental input.

Hopefully, the reader has been convinced the BAU is a fascinating problem and is at the heart of *how* we exist. We reviewed two of the most popular in Section 4 and it was evident there remains tension between the viability and testability of such theories. In general, EWBG predicts New Physics at the EW-scale and therefore has the benefit of being testable and indeed many variants of EWBG are no longer viable.

High-scale leptogenesis is a relatively simple and plausible scenario that has deep connections with the neutrino sector. However, the possibility of being fully testable is unlikely in the foreseeable future, given that the mass scale of the heavy see-saw mediators ranges from $10^6 - 10^{15}$ GeV. In spite of this, there are indirect methods of excluding or constraining the theory parameter space. There has been work that investigated the possibility of falsifying high-scale leptogenesis in two ways: the first studied constraints from lepton-number violating (LNV) processes at the Large Hadron Collider (LHC) [258] and the second constraints from $0\nu\beta\beta$ [259]. In [258], the authors showed that observation of LNV at the LHC would put strong lower limits on leptogenesis washout processes. The authors investigated N_1-leptogenesis while ignoring flavour effects and therefore the conclusions of this work may only be applied to leptogenesis at very high temperatures. Moreover, it is worth stressing that the non-observation of LNV cannot constrain leptogenesis in any way. However, given the robustness of the SM to date, any New Physics including LNV at LHC (in spite of putting high-scale scenarios under considerable stress) would be welcomed by me. The second work, concluded that if $0\nu\beta\beta$ is triggered by non-standard effects, then it is likely high-scale leptogenesis is unfeasible (given the lower limit on

washout processes). However, $0\nu\beta\beta$ is a very challenging measurement and it will be very difficult to disentangle which particular non-standard mechanism is responsible even if $0\nu\beta\beta$ is observed. In spite of the aforementioned tension, it is worthwhile exploring all possible avenues.

The focal point of Chapter 4 was the presentation of a new mechanism of producing the matter anti-matter asymmetry via lepto-bubble nucleation. This mechanism has deep connections with leptonic flavour symmetries and therefore low-energy neutrino observables. The lepton asymmetry is produced at high temperatures, $T \sim 10^{11}$ GeV, after a flavon undergoes a phase transition; however, there are several modifications that could be made to the calculation in order to lower the scale.

In conclusion, we have demonstrated that with the accumulation of more precise neutrino oscillation data, it is possible to test the predictions of non-Abelian discrete symmetries, in particular using A_5 in conjunction with a generalised CP symmetry. In addition, we explored the possible connection between leptonic flavour symmetries and the BAU by discussing a non-standard leptogenesis scenario. We calculated the lepton asymmetry using a technique that captures memory effects and we found the scale of this mechanism is similar to that of high-scale thermal leptogenesis. There remains work to be done in further developing this mechanism and exploring the exciting possible connections with specific flavour models and their associated phenomenology.

Appendix A

A_5 Group Structure

We follow the discussion of [126]. A_5 is isomorphic to the icosahedral symmetry group which consist of all the rotations that preserve the orientation of the icosahedron, the platonic solid which consist of 20 equilateral triangles. The icosahedral group is of order 60 and has an identity element, rotations by $2\pi/5$, $4\pi/5$ (both order 5) through each of the twelve vertices, rotations by $2\pi/3$ (order 3) about the axis through each of the twenty equilateral triangles and rotations of π (order 2) around the midpoint of the thirty edges which result in fifteen different rotations. From these rotations, we can observe there are five different conjugacy classes

$$\mathbb{1}, 15C_2, 20C_3, 15C_5, 15C_5'.$$

A_5 has irreducible representations of order 1, 2, 3, 4 and 5. We can deduce this from the result that the order of the group equal to the sum of the squares of the irreducible representations,

$$1 + 12 + 12 + 15 + 20 = 60 = 1^2 + 3^2 + 3^3 + 4^2 + 5^2.$$

$$\langle S, T | S^2 \rangle = T^5 = (ST)^3 = \mathbb{1} \rangle.$$

The group consists of elements of (15) order 2, (20) 3 and 5 and their respective subgroups are given by C_2, C_3 and C_5.

We list the group elements below

$C_2 : \{ST^2ST^3S, TST^4, T^4(ST^2)^2, T^2DT^3, T^2ST^2ST^3S, ST^2ST, S, T^3ST^2ST^3, T^3ST^2ST^3S,$
$T^3ST^2, T^4ST^2ST^3S, TST^2S, ST^3ST^2S, T^4ST, (T^2S)T^4\}$

$C_3 : \{ST, TS, ST^4, T^4S, TST^3, T^2ST^2, T^2ST^4, T^3ST, T^3ST^3, T^4ST^2, TST^3S, T^2ST^3S,$
$T^3ST^2S, ST^2ST^3, ST^3ST, ST^3ST^2, (T^2S)^2T^2, T^2(T^2S)^2, (ST^2)^2S, (ST^2)^2T^2\}$

$C_5 : \{T, T^4, ST^2, T^2S, ST^3, T^3S, STS, TST, TST^2, T^2ST, T^3ST^4, T^4ST^3\}$

$C_5' : \{T^2, T^3, ST^2S, ST^3S, ST^2ST^2, T^2ST^2S, ST^3ST^3, T^3ST^3S, T^2ST^2ST^3,$
$T^3ST^2ST^2, T^3ST^2ST^4, T^4ST^2ST^3\}$

Appendix B

Chern-Simons Number

The YM Lagrangian has the following form

$$\mathcal{L} = \frac{1}{4} G^a_{\mu\nu} G_{a\mu\nu}, \quad G^a_{\mu\nu} = \partial_\mu A_\nu - \partial_\nu A_\mu + g f^{abc} A^a_\mu A^b_\nu \tag{B.0.1}$$

where g is the gauge coupling and f^{abc} is the structure constant of the gauge group. For this example we will use the gauge group, SU (2), as this is particularly relevant given that we discussed electroweak sphaleron processes. From Eq. (B.0.1), it is not immediately clear the vacua of the theory are discrete and degenerate. The way to see this is to consider the set of gauge field configurations that correspond to states with the minimal energy[1]

$$A_i(x) = iU(x)\partial_i U^\dagger(x), \tag{B.0.2}$$

where x is a spatial coordinate and U is a matrix representation of SU (2) element. Moreover the matrix notation has been introduced

$$A_\mu = g A^a_\mu \frac{\tau^a}{2}$$

where τ^a are the Pauli matrices. The gauge field configuration of Eq. (B.0.2) is referred to as *pure gauge*. As we are interested in tunnelling processes between vacua, which are zero-energy states, the action must be finite. In order to ensure the action is finite, U must behave as follows

$$U \to U_0, \quad |x| \to \infty,$$

[1]The pure gauge configuration corresponds to $F_{\mu\nu} = 0$ and thus a minimal energy configuration.

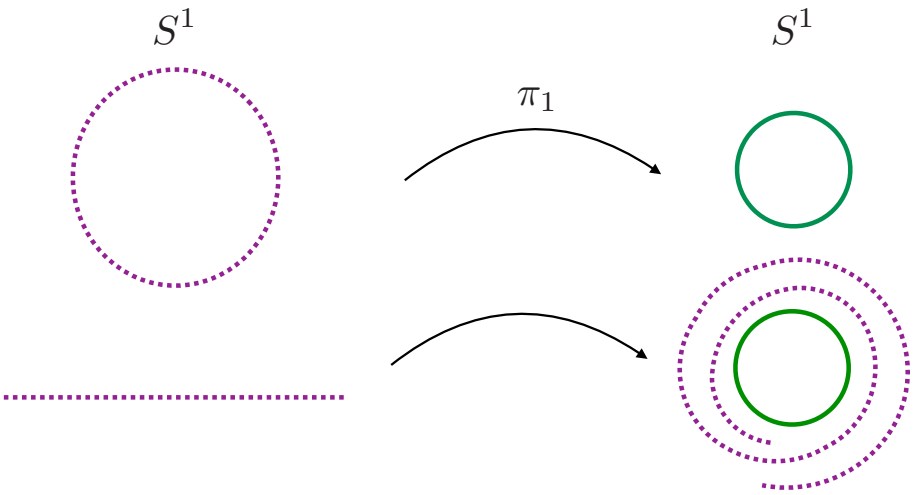

Figure B.1: Schematic mapping $f : S_1 \to S_1$

where U_0 is a constant matrix. At spatial infinity our three-dimensional space becomes equivalent to a three-sphere, S_3. Additionally, the group space of SU (2) is also the three-sphere. Indeed, this boundary condition has realised a set of continuous maps between the sphere in coordinate space (x) to the sphere in the group space (SU (2)): $\mathrm{S}_3 \to \mathrm{S}_3$. Such mapping corresponds to

$$\pi_3(S_3) = \mathbb{Z}.$$

The above result derives from algebraic topology and its meaning is more easily understood in a lower-dimensional example [2]. The Chern-Simons (CS) current may be defined as a function of gauge fields

$$\mathcal{K}^\nu = 2\epsilon^{\nu\mu\alpha\beta}\left(A^a_\mu \partial_\alpha A^a_\beta + \frac{g}{3} f^{abc} A^a_\mu A^b_\alpha A^c_\beta\right) \quad \text{with} \quad \epsilon^{0123} = 1.$$

K^ν is the CS current. As the case with most currents in physical systems, we can define a charge associated to that current which is the usual integration over spatial dimension with respect to the zeroth component

$$\mathcal{K} = \int d^3x \mathcal{K}^0(x).$$

[2] This result generalises to $\pi_N(\mathrm{S}_N) = \mathbb{Z}$. The most easily visualised example is $\pi_1(\mathrm{S}_1)$, which is the homotopy group of a circle, i.e. the mappings of a circle to a circle which is characterised by how many times one can wrap or *wind* one circle around another; clearly an integer number.

For pure gauge field configurations the above reduces to an integer i.e. the CS charge gives a measure of the winding number.

Appendix C

Lepton Asymmetry

There are several steps that need to be completed in order to massage the lepton asymmetry into a numerically integrable form. First, we shall write down the lepton asymmetry and note that it factorises into a part proportional to the time-dependent coupling (the prefactor) and another part which involves integrating the finite-temperature matrix element over phase space. To evaluate the prefactor, we will assume a **thin-bubble wall** and **fast-bubble expansion**, change variables from times t_1, t_2 to the relative and average coordinate $y = t_2 - t_1$ and $t = (t_1 + t_2)/2$ and complete the time-integration. Subsequently, the integration of the matrix-element will be completed and much of this calculation follows [227], e.g. the Feynman rules and phase space integration.

C.1 Factorising the Lepton Asymmetry

We will calculate the self-energy correction using the Weinberg operator: $\mathcal{L}_W = \frac{Y_{ij} L_i \phi \phi L_j}{M}$. The following diagrams are CP-violating and using the CTP formalism there are two possible ways of time ordering the self-energy correction. Therefore, to leading order the lepton asymmetry is [227],

$$L_{\mathbf{k}}(t,t) = -\int_0^t dt_1 \int_0^t dt_2 \mathrm{tr}[\underbrace{\Pi^{>}_{\mathbf{k}}(t_1,t_2)}_{\text{self-energy}} S^{<}_{\mathbf{k}}(t_2,t_1) - \Pi^{<}_{\mathbf{k}}(t_1,t_2) S^{>}_{\mathbf{k}}(t_2,t_1)]. \quad \text{(C.1.1)}$$

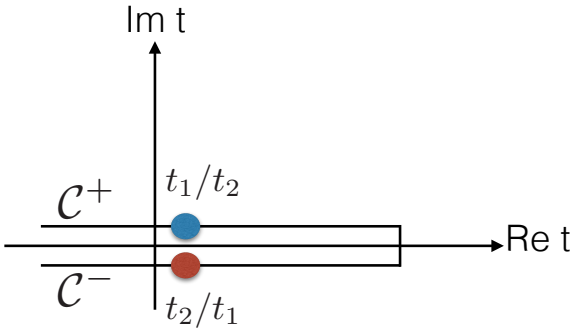

Figure C.1: Time-Ordering

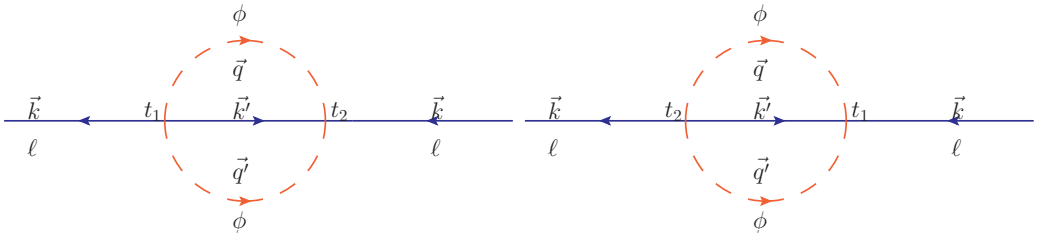

Figure C.2: Two ways of time-ordering the CP-violating diagrams with $q' = k - q - k'$.

The loop integrals of C.1.1 are shown in the two diagrams of Fig. C.2 and are written below,

$$\begin{aligned}\Pi^{>}_{\mathbf{k}}(t_1,t_2) &= \int \frac{dq^3}{(2\pi)^3}\frac{dq'^3}{(2\pi)^3} \times \Big[\Delta^{<}_{\mathbf{q}'}(t_2-t_1)\Delta^{<}_{\mathbf{q}}(t_2-t_1)S^{<}_{\mathbf{k}'}(t_2-t_1)\Big]P_L \\ \Pi^{<}_{\mathbf{k}}(t_1,t_2) &= \int \frac{dq^3}{(2\pi)^3}\frac{dq'^3}{(2\pi)^3} \times \Big[\Delta^{>}_{\mathbf{q}'}(t_2-t_1)\Delta^{>}_{\mathbf{q}}(t_2-t_1)S^{>}_{\mathbf{k}'}(t_2-t_1)\Big]P_L,\end{aligned} \tag{C.1.2}$$

Substituting C.1.2 into C.1.1 and henceforth using the relative ($y = t_2 - t_1$) and average time ($t = (t_1 + t_2)/2$), we find that the lepton asymmetry may be rewritten as

$$L_{\mathbf{k}}(t,t) = -\mathcal{C}\int_0^t dt_1 \int_0^t dt_2 \mathrm{tr}\Big\{\Delta^{<}_{\mathbf{q}'}(y)\Delta^{<}_{\mathbf{q}}(y)S^{<}_{\mathbf{k}'}(y)S^{<}_{\mathbf{k}}(y) - \Delta^{>}_{\mathbf{q}'}(y)\Delta^{>}_{\mathbf{q}}(y)S^{>}_{\mathbf{k}'}(y)S^{>}_{\mathbf{k}}(y)\Big\}, \tag{C.1.3}$$

and simplified using the following set of symmetry relations

$$\begin{aligned}\Delta^{>}_{\mathbf{q}}(y)^* = \Delta^{<}_{\mathbf{q}}(y) &\implies \Delta^{>}_{\mathbf{q}}(y) = \Delta^{<}_{\mathbf{q}}(y)^*, \\ S^{>}_{\mathbf{k}}(y)^* = CS^{<}_{\mathbf{k}}(y)C^{-1} &\implies S^{>}_{\mathbf{k}}(y) = C^*S^{<}_{\mathbf{k}}(y)^*C^T.\end{aligned} \tag{C.1.4}$$

As a consequence the lepton asymmetry is given by

$$\begin{aligned} L_{\mathbf{k}}(t,t) &= \mathcal{C}\int_0^t dt_1\int_0^t dt_2 \mathrm{tr}\Big\{\Delta^<_{\mathbf{q}'}(y)\Delta^<_{\mathbf{q}}(y)S^<_{\mathbf{k}'}(y)S^<_{\mathbf{k}}(y) \\ &\quad - \Delta^<_{\mathbf{q}'}(y)^*\Delta^<_{\mathbf{q}}(y)^*C^*S^<_{\mathbf{k}'}(y)C^TC^*S^>_{\mathbf{k}}(y)C^T\Big\} \\ &= -2i\times\int_0^t dt_1\int_0^t dt_2\underbrace{\mathrm{Im}(\mathcal{C})}_{\text{prefactor}}\underbrace{\mathrm{Im}\Big(\mathrm{tr}\Big\{\Delta^<_{\mathbf{q}'}(y)\Delta^<_{\mathbf{q}}(y)S^<_{\mathbf{k}'}(y)S^<_{\mathbf{k}}(y)\Big\}\Big)}_{\text{Matrix-Element}}. \end{aligned} \tag{C.1.5}$$

It is easy to see the lepton asymmetry has factorised in two parts: one involves calculating $\mathcal{C}$, which is a prefactor dependent upon the Weinberg operator coefficient, λ and the other involves calculating the finite-temperature matrix element of the self-energy correction. The integral evaluation and prefactor and matrix element will be discussed in Section C.2 and Section C.3 respectively.

C.2 Prefactor

The prefactor is part of the lepton asymmetry which is dependent upon the coefficient of the Weinberg operator. As this prefactor is a function of time, we will need to integrate over time

$$L(t,t)\propto\int_{t_i}^{t_f}dt_1\int_{t_i}^{t_f}dt_2\mathrm{Im}\left(\lambda^*_{\alpha\beta}(t_1)\lambda_{\alpha\beta}(t_2)\right).$$

For the remainder of this calculation, the matrix structure of λ will be dropped in order to simplify the discussion. We make the following ansatz for the time dependent form of the coupling

$$\lambda\left(t\right)=\lambda^0+\frac{\lambda^1}{2}\left(1+\tanh\left(\frac{z-v_wt}{L_w}\right)\right), \tag{C.2.6}$$

where v_w is the velocity of the bubble wall, L_w is the width of the bubble wall and z is the direction of expansion of the bubble wall. However as mentioned in earlier sections, bubble properties do not affect the final lepton asymmetry due to the fast-bubble expansion and a thin-wall assumption. Eq. (C.2.6) shows a typical functional form of the bubble-wall we assume and this is similar to EWBG examples.

The imaginary part may be found in the following way

$$\begin{aligned}
\lambda^*(t_1) &= \lambda_0^* + \frac{\lambda_1^*}{2}\left(1+\tanh\left(\frac{z-v_w t_1}{L_w}\right)\right)\\
\lambda(t_2) &= \lambda_0 + \frac{\lambda_1}{2}\left(1+\tanh\left(\frac{z-v_w t_2}{L_w}\right)\right) \implies\\
\mathrm{Im}\left[\lambda^*(t_1)\lambda(t_2)\right] &= \mathrm{Im}\left[\frac{\lambda_0^*\lambda_1}{2}\left(1+\tanh\left(\frac{z-v_w t_2}{L_w}\right)\right)+\frac{\lambda_0\lambda_1^*}{2}\left(1+\tanh\left(\frac{z-v_w t_1}{L_w}\right)\right)\right]\\
&= \mathrm{Im}\left[\lambda_0^*\lambda_1\right]\left\{\left(1+\tanh\left(\frac{z-v_w t_2}{L_w}\right)\right)-\left(1+\tanh\left(\frac{z-v_w t_1}{L_w}\right)\right)\right\}\\
&= \mathrm{Im}\left[\lambda_0^*\lambda_1\right]\left\{\tanh\left(\frac{z-v_w t_2}{L_w}\right)-\tanh\left(\frac{z-v_w t_1}{L_w}\right)\right\}\\
&= \mathrm{Im}\left[\lambda_0^*\lambda_1\right]\left\{\frac{\sinh\left(z-v_w t_2/L_w\right)}{\cosh\left(z-v_w t_2/L_w\right)}-\frac{\sinh\left(z-v_w t_1/L_w\right)}{\cosh\left(z-v_w t_1/L_w\right)}\right\}.
\end{aligned} \tag{C.2.7}$$

The numerator of Eq. (C.2.7) may be found using the following identity

$$\sinh(a-b)\cosh(a-c)-\sinh(a-c)\cosh(a-b)=-\sinh(b-c),$$

and gives the result

$$\text{numerator} = -\sinh\left(\frac{v_w}{L_w}(t_2-t_1)\right) = -\sinh\left(\frac{v_w}{L_w}y\right).$$

To simplify the denominator, we can make use of the relative and average coordinates

$$y = t_2 - t_1 \quad \text{and} \quad t = \frac{t_1+t_2}{2} \implies t_1 = \frac{2t-y}{2} \quad \text{and} \quad t_2 = \frac{y+2t}{2}.$$

Applying this change of coordinate, we may rewrite the denominator as

$$\text{denominator} = \cosh\left(\frac{z-v_w\left(t+y/2\right)}{L_w}\right)\cosh\left(\frac{z-v_w\left(t-y/2\right)}{L_w}\right). \tag{C.2.8}$$

Expanding Eq. (C.2.8) and multiplying out the denominator we find

$$\text{denominator} = \frac{1}{2}\cosh\left(2\frac{z-v_w t}{L_w}\right)+\frac{1}{2}\cosh\left(\frac{v_w y}{L_w}\right).$$

This implies that

$$\mathrm{Im}\left(\lambda^*(t_1)\lambda(t_2)\right) = \mathrm{Im}\left[\lambda_0^*\lambda_1\right]\frac{\sinh\left(\frac{v_w}{L_w}y\right)}{\cosh\left(2\frac{z-v_w t}{L_w}\right)+\cosh\left(\frac{v_w y}{L_w}\right)}. \tag{C.2.9}$$

As $\mathrm{Im}\left(\lambda^*(t_1)\lambda(t_2)\right)$ has been rewritten as a function of y and t, we may change integration variables as well

$$\int_{t_i}^{t_f} dt_1 \int_{t_i}^{t_f} dt_2 = \int_{t_i-t_f}^{0} dy \int_{t_i-\frac{y}{2}}^{t_f+\frac{y}{2}} dt + \int_{0}^{t_f-t_i} dy \int_{t_i+\frac{y}{2}}^{t_f-\frac{y}{2}} dt.$$

In addition, we apply the formula

$$\int_{-\infty}^{\infty} dx_2 \frac{\sinh\left(2x_1\right)}{\cosh\left(2x_2\right)+\cosh\left(x_1\right)} = \frac{1}{2}\frac{\cosh\left(x_1+x_2\right)}{\cosh\left(x_1-x_2\right)}\Bigg|_{-\infty}^{\infty} = 2y,$$

and we find that

$$\int_0^t dt_1 \int_0^t dt_2 \mathrm{Im}\left[\lambda^*\left(t_1\right)\lambda\left(t_2\right)\right] = \mathrm{Im}\left[\lambda_0^*\lambda_1\right] y.$$

C.3 Matrix Element

To calculate the matrix element we will apply the CTP Feynman rules and use the free equilibrium propagators of the massless leptons and Higgs field which are given by [227]

$$\begin{aligned} \Delta_q^< &= \left(\frac{1}{2q}\coth\left(\frac{\beta q}{2}\right)\cos\left(qy\right) + i\sin(qy)\right) e^{-\gamma_H|y|}, \\ S_k^< &= \frac{e^{-\gamma_\ell|y|}}{2}\left\{\gamma^0\left(\cos\left(ky\right) - i\tanh\left(\frac{\beta k}{2}\right)\sin\left(ky\right)\right)\right. \\ &\qquad \left. -\gamma\hat{k}\left(\tanh\left(\frac{\beta k}{2}\right)\cos\left(ky\right) + i\sin\left(ky\right)\right)\right\}, \end{aligned} \tag{C.3.10}$$

where γ_H (γ_ℓ) is the Higgs (lepton) thermal width and we apply the notation $k = \vec{k}$, $q = \vec{q}$ and $\hat{k} = \vec{k}/k$. These propagators may be simplified using the redefinition of

the relative coordinate $y^- = y - i\beta/2$ where $\beta = 1/T$

$$\Delta_q^< = \frac{1}{2q}\left(\coth\left(\frac{\beta q}{2}\right)\cos(qy) + i\sin(qy)\right) \tag{C.3.11}$$

$$= \frac{1}{2q}\left(\coth\left(\frac{\beta q}{2}\right)\cos\left(qy^- + \frac{i\beta q}{2}\right) + i\sin\left(qy^- + \frac{iq\beta}{2}\right)\right) \tag{C.3.12}$$

$$= \frac{1}{2q}\frac{\cos(qy^-)}{\sinh\left(\frac{q\beta}{2}\right)}, \tag{C.3.13}$$

$$S_k^< = \frac{\gamma^0}{2}\left(\cos\left(ky^-\right) - i\tanh\left(\frac{\beta k}{2}\right)\sin\left(ky^-\right)\right) \tag{C.3.14}$$

$$- \frac{\gamma\hat{k}}{2}\left(\tanh\left(\frac{\beta k}{2}\right)\cos\left(ky^-\right) + i\sin(ky)\right) \tag{C.3.15}$$

$$= \frac{\gamma^0}{2}\left(\cos\left(ky^- + \frac{i\beta k}{2}\right) - i\tanh\left(\frac{\beta k}{2}\right)\sin\left(ky^- + \frac{i\beta k}{2}\right)\right) \tag{C.3.16}$$

$$- \frac{\gamma\hat{k}}{2}\left(\tanh\left(\frac{\beta k}{2}\right)\cos\left(ky^- + \frac{i\beta k}{2}\right) + i\sin\left(ky^- + \frac{i\beta k}{2}\right)\right) \tag{C.3.17}$$

$$= -\frac{\gamma^0}{2}\frac{\cos(ky^-)}{\cosh\left(\frac{\beta k}{2}\right)} - i\frac{\hat{k}\gamma\sin(ky^-)}{2\cosh\frac{\beta k}{2}}. \tag{C.3.18}$$

Substituting Eq. (C.3.11) into Eq. (C.1.5), the trace will pick up the gamma matrices

$$\begin{aligned}\mathrm{tr}\left\{\Delta_{q'}^<\Delta_q^< S_{k'}^< S_k^<\right\} &= \left(\frac{\cos(qy^-)\cos(q'y^-)}{4qq'\sinh\left(\frac{q\beta}{2}\right)\sinh\left(\frac{q'\beta}{2}\right)}\right) \\ &\left(\underbrace{\mathrm{Tr}\left(\frac{\gamma^0\gamma^0}{4}\right)}_{1}\frac{\cos(ky^-)\cos(k'y^-)}{\cosh\left(\frac{k\beta}{2}\right)\cosh\left(\frac{k'\beta}{2}\right)} - \underbrace{\mathrm{Tr}\left(\frac{\gamma\gamma}{4}\right)}_{-\delta}\frac{\hat{k}\hat{k}'\sin(ky^-)\sin(k'y^-)}{\cosh\left(\frac{k\beta}{2}\right)\cosh\left(\frac{k'\beta}{2}\right)}\right) \\ &= \frac{1}{8qq'}\left(\frac{\cos(qy^-)\cos(q'y^-)}{\sinh\left(\frac{q\beta}{2}\right)\sinh\left(\frac{q'\beta}{2}\right)\cosh\left(\frac{k\beta}{2}\right)\cosh\left(\frac{k'\beta}{2}\right)}\right) \\ &\left\{\cos\left(ky^-\right)\cos\left(k'y^-\right) + \delta_{ij}\hat{k^i}\hat{k'^j}\sin\left(ky^-\right)\sin\left(k'y^-\right)\right\},\end{aligned} \tag{C.3.19}$$

This integrand must be integrated over phase space, however for the moment we shall concentrate on the simplifying $\mathrm{tr}\left\{\Delta_{q'}^<\Delta_q^< S_{k'}^< S_k^<\right\}$

$$\text{numerator} = \underbrace{\cos\left(qy^-\right)\cos\left(q'y^-\right)}_{A}\left(\underbrace{\cos\left(ky^-\right)\cos\left(k'y^-\right)}_{B} + \underbrace{\delta_{ij}\hat{k^i}\hat{k'^j}\sin\left(ky^-\right)\sin\left(k'y^-\right)}_{C}\right). \tag{C.3.20}$$

Multiplying out $A \times B$ and then $A \times C$

$$\begin{aligned} A \times B = &\left(\frac{e^{i(q+q')y'} + e^{i(q-q')y^-} + e^{i(q'-q)y'} + e^{-i(q+q')y^-}}{4} \right) \\ &\times \left(\frac{e^{i(k+k')y'} + e^{i(k-k')y^-} + e^{i(k'-k)y'} + e^{-i(k+k')y^-}}{4} \right) \\ &= \frac{1}{16}\Big(e^{i(q+q'+k+k')y^-} + e^{i(q-q'+k+k')y^-} + e^{i(-q+q'+k+k')y^-} + e^{i(-q-q'+k+k')y^-} \\ &+ e^{i(q+q'+k-k')y^-} + e^{i(q-q'+k-k')y^-} + e^{i(-q+q'+k-k')y^-} + e^{i(-q-q'+k-k')y^-} + \text{C.C} \Big). \end{aligned} \tag{C.3.21}$$

Recalling $y^- = y - i\beta/2$, we may make the expansion $e^{i(xy - ix\beta/2)} \equiv e^{ixy}e^{\beta x/2}$. To find the imaginary part this implies $\text{Im}[e^{ixy}e^{\beta x/2}] \equiv \sin(xy)e^{\beta x/2}$. Applying this to Eq. (C.3.21) we find

$$\begin{aligned} A \times B = \frac{1}{16}\Big(&\sin\left(q + q' + k + k'\right) e^{\beta/2(q+q'+k+k')} \\ &+ \sin\left(q - q' + k + k'\right) e^{\beta/2(q-q'+k+k')} \\ &+ \sin\left(-q + q' + k + k'\right) e^{\beta/2(-q+q'+k+k')} \\ &+ \sin\left(-q - q' + k + k'\right) e^{\beta/2(-q-q'+k+k')} \\ &+ \sin\left(q + q' + k - k'\right) e^{\beta/2(q+q'+k-k')} \\ &+ \sin\left(q - q' + k - k'\right) e^{\beta/2(q-q'+k-k')} \\ &+ \sin\left(-q + q' + k - k'\right) e^{\beta/2(-q+q'+k-k')} \\ &+ \sin\left(-q - q' + k - k'\right) e^{\beta/2(-q-q'+k-k')} + \text{C.C} \Big). \end{aligned} \tag{C.3.22}$$

How do we handle the complex conjugate (C.C) part of the above equation? Consider $e^{-ixy^-} \equiv e^{-i(xy - i\beta/2)} = e^{-ixy}e^{-\beta/2} \implies \text{Im}[e^{-ixy}e^{-\beta/2}] = -\sin(xy)\, e^{-\beta/2}$. There adding to its complex conjugate, we find $\sin(xy)\, e^{\beta x/2} - \sin(xy)\, e^{-\beta x/2} = 2\sin(xy)\sinh(\beta x/2)$. This implies Eq. (C.3.21) may be written as

$$\begin{aligned} A \times B = \frac{2}{16}\Bigg\{ &\sin\left(K_{+++}y\right)\sinh\left(\frac{\beta K_{+++}}{2}\right) + \sin\left(K_{++-}y\right)\sinh\left(\frac{\beta K_{++-}}{2}\right) \\ &+ \sin\left(K_{+-+}y\right)\sinh\left(\frac{\beta K_{+-+}}{2}\right) + \sin\left(K_{+--}y\right)\sinh\left(\frac{\beta K_{+--}}{2}\right) \\ &+ \sin\left(K_{-++}y\right)\sinh\left(\frac{\beta K_{-++}}{2}\right) + \sin\left(K_{-+-}y\right)\sinh\left(\frac{\beta K_{-+-}}{2}\right) \\ &+ \sin\left(K_{--+}y\right)\sinh\left(\frac{\beta K_{--+}}{2}\right) + \sin\left(K_{---}y\right)\sinh\left(\frac{\beta K_{---}}{2}\right) \Bigg\}, \end{aligned} \tag{C.3.23}$$

where we have applied the following definitions for ease of notation

$$\begin{aligned}
K_{+++} &= k + k' + q + q' \\
K_{++-} &= k + k' + q - q' \\
K_{+-+} &= k + k' - q + q' \\
K_{+--} &= k + k' - q - q' \\
K_{-++} &= k - k' + q + q' \\
K_{-+-} &= k - k' + q - q' \\
K_{--+} &= k - k' - q + q' \\
K_{---} &= k - k' - q - q'
\end{aligned} \tag{C.3.24}$$

where $K_{\eta_2\eta_3\eta_4} = k + \eta_2 k' + \eta_3 q + \eta_4 q'$ and $\eta_i = \pm 1$. Applying the same procedure, we calculate $A \times C$

$$\begin{aligned}
A \times C = \frac{\hat{k}\hat{k}'}{16}\Big\{ &- \sin\left(K_{+++}y\right) e^{\beta K_{+++}/2} - \sin\left(K_{++-}y\right) e^{\beta K_{++-}/2} \\
&- \sin\left(K_{+-+}y\right) e^{\beta K_{+-+}/2} - \sin\left(K_{+--}y\right) e^{\beta K_{+--}/2} \\
&+ \sin\left(K_{-++}y\right) e^{\beta K_{-++}/2} + \sin\left(K_{-+-}y\right) e^{\beta K_{-+-}/2} \\
&- \sin\left(K_{--+}y\right) e^{\beta K_{--+}/2} + \sin\left(K_{---}y\right) e^{\beta K_{---}/2} + \text{C.C.}\Big\}.
\end{aligned} \tag{C.3.25}$$

Adding the complex conjugate part in the same way as before we find

$$\begin{aligned}
A \times C = \frac{2\hat{k}\hat{k}'}{16}\Big\{ &- \sin\left(K_{+++}y\right) \sinh\left(\frac{\beta K_{+++}}{2}\right) - \sin\left(K_{++-}y\right) \sinh\left(\frac{\beta K_{++-}}{2}\right) \\
&- \sin\left(K_{+-+}y\right) \sinh\left(\frac{\beta K_{+-+}}{2}\right) - \sin\left(K_{+--}y\right) \sinh\left(\frac{\beta K_{+--}}{2}\right) \\
&+ \sin\left(K_{-++}y\right) \sinh\left(\frac{\beta K_{-++}}{2}\right) + \sin\left(K_{-+-}y\right) \sinh\left(\frac{\beta K_{-+-}}{2}\right) \\
&+ \sin\left(K_{--+}y\right) \sinh\left(\frac{\beta K_{--+}}{2}\right) + \sin\left(K_{---}y\right) \sinh\left(\frac{\beta K_{---}}{2}\right)\Big\}.
\end{aligned} \tag{C.3.26}$$

Adding $A\times B$ to $A\times C$, and using the Lorentz-invariance of the vacuum contribution, we find the integrand may be written as

$$\begin{aligned}\mathcal{M} = \mathrm{Im}\left(\mathrm{tr}\left\{\Delta^{<}_{\mathbf{q}'}\Delta^{<}_{\mathbf{q}}S^{<}_{\mathbf{k}'}S^{<}_{\mathbf{k}}\right\}\right) &= \frac{1}{8qq'\sinh\left(\frac{\mathbf{q}\beta}{2}\right)\sinh\left(\frac{q'\beta}{2}\right)\cosh\left(\frac{k\beta}{2}\right)\cosh\left(\frac{k'\beta}{2}\right)} \\ &\frac{k.k'}{8kk'}\Bigg\{-\sin\left(K_{+++}y\right)\sinh\left(\frac{\beta K_{+++}}{2}\right)-\sin\left(K_{++-}y\right)\sinh\left(\frac{\beta K_{++-}}{2}\right) \\ &-\sin\left(K_{+-+}y\right)\sinh\left(\frac{\beta K_{+-+}}{2}\right)-\sin\left(K_{+--}y\right)\sinh\left(\frac{\beta K_{+--}}{2}\right) \\ &+\sin\left(K_{-++}y\right)\sinh\left(\frac{\beta K_{-++}}{2}\right)+\sin\left(K_{-+-}y\right)\sinh\left(\frac{\beta K_{-+-}}{2}\right) \\ &+\sin\left(K_{--+}y\right)\sinh\left(\frac{\beta K_{--+}}{2}\right)+\sin\left(K_{---}y\right)\sinh\left(\frac{\beta K_{---}}{2}\right)\Bigg\}e^{-2\gamma|y|}.\end{aligned} \tag{C.3.27}$$

In summary the matrix element integration is given by

$$\int\frac{d^3k}{(2\pi)^3}\int\frac{d^3q}{(2\pi)^3}\int\frac{d^3q'}{(2\pi)^3}\int dyy\mathcal{M}. \tag{C.3.28}$$

where $\gamma=\gamma_\ell+\gamma_H$, $k'=-\left(k+q+q'\right)$ and note that the y factor came from the prefactor time integration. We may make use of the fact $\mathcal{M}$ is an odd function of y

$$\begin{aligned}\int_{-\infty}^{+\infty}dyyM &= 2\int_0^{+\infty}dyyM \\ &= 2\int dyy\frac{\mathrm{Im}\left\{\cos\left(qy\right)\cos\left(q'y\right)\cos\left(qy\right)\left[\cos\left(ky\right)\cos\left(k'y\right)+kk'\cos\left(ky\right)\cos\left(k'y\right)\right]\right\}}{8q'q\left(\sinh\left(q\beta/2\right)\sinh\left(q'\beta/2\right)\cosh\left(q\beta/2\right)\cosh\left(q'\beta/2\right)\right)}e^{-2|\gamma|y} \\ &= -\sum_{\eta_2,\eta_3,\eta_4=\pm1}\frac{K_{\eta_2\eta_3\eta_4}\gamma\sinh\left(\beta K_{\eta_2\eta_3\eta_4}/2\right)\left[1-\eta_2\hat{k}\hat{k}'\right]}{16qq'\left(K^2_{\eta_2\eta_3\eta_4}+4\gamma^2\right)^2\sinh\left(q\beta/2\right)\sinh\left(q'\beta/2\right)\cosh\left(q\beta/2\right)\cosh\left(q'\beta/2\right)}.\end{aligned} \tag{C.3.29}$$

The blue coloured parts of Eq. (C.3.29) uses the formula

$$\int_0^\infty x\sin\left(ax\right)e^{-2bx}=\frac{4ab}{\left(a^2+4b^2\right)^2}.$$

In order to calculate the momentum integration we use technique similar to those of [227] and, for these reasons, will not repeat the phase space integration and instead refer the reader to the aforementioned reference. We assume $p\equiv k-q$ and replace the momentum integration $d^3q'd^3q$ with $d^3k'd^3p$ where $p\equiv k'+p'$. Using

the parametrisation of [227]

$$\begin{aligned} p &= |p|\,(1,0,0)\,, \\ k &= |k|\,(\sin\theta,0,\cos\theta)\,, \\ k' &= |k'|\,(\sin\theta'\cos\varphi',\sin\theta'\sin\varphi',\cos\theta')\,. \end{aligned} \tag{C.3.30}$$

$$\begin{aligned} &\int \frac{d^3k}{(2\pi)^3}\int \frac{d^3q}{(2\pi)^3}\int \frac{d^3q'}{(2\pi)^3} = \int \frac{d^3k}{(2\pi)^3}\int \frac{d^3p}{(2\pi)^3}\int \frac{d^3k'}{(2\pi)^3} \\ &\frac{1}{(2\pi)^2}\int_0^\infty dp\int_0^\infty pdp\int_0^\infty k'dk'\int_{k-p}^{k+p} qdq\int_{k'-p}^{k'+p} q'dq' \end{aligned} \tag{C.3.31}$$

where we have used

$$q^2 = k^2+p^2-2kp\cos\theta \quad \text{and} \quad q'^2 = k'^2+p^2-2k'p\cos\theta.$$

Finally, we may rescale the momentum by temperature i.e $k \to k\beta/2$ and use the following substitution

$$x_1 = k\beta/2, \quad x_2 = k'\beta/2, \quad x_3 = q\beta/2, \quad x_4 = q'\beta/2, \quad x_\gamma = \gamma\beta \quad \text{and} \quad x = p\beta/2. \tag{C.3.32}$$

The final lepton asymmetry is given by[1]

$$L = \frac{3\mathrm{Im}\left[m_\nu^0 m_\nu^*\right]T^5}{(2\pi)^4\, v_H^4} F\left(x_1, x_\gamma\right).$$

$F\left(x_1, x_\gamma\right)$ is a loop factor and is given by

$$\begin{aligned} F\left(x_1,x_\gamma\right) = \frac{1}{x_1}\int_0^\infty dx\int_0^\infty x_1dx_1\int_0^\infty x_2dx_2\int_{x_1-x}^{x_1+x} dx_3\int_{x_2-x}^{x_2+x} dx_4 \sum_{\eta_2,\eta_3,\eta_4=\pm1} \\ \left[1-\frac{\left(x_1^2+x^2-x_3^2\right)\left(x_2^2+x^2-x_4^2\right)}{4\eta_2 x_1x_2x^2}\right]\frac{K_{\eta_2\eta_3\eta_4}\gamma\sinh\left(\beta K_{\eta_2\eta_3\eta_4}/2\right)}{\left(K_{\eta_2\eta_3\eta_4}^2+4\gamma^2\right)^2\sinh x_1\sinh x_2\cosh x_3\cosh x_4}. \end{aligned} \tag{C.3.33}$$

For fixed values of γ ($\gamma_{\rm SM} \simeq 0.1$), we may integrate over x_1 which is the temperature normalised three-momentum of the external lepton and the results are shown in Fig. 4.17.

[1]Note the temperature to the fifth power comes from the five-variable integration.

Bibliography

[1] P. Ballett, S. Pascoli, and J. Turner. "Mixing angle and phase correlations from A5 with generalized CP and their prospects for discovery". In: *Phys. Rev.* D92.9 (2015), p. 093008. DOI: 10.1103/PhysRevD.92.093008. arXiv: 1503.07543 [hep-ph].

[2] J. Turner. "Predictions for leptonic mixing angle correlations and nontrivial Dirac CP violation from A_5 with generalized CP symmetry". In: *Phys. Rev.* D92.11 (2015), p. 116007. DOI: 10.1103/PhysRevD.92.116007. arXiv: 1507.06224 [hep-ph].

[3] S. Pascoli, J. Turner, and Y.-L. Zhou. "Baryogenesis via leptonic CP-violating phase transition". In: (2016). arXiv: 1609.07969 [hep-ph].

[4] E. Fermi. "An attempt of a theory of beta radiation. 1." In: *Z. Phys.* 88 (1934), pp. 161–177. DOI: 10.1007/BF01351864.

[5] H. Bethe and R. Peierls. "The 'neutrino'". In: *Nature* 133 (1934), p. 532. DOI: 10.1038/133532a0.

[6] F. Reines and C. L. Cowan. "Detection of the free neutrino". In: *Phys. Rev.* 92 (1953), pp. 830–831. DOI: 10.1103/PhysRev.92.830.

[7] M. Goldhaber, L. Grodzins, and A. W. Sunyar. "Helicity of Neutrinos". In: *Phys. Rev.* 109 (1958), pp. 1015–1017. DOI: 10.1103/PhysRev.109.1015.

[8] B. Pontecorvo. "Neutrino Experiments and the Problem of Conservation of Leptonic Charge". In: *Sov. Phys. JETP* 26 (1968). [Zh. Eksp. Teor. Fiz.53,1717(1967)], pp. 984–988.

[9] Z. Maki, M. Nakagawa, and S. Sakata. "Remarks on the unified model of elementary particles". In: *Prog. Theor. Phys.* 28 (1962), pp. 870–880. DOI: 10.1143/PTP.28.870.

[10] B. T. Cleveland et al. "Measurement of the solar electron neutrino flux with the Homestake chlorine detector". In: *Astrophys. J.* 496 (1998), pp. 505–526. DOI: 10.1086/305343.

[11] S. P. Mikheev and A. Yu. Smirnov. "Resonance Amplification of Oscillations in Matter and Spectroscopy of Solar Neutrinos". In: *Sov. J. Nucl. Phys.* 42 (1985). [Yad. Fiz.42,1441(1985)], pp. 913–917.

[12] L Wolfenstein. "Neutrino Oscillations in Matter". In: *Phys. Rev.* D17 (1978).

[13] M. L. Perl et al. "Evidence for Anomalous Lepton Production in e+ - e- Annihilation". In: *Phys. Rev. Lett.* 35 (1975), pp. 1489–1492. DOI: 10.1103/PhysRevLett.35.1489.

[14] M. Acciarri et al. "Determination of the number of light neutrino species from single photon production at LEP". In: *Phys. Lett.* B431 (1998), pp. 199–208. DOI: 10.1016/S0370-2693(98)00519-X.

[15] K. Kodama et al. "Detection and analysis of tau neutrino interactions in DONUT emulsion target". In: *Nucl. Instrum. Meth.* A493 (2002), pp. 45–66. DOI: 10.1016/S0168-9002(02)01555-3.

[16] Y. Fukuda et al. "Evidence for oscillation of atmospheric neutrinos". In: *Phys. Rev. Lett.* 81 (1998), pp. 1562–1567. DOI: 10.1103/PhysRevLett.81.1562. arXiv: hep-ex/9807003 [hep-ex].

[17] Q. R. Ahmad et al. "Measurement of the rate of $\nu_e + d \rightarrow p + p + e^-$ interactions produced by ^8B solar neutrinos at the Sudbury Neutrino Observatory". In: *Phys. Rev. Lett.* 87 (2001), p. 071301. DOI: 10.1103/PhysRevLett.87.071301. arXiv: nucl-ex/0106015 [nucl-ex].

[18] Q. R. Ahmad et al. "Direct evidence for neutrino flavor transformation from neutral current interactions in the Sudbury Neutrino Observatory". In: *Phys.*

Rev. Lett. 89 (2002), p. 011301. DOI: 10.1103/PhysRevLett.89.011301. arXiv: nucl-ex/0204008 [nucl-ex].

[19] N. Cabibbo. "Unitary Symmetry and Leptonic Decays". In: *Phys. Rev. Lett.* 10 (1963). [,648(1963)], pp. 531–533. DOI: 10.1103/PhysRevLett.10.531.

[20] M. Kobayashi and T. Maskawa. "CP Violation in the Renormalizable Theory of Weak Interaction". In: *Prog. Theor. Phys.* 49 (1973), pp. 652–657. DOI: 10.1143/PTP.49.652.

[21] K. A. Olive et al. "Review of Particle Physics". In: *Chin. Phys.* C38 (2014), p. 090001. DOI: 10.1088/1674-1137/38/9/090001.

[22] E. K. Akhmedov and A. Yu. Smirnov. "Paradoxes of neutrino oscillations". In: *Phys. Atom. Nucl.* 72 (2009), pp. 1363–1381. DOI: 10.1134/S1063778809080122. arXiv: 0905.1903 [hep-ph].

[23] I. Esteban et al. "Updated fit to three neutrino mixing: exploring the accelerator-reactor complementarity". In: *JHEP* 01 (2017), p. 087. DOI: 10.1007/JHEP01(2017)087. arXiv: 1611.01514 [hep-ph].

[24] W. W. M. Allison et al. "The Atmospheric neutrino flavor ratio from a 3.9 fiducial kiloton year exposure of Soudan-2". In: *Phys. Lett.* B449 (1999), pp. 137–144. DOI: 10.1016/S0370-2693(99)00056-8. arXiv: hep-ex/9901024 [hep-ex].

[25] K. S. Hirata et al. "Observation of a small atmospheric muon-neutrino / electron-neutrino ratio in Kamiokande". In: *Phys. Lett.* B280 (1992), pp. 146–152. DOI: 10.1016/0370-2693(92)90788-6.

[26] A. Radovic. "Current Status and Future Plans of NOνA". Neutrino 2016. 2016. URL: https://indico.ph.qmul.ac.uk/indico/getFile.py/access?contribId=43&resId=0&materialId=slides&confId=112.

[27] G. Mention et al. "The Reactor Antineutrino Anomaly". In: *Phys. Rev.* D83 (2011), p. 073006. DOI: 10.1103/PhysRevD.83.073006. arXiv: 1101.2755 [hep-ex].

[28] F. P. An et al. "Observation of electron-antineutrino disappearance at Daya Bay". In: *Phys. Rev. Lett.* 108 (2012), p. 171803. DOI: 10.1103/PhysRevLett.108.171803. arXiv: 1203.1669 [hep-ex].

[29] F. P. An et al. "Improved Measurement of Electron Antineutrino Disappearance at Daya Bay". In: *Chin. Phys.* C37 (2013), p. 011001. DOI: 10.1088/1674-1137/37/1/011001. arXiv: 1210.6327 [hep-ex].

[30] J. K. Ahn et al. "Observation of Reactor Electron Antineutrino Disappearance in the RENO Experiment". In: *Phys. Rev. Lett.* 108 (2012), p. 191802. DOI: 10.1103/PhysRevLett.108.191802. arXiv: 1204.0626 [hep-ex].

[31] F. Ardellier et al. "Double Chooz: A Search for the neutrino mixing angle theta(13)". In: (2006). arXiv: hep-ex/0606025 [hep-ex].

[32] W. Hampel et al. "Final results of the Cr-51 neutrino source experiments in GALLEX". In: *Phys. Lett.* B420 (1998), pp. 114–126. DOI: 10.1016/S0370-2693(97)01562-1.

[33] M. Altmann et al. "Complete results for five years of GNO solar neutrino observations". In: *Phys. Lett.* B616 (2005), pp. 174–190. DOI: 10.1016/j.physletb.2005.04.068. arXiv: hep-ex/0504037 [hep-ex].

[34] J. N. Abdurashitov et al. "Measurement of the solar neutrino capture rate with gallium metal. III: Results for the 2002–2007 data-taking period". In: *Phys. Rev.* C80 (2009), p. 015807. DOI: 10.1103/PhysRevC.80.015807. arXiv: 0901.2200 [nucl-ex].

[35] H. A. Tanaka. "T2K: Latest Results". Neutrino 2016. 2016. URL: http://neutrino2016.iopconfs.org/IOP/media/uploaded/EVIOP/event_582/T2K_Neutrino_2016.pdf.

[36] P. B. Pal. "Dirac, Majorana and Weyl fermions". In: *Am. J. Phys.* 79 (2011), pp. 485–498. DOI: 10.1119/1.3549729. arXiv: 1006.1718 [hep-ph].

[37] P. Langacker, J. Erler, and E. Peinado. "Neutrino physics". In: *J. Phys. Conf. Ser.* 18 (2005), pp. 154–187. DOI: 10.1088/1742-6596/18/1/004. arXiv: hep-ph/0506257 [hep-ph].

[38] S. Weinberg. "Cosmological Production of Baryons". In: *Phys. Rev. Lett.* 42 (1979), pp. 850–853. DOI: 10.1103/PhysRevLett.42.850.

[39] P. Minkowski. "$\mu \to e\gamma$ at a Rate of One Out of 10^9 Muon Decays?" In: *Phys. Lett.* B67 (1977), pp. 421–428. DOI: 10.1016/0370-2693(77)90435-X.

[40] T. Yanagida. "HORIZONTAL SYMMETRY AND MASSES OF NEUTRINOS". In: *Conf. Proc.* C7902131 (1979), pp. 95–99.

[41] M. Gell-Mann, P. Ramond, and R. Slansky. "Complex Spinors and Unified Theories". In: *Conf. Proc.* C790927 (1979), pp. 315–321. arXiv: 1306.4669 [hep-th].

[42] R. N. Mohapatra and G. Senjanovic. "Neutrino Masses and Mixings in Gauge Models with Spontaneous Parity Violation". In: *Phys. Rev.* D23 (1981), p. 165. DOI: 10.1103/PhysRevD.23.165.

[43] P.-H. Gu et al. "Neutrino masses, leptogenesis and dark matter in hybrid seesaw". In: *Phys. Rev.* D79 (2009), p. 033010. DOI: 10.1103/PhysRevD.79.033010. arXiv: 0811.0953 [hep-ph].

[44] P.-H. Gu et al. "Double Type-II Seesaw, Baryon Asymmetry and Dark Matter for Cosmic $e^{\pm}$ Excesses". In: *Phys. Rev.* D80 (2009), p. 053004. DOI: 10.1103/PhysRevD.80.053004. arXiv: 0906.0442 [hep-ph].

[45] D. Aristizabal Sierra, M. Dhen, and T. Hambye. "Scalar triplet flavored leptogenesis: a systematic approach". In: *JCAP* 1408 (2014), p. 003. DOI: 10.1088/1475-7516/2014/08/003. arXiv: 1401.4347 [hep-ph].

[46] W. Chao, S. Luo, and Z.-z. Xing. "Neutrino mixing and leptogenesis in type-II seesaw scenarios with left-right symmetry". In: *Phys. Lett.* B659 (2008), pp. 281–289. DOI: 10.1016/j.physletb.2007.11.028. arXiv: 0704.3838 [hep-ph].

[47] J. McDonald, N. Sahu, and U. Sarkar. "Type-II Seesaw at Collider, Lepton Asymmetry and Singlet Scalar Dark Matter". In: *JCAP* 0804 (2008), p. 037. DOI: 10.1088/1475-7516/2008/04/037. arXiv: 0711.4820 [hep-ph].

[48] S. Antusch and S. F. King. "Leptogenesis in unified theories with type II see-saw". In: *JHEP* 01 (2006), p. 117. DOI: 10.1088/1126-6708/2006/01/117. arXiv: hep-ph/0507333 [hep-ph].

[49] B. Brahmachari, E. Ma, and U. Sarkar. "Supersymmetric model of neutrino mass and leptogenesis with string scale unification". In: *Phys. Lett.* B520 (2001), pp. 152–158. DOI: 10.1016/S0370-2693(01)01123-6. arXiv: hep-ph/0105278 [hep-ph].

[50] T. Hambye et al. "Constraints on neutrino masses from leptogenesis models". In: *Nucl. Phys.* B695 (2004), pp. 169–191. DOI: 10.1016/j.nuclphysb.2004.06.027. arXiv: hep-ph/0312203 [hep-ph].

[51] S. Blanchet and P. Fileviez Perez. "Baryogenesis via Leptogenesis in Adjoint SU(5)". In: *JCAP* 0808 (2008), p. 037. DOI: 10.1088/1475-7516/2008/08/037. arXiv: 0807.3740 [hep-ph].

[52] D. Aristizabal Sierra, J. F. Kamenik, and M. Nemevsek. "Implications of Flavor Dynamics for Fermion Triplet Leptogenesis". In: *JHEP* 10 (2010), p. 036. DOI: 10.1007/JHEP10(2010)036. arXiv: 1007.1907 [hep-ph].

[53] R. N. Mohapatra. "Mechanism for Understanding Small Neutrino Mass in Superstring Theories". In: *Phys. Rev. Lett.* 56 (1986), pp. 561–563. DOI: 10.1103/PhysRevLett.56.561.

[54] R. N. Mohapatra and J. W. F. Valle. "Neutrino Mass and Baryon Number Nonconservation in Superstring Models". In: *Phys. Rev.* D34 (1986), p. 1642. DOI: 10.1103/PhysRevD.34.1642.

[55] J. Bernabeu et al. "Lepton Flavor Nonconservation at High-Energies in a Superstring Inspired Standard Model". In: *Phys. Lett.* B187 (1987), pp. 303–308. DOI: 10.1016/0370-2693(87)91100-2.

[56] A. Zee. "A Theory of Lepton Number Violation, Neutrino Majorana Mass, and Oscillation". In: *Phys. Lett.* B93 (1980). [Erratum: Phys. Lett.B95,461(1980)], p. 389. DOI: 10.1016/0370-2693(80)90349-4,10.1016/0370-2693(80)90193-8.

[57] L. Wolfenstein. "A Theoretical Pattern for Neutrino Oscillations". In: *Nucl. Phys.* B175 (1980), pp. 93–96. DOI: 10.1016/0550-3213(80)90004-8.

[58] A. Zee. "Charged Scalar Field and Quantum Number Violations". In: *Phys. Lett.* B161 (1985), pp. 141–145. DOI: 10.1016/0370-2693(85)90625-2.

[59] K. S. Babu. "Model of 'Calculable' Majorana Neutrino Masses". In: *Phys. Lett.* B203 (1988), pp. 132–136. DOI: 10.1016/0370-2693(88)91584-5.

[60] E. Ma. "Pathways to naturally small neutrino masses". In: *Phys. Rev. Lett.* 81 (1998), pp. 1171–1174. DOI: 10.1103/PhysRevLett.81.1171. arXiv: hep-ph/9805219 [hep-ph].

[61] P. Fileviez Perez and M. B. Wise. "On the Origin of Neutrino Masses". In: *Phys. Rev.* D80 (2009), p. 053006. DOI: 10.1103/PhysRevD.80.053006. arXiv: 0906.2950 [hep-ph].

[62] K. S. Babu and S. Nandi. "Natural fermion mass hierarchy and new signals for the Higgs boson". In: *Phys. Rev.* D62 (2000), p. 033002. DOI: 10.1103/PhysRevD.62.033002. arXiv: hep-ph/9907213 [hep-ph].

[63] M.-C. Chen, A. de Gouvea, and B. A. Dobrescu. "Gauge Trimming of Neutrino Masses". In: *Phys. Rev.* D75 (2007), p. 055009. DOI: 10.1103/PhysRevD.75.055009. arXiv: hep-ph/0612017 [hep-ph].

[64] I. Gogoladze, N. Okada, and Q. Shafi. "NMSSM and Seesaw Physics at LHC". In: *Phys. Lett.* B672 (2009), pp. 235–239. DOI: 10.1016/j.physletb.2008.12.068. arXiv: 0809.0703 [hep-ph].

[65] G. F. Giudice and O. Lebedev. "Higgs-dependent Yukawa couplings". In: *Phys. Lett.* B665 (2008), pp. 79–85. DOI: 10.1016/j.physletb.2008.05.062. arXiv: 0804.1753 [hep-ph].

[66] J. Alexandre, C. M. Bender, and P. Millington. "Non-Hermitian extension of gauge theories and implications for neutrino physics". In: *JHEP* 11 (2015), p. 111. DOI: 10.1007/JHEP11(2015)111. arXiv: 1509.01203 [hep-th].

[67] Y. Grossman and M. Neubert. "Neutrino masses and mixings in nonfactorizable geometry". In: *Phys. Lett.* B474 (2000), pp. 361–371. DOI: 10.1016/S0370-2693(00)00054-X. arXiv: hep-ph/9912408 [hep-ph].

[68] N. Arkani-Hamed et al. "Neutrino masses from large extra dimensions". In: *Phys. Rev.* D65 (2001), p. 024032. DOI: 10.1103/PhysRevD.65.024032. arXiv: hep-ph/9811448 [hep-ph].

[69] L. J. Hall, H. Murayama, and N. Weiner. "Neutrino mass anarchy". In: *Phys. Rev. Lett.* 84 (2000), pp. 2572–2575. DOI: 10.1103/PhysRevLett.84.2572. arXiv: hep-ph/9911341 [hep-ph].

[70] N. Haba and H. Murayama. "Anarchy and hierarchy". In: *Phys. Rev.* D63 (2001), p. 053010. DOI: 10.1103/PhysRevD.63.053010. arXiv: hep-ph/0009174 [hep-ph].

[71] A. de Gouvea and H. Murayama. "Statistical test of anarchy". In: *Phys. Lett.* B573 (2003), pp. 94–100. DOI: 10.1016/j.physletb.2003.08.045. arXiv: hep-ph/0301050 [hep-ph].

[72] R. Barbieri et al. "Fermion masses and symmetry breaking of a U(2) flavor symmetry". In: *Nucl. Phys.* B550 (1999), pp. 32–40. DOI: 10.1016/S0550-3213(99)00195-9. arXiv: hep-ph/9812239 [hep-ph].

[73] R. Barbieri et al. "Unified theories with U(2) flavor symmetry". In: *Nucl. Phys.* B493 (1997), pp. 3–26. DOI: 10.1016/S0550-3213(97)00134-X. arXiv: hep-ph/9610449 [hep-ph].

[74] S. F. King and G. G. Ross. "Fermion masses and mixing angles from SU(3) family symmetry". In: *Phys. Lett.* B520 (2001), pp. 243–253. DOI: 10.1016/S0370-2693(01)01139-X. arXiv: hep-ph/0108112 [hep-ph].

[75] S. F. King and G. G. Ross. "Fermion masses and mixing angles from SU (3) family symmetry and unification". In: *Phys. Lett.* B574 (2003), pp. 239–252. DOI: 10.1016/j.physletb.2003.09.027. arXiv: hep-ph/0307190 [hep-ph].

[76] C. D. Froggatt and H. B. Nielsen. "Hierarchy of Quark Masses, Cabibbo Angles and CP Violation". In: *Nucl. Phys.* B147 (1979), pp. 277–298. DOI: 10.1016/0550-3213(79)90316-X.

[77] K. Abe et al. "Indication of Electron Neutrino Appearance from an Accelerator-produced Off-axis Muon Neutrino Beam". In: *Phys. Rev. Lett.* 107 (2011), p. 041801. DOI: 10.1103/PhysRevLett.107.041801. arXiv: 1106.2822 [hep-ex].

[78] Y. Abe et al. "Indication of Reactor $\bar{\nu}_e$ Disappearance in the Double Chooz Experiment". In: *Phys. Rev. Lett.* 108 (2012), p. 131801. DOI: 10.1103/PhysRevLett.108.131801. arXiv: 1112.6353 [hep-ex].

[79] M. Fukugita, M. Tanimoto, and T. Yanagida. "Atmospheric neutrino oscillation and a phenomenological lepton mass matrix". In: *Phys. Rev.* D57 (1998), pp. 4429–4432. DOI: 10.1103/PhysRevD.57.4429. arXiv: hep-ph/9709388 [hep-ph].

[80] V. D. Barger et al. "Bimaximal mixing of three neutrinos". In: *Phys. Lett.* B437 (1998), pp. 107–116. DOI: 10.1016/S0370-2693(98)00880-6. arXiv: hep-ph/9806387 [hep-ph].

[81] S. Davidson and S. F. King. "Bimaximal neutrino mixing in the MSSM with a single right-handed neutrino". In: *Phys. Lett.* B445 (1998), pp. 191–198. DOI: 10.1016/S0370-2693(98)01442-7. arXiv: hep-ph/9808296 [hep-ph].

[82] G. Altarelli, F. Feruglio, and L. Merlo. "Revisiting Bimaximal Neutrino Mixing in a Model with S(4) Discrete Symmetry". In: *JHEP* 05 (2009), p. 020. DOI: 10.1088/1126-6708/2009/05/020. arXiv: 0903.1940 [hep-ph].

[83] P. F. Harrison, D. H. Perkins, and W. G. Scott. "Tri-bimaximal mixing and the neutrino oscillation data". In: *Phys. Lett.* B530 (2002), p. 167. DOI: 10.1016/S0370-2693(02)01336-9. arXiv: hep-ph/0202074 [hep-ph].

[84] P. F. Harrison and W. G. Scott. "Permutation symmetry, tri - bimaximal neutrino mixing and the S3 group characters". In: *Phys. Lett.* B557 (2003), p. 76. DOI: 10.1016/S0370-2693(03)00183-7. arXiv: hep-ph/0302025 [hep-ph].

[85] F. Feruglio and A. Paris. "The Golden Ratio Prediction for the Solar Angle from a Natural Model with A5 Flavour Symmetry". In: *JHEP* 03 (2011), p. 101. DOI: 10.1007/JHEP03(2011)101. arXiv: 1101.0393 [hep-ph].

[86] S. F. King and C. Luhn. "Neutrino Mass and Mixing with Discrete Symmetry". In: *Rept. Prog. Phys.* 76 (2013), p. 056201. DOI: 10.1088/0034-4885/76/5/056201. arXiv: 1301.1340 [hep-ph].

[87] I. K. Cooper, S. F. King, and C. Luhn. "A4xSU(5) SUSY GUT of Flavour with Trimaximal Neutrino Mixing". In: *JHEP* 06 (2012), p. 130. DOI: 10.1007/JHEP06(2012)130. arXiv: 1203.1324 [hep-ph].

[88] G. Altarelli, F. Feruglio, and L. Merlo. "Tri-Bimaximal Neutrino Mixing and Discrete Flavour Symmetries". In: *Fortsch. Phys.* 61 (2013), pp. 507–534. DOI: 10.1002/prop.201200117. arXiv: 1205.5133 [hep-ph].

[89] Y. BenTov, X.-G. He, and A. Zee. "An A_4 x Z_4 model for neutrino mixing". In: *JHEP* 12 (2012), p. 093. DOI: 10.1007/JHEP12(2012)093. arXiv: 1208.1062 [hep-ph].

[90] M.-C. Chen et al. "Compatibility of θ_{13} and the Type I Seesaw Model with A_4 Symmetry". In: *JHEP* 02 (2013), p. 021. DOI: 10.1007/JHEP02(2013)021. arXiv: 1210.6982 [hep-ph].

[91] M. Holthausen, M. Lindner, and M. A. Schmidt. "Lepton flavor at the electroweak scale: A complete A_4 model". In: *Phys. Rev.* D87.3 (2013), p. 033006. DOI: 10.1103/PhysRevD.87.033006. arXiv: 1211.5143 [hep-ph].

[92] N. Memenga, W. Rodejohann, and H. Zhang. "A_4 flavor symmetry model for Dirac neutrinos and sizable U_{e3}". In: *Phys. Rev.* D87.5 (2013), p. 053021. DOI: 10.1103/PhysRevD.87.053021. arXiv: 1301.2963 [hep-ph].

[93] R. de Adelhart Toorop, F. Feruglio, and C. Hagedorn. "Discrete Flavour Symmetries in Light of T2K". In: *Phys. Lett.* B703 (2011), pp. 447–451. DOI: 10.1016/j.physletb.2011.08.013. arXiv: 1107.3486 [hep-ph].

[94] G.-J. Ding. "TFH Mixing Patterns, Large θ_{13} and $\Delta(96)$ Flavor Symmetry". In: *Nucl. Phys.* B862 (2012), pp. 1–42. DOI: 10.1016/j.nuclphysb.2012.04.002. arXiv: 1201.3279 [hep-ph].

[95] C. S. Lam. "Finite Symmetry of Leptonic Mass Matrices". In: *Phys. Rev.* D87.1 (2013), p. 013001. DOI: 10.1103/PhysRevD.87.013001. arXiv: 1208.5527 [hep-ph].

[96] C. S. Lam. "Horizontal symmetries ?(150) and ?(600)". In: *Phys. Rev.* D87.5 (2013), p. 053012. DOI: 10.1103/PhysRevD.87.053012. arXiv: 1301.1736 [hep-ph].

[97] M. Holthausen, K. S. Lim, and M. Lindner. "Lepton Mixing Patterns from a Scan of Finite Discrete Groups". In: *Phys. Lett.* B721 (2013), pp. 61–67. DOI: 10.1016/j.physletb.2013.02.047. arXiv: 1212.2411 [hep-ph].

[98] D. Hernandez and A. Yu. Smirnov. "Lepton mixing and discrete symmetries". In: *Phys. Rev.* D86 (2012), p. 053014. DOI: 10.1103/PhysRevD.86.053014. arXiv: 1204.0445 [hep-ph].

[99] D. Hernandez and A. Yu. Smirnov. "Discrete symmetries and model-independent patterns of lepton mixing". In: *Phys. Rev.* D87.5 (2013), p. 053005. DOI: 10.1103/PhysRevD.87.053005. arXiv: 1212.2149 [hep-ph].

[100] P. Ballett et al. "Testing atmospheric mixing sum rules at precision neutrino facilities". In: *Phys. Rev.* D89.1 (2014), p. 016016. DOI: 10.1103/PhysRevD.89.016016. arXiv: 1308.4314 [hep-ph].

[101] D. Meloni. "Checking Flavour Models at Neutrino Facilities". In: *Phys. Lett.* B728 (2014), pp. 118–124. DOI: 10.1016/j.physletb.2013.11.033. arXiv: 1308.4578 [hep-ph].

[102] A. D. Hanlon, S.-F. Ge, and W. W. Repko. "Phenomenological consequences of residual $\mathbb{Z}_2^s$ and $\overline{\mathbb{Z}}_2^s$ symmetries". In: *Phys. Lett.* B729 (2014), pp. 185–191. DOI: 10.1016/j.physletb.2013.12.063. arXiv: 1308.6522 [hep-ph].

[103] S. T. Petcov. "Predicting the values of the leptonic CP violation phases in theories with discrete flavour symmetries". In: *Nucl. Phys.* B892 (2015), pp. 400–428. DOI: 10.1016/j.nuclphysb.2015.01.011. arXiv: 1405.6006 [hep-ph].

[104] P. Ballett et al. "Testing solar lepton mixing sum rules in neutrino oscillation experiments". In: *JHEP* 12 (2014), p. 122. DOI: 10.1007/JHEP12(2014)122. arXiv: 1410.7573 [hep-ph].

[105] S. Antusch et al. "Neutrino mixing sum rules and oscillation experiments". In: *JHEP* 04 (2007), p. 060. DOI: 10.1088/1126-6708/2007/04/060. arXiv: hep-ph/0702286 [HEP-PH].

[106] P. Ballett et al. "Precision measurements of θ_{12} for testing models of discrete leptonic flavour symmetries". In: *J. Phys. Conf. Ser.* 598.1 (2015), p. 012014. DOI: 10.1088/1742-6596/598/1/012014. arXiv: 1406.0308 [hep-ph].

[107] I. Girardi, S. T. Petcov, and A. V. Titov. "Determining the Dirac CP Violation Phase in the Neutrino Mixing Matrix from Sum Rules". In: *Nucl. Phys.* B894 (2015), pp. 733–768. DOI: 10.1016/j.nuclphysb.2015.03.026. arXiv: 1410.8056 [hep-ph].

[108] F. Feruglio, C. Hagedorn, and R. Ziegler. "Lepton Mixing Parameters from Discrete and CP Symmetries". In: *JHEP* 07 (2013), p. 027. DOI: 10.1007/JHEP07(2013)027. arXiv: 1211.5560 [hep-ph].

[109] P. F. Harrison and W. G. Scott. "Symmetries and generalizations of tri - bimaximal neutrino mixing". In: *Phys. Lett.* B535 (2002), pp. 163–169. DOI: 10.1016/S0370-2693(02)01753-7. arXiv: hep-ph/0203209 [hep-ph].

[110] P. F. Harrison and W. G. Scott. "mu - tau reflection symmetry in lepton mixing and neutrino oscillations". In: *Phys. Lett.* B547 (2002), pp. 219–228. DOI: 10.1016/S0370-2693(02)02772-7. arXiv: hep-ph/0210197 [hep-ph].

[111] W. Grimus and L. Lavoura. "A Nonstandard CP transformation leading to maximal atmospheric neutrino mixing". In: *Phys. Lett.* B579 (2004), pp. 113–122. DOI: 10.1016/j.physletb.2003.10.075. arXiv: hep-ph/0305309 [hep-ph].

[112] P. M. Ferreira et al. "Maximal CP Violation in Lepton Mixing from a Model with Delta(27) flavour Symmetry". In: *JHEP* 09 (2012), p. 128. DOI: 10.1007/JHEP09(2012)128. arXiv: 1206.7072 [hep-ph].

[113] Y. Farzan and A. Yu. Smirnov. "Leptonic CP violation: Zero, maximal or between the two extremes". In: *JHEP* 01 (2007), p. 059. DOI: 10.1088/1126-6708/2007/01/059. arXiv: hep-ph/0610337 [hep-ph].

[114] M. Holthausen, M. Lindner, and M. A. Schmidt. "CP and Discrete Flavour Symmetries". In: *JHEP* 04 (2013), p. 122. DOI: 10.1007/JHEP04(2013)122. arXiv: 1211.6953 [hep-ph].

[115] M.-C. Chen et al. "CP Violation from Finite Groups". In: *Nucl. Phys.* B883 (2014), pp. 267–305. DOI: 10.1016/j.nuclphysb.2014.03.023. arXiv: 1402.0507 [hep-ph].

[116] G.-J. Ding, S. F. King, and A. J. Stuart. "Generalised CP and A_4 Family Symmetry". In: *JHEP* 12 (2013), p. 006. DOI: 10.1007/JHEP12(2013)006. arXiv: 1307.4212 [hep-ph].

[117] F. Feruglio, C. Hagedorn, and R. Ziegler. "A realistic pattern of lepton mixing and masses from S_4 and CP". In: *Eur. Phys. J.* C74 (2014), p. 2753. DOI: 10.1140/epjc/s10052-014-2753-2. arXiv: 1303.7178 [hep-ph].

[118] R. N. Mohapatra and C. C. Nishi. "S_4 Flavored CP Symmetry for Neutrinos". In: *Phys. Rev.* D86 (2012), p. 073007. DOI: 10.1103/PhysRevD.86.073007. arXiv: 1208.2875 [hep-ph].

[119] J. T. Penedo, S. T. Petcov, and A. V. Titov. "Neutrino Mixing and Leptonic CP Violation from S_4 Flavour and Generalised CP Symmetries". In: (2017). arXiv: 1705.00309 [hep-ph].

[120] C. Hagedorn, A. Meroni, and E. Molinaro. "Lepton mixing from ?($3n^2$) and ?($6n^2$) and CP". In: *Nucl. Phys.* B891 (2015), pp. 499–557. DOI: 10.1016/j.nuclphysb.2014.12.013. arXiv: 1408.7118 [hep-ph].

[121] G.-J. Ding, S. F. King, and T. Neder. "Generalised CP and $\Delta(6n^2)$ family symmetry in semi-direct models of leptons". In: *JHEP* 12 (2014), p. 007. DOI: 10.1007/JHEP12(2014)007. arXiv: 1409.8005 [hep-ph].

[122] C.-C. Li and G.-J. Ding. "Lepton Mixing in A_5 Family Symmetry and Generalized CP". In: *JHEP* 05 (2015), p. 100. DOI: 10.1007/JHEP05(2015)100. arXiv: 1503.03711 [hep-ph].

[123] A. Di Iura, C. Hagedorn, and D. Meloni. "Lepton mixing from the interplay of the alternating group A_5 and CP". In: *JHEP* 08 (2015), p. 037. DOI: 10.1007/JHEP08(2015)037. arXiv: 1503.04140 [hep-ph].

[124] G. Ecker, W. Grimus, and H. Neufeld. "A Standard Form for Generalized CP Transformations". In: *J. Phys.* A20 (1987), p. L807. DOI: 10.1088/0305-4470/20/12/010.

[125] G. C. Branco, R. G. Felipe, and F. R. Joaquim. "Leptonic CP Violation". In: *Rev. Mod. Phys.* 84 (2012), pp. 515–565. DOI: 10.1103/RevModPhys.84.515. arXiv: 1111.5332 [hep-ph].

[126] L. L. Everett and A. J. Stuart. "The Double Cover of the Icosahedral Symmetry Group and Quark Mass Textures". In: *Phys. Lett.* B698 (2011), pp. 131–139. DOI: 10.1016/j.physletb.2011.02.054. arXiv: 1011.4928 [hep-ph].

[127] G.-J. Ding, L. L. Everett, and A. J. Stuart. "Golden Ratio Neutrino Mixing and A_5 Flavor Symmetry". In: *Nucl. Phys.* B857 (2012), pp. 219–253. DOI: 10.1016/j.nuclphysb.2011.12.004. arXiv: 1110.1688 [hep-ph].

[128] R. de Adelhart Toorop, F. Feruglio, and C. Hagedorn. "Finite Modular Groups and Lepton Mixing". In: *Nucl. Phys.* B858 (2012), pp. 437–467. DOI: 10.1016/j.nuclphysb.2012.01.017. arXiv: 1112.1340 [hep-ph].

[129] Y. Au-Yeung. "A necessary and sufficient condition for simultaneous diagonalisation of two hermitian matrices and its application". In: *Glasgow Math Journal, 11:81-83, (1970)* (1970).

[130] C. Jarlskog. "Commutator of the Quark Mass Matrices in the Standard Electroweak Model and a Measure of Maximal CP Violation". In: *Phys. Rev. Lett.* 55 (1985), p. 1039. DOI: 10.1103/PhysRevLett.55.1039.

[131] O. W. Greenberg. "Rephase Invariant Formulation of CP Violation in the Kobayashi-Maskawa Framework". In: *Phys. Rev.* D32 (1985), p. 1841. DOI: 10.1103/PhysRevD.32.1841.

[132] I. Dunietz, O. W. Greenberg, and D.-d. Wu. "A Priori Definition of Maximal CP Violation". In: *Phys. Rev. Lett.* 55 (1985), p. 2935. DOI: 10.1103/PhysRevLett.55.2935.

[133] E. E. Jenkins and A. V. Manohar. "Rephasing Invariants of Quark and Lepton Mixing Matrices". In: *Nucl. Phys.* B792 (2008), pp. 187–205. DOI: 10.1016/j.nuclphysb.2007.09.031. arXiv: 0706.4313 [hep-ph].

[134] S. F. King. "Parametrizing the lepton mixing matrix in terms of deviations from tri-bimaximal mixing". In: *Phys. Lett.* B659 (2008), pp. 244–251. DOI: 10.1016/j.physletb.2007.10.078. arXiv: 0710.0530 [hep-ph].

[135] Y. Kajiyama, M. Raidal, and A. Strumia. "The Golden ratio prediction for the solar neutrino mixing". In: *Phys. Rev.* D76 (2007), p. 117301. DOI: 10.1103/PhysRevD.76.117301. arXiv: 0705.4559 [hep-ph].

[136] A. Datta, F.-S. Ling, and P. Ramond. "Correlated hierarchy, Dirac masses and large mixing angles". In: *Nucl. Phys.* B671 (2003), pp. 383–400. DOI: 10.1016/j.nuclphysb.2003.08.026. arXiv: hep-ph/0306002 [hep-ph].

[137] R. N. Mohapatra and W. Rodejohann. "Broken mu-tau symmetry and leptonic CP violation". In: *Phys. Rev.* D72 (2005), p. 053001. DOI: 10.1103/PhysRevD.72.053001. arXiv: hep-ph/0507312 [hep-ph].

[138] H.-J. He, W. Rodejohann, and X.-J. Xu. "Origin of Constrained Maximal CP Violation in Flavor Symmetry". In: *Phys. Lett.* B751 (2015), pp. 586–594. DOI: 10.1016/j.physletb.2015.10.066. arXiv: 1507.03541 [hep-ph].

[139] F. An et al. "Neutrino Physics with JUNO". In: *J. Phys.* G43.3 (2016), p. 030401. DOI: 10.1088/0954-3899/43/3/030401. arXiv: 1507.05613 [physics.ins-det].

[140] Y.-F. Li. "Overview of the Jiangmen Underground Neutrino Observatory (JUNO)". In: *Int. J. Mod. Phys. Conf. Ser.* 31 (2014), p. 1460300. DOI: 10.1142/S2010194514603007. arXiv: 1402.6143 [physics.ins-det].

[141] S.-B. Kim. "New results from RENO and prospects with RENO-50". In: *Nucl. Part. Phys. Proc.* 265-266 (2015), pp. 93–98. DOI: 10.1016/j.nuclphysbps.2015.06.024. arXiv: 1412.2199 [hep-ex].

[142] S. T. Petcov and M. Piai. "The LMA MSW solution of the solar neutrino problem, inverted neutrino mass hierarchy and reactor neutrino experiments". In: *Phys. Lett.* B533 (2002), pp. 94–106. DOI: 10.1016/S0370-2693(02)01591-5. arXiv: hep-ph/0112074 [hep-ph].

[143] G.-J. Ding and Y.-L. Zhou. "Predicting lepton flavor mixing from $\Delta(48)$ and generalized CP symmetries". In: *Chin. Phys.* C39.2 (2015), p. 021001. DOI: 10.1088/1674-1137/39/2/021001. arXiv: 1312.5222 [hep-ph].

[144] G.-J. Ding and Y.-L. Zhou. "Lepton mixing parameters from $\Delta(48)$ family symmetry and generalised CP". In: *JHEP* 06 (2014), p. 023. DOI: 10.1007/JHEP06(2014)023. arXiv: 1404.0592 [hep-ph].

[145] G.-J. Ding and S. F. King. "Generalized CP and $\Delta(96)$ family symmetry". In: *Phys. Rev.* D89.9 (2014), p. 093020. DOI: 10.1103/PhysRevD.89.093020. arXiv: 1403.5846 [hep-ph].

[146] K. Abe et al. "Neutrino oscillation physics potential of the T2K experiment". In: *PTEP* 2015.4 (2015), p. 043C01. DOI: 10.1093/ptep/ptv031. arXiv: 1409.7469 [hep-ex].

[147] R. B. Patterson. "The NOvA Experiment: Status and Outlook". In: (2012). [Nucl. Phys. Proc. Suppl.235-236,151(2013)]. DOI: 10.1016/j.nuclphysbps.2013.04.005. arXiv: 1209.0716 [hep-ex].

[148] R. Acciarri et al. "Long-Baseline Neutrino Facility (LBNF) and Deep Underground Neutrino Experiment (DUNE)". In: (2016). arXiv: 1601.05471 [physics.ins-det].

[149] T. Alion et al. "Experiment Simulation Configurations Used in DUNE CDR". In: (2016). arXiv: 1606.09550 [physics.ins-det].

[150] P. Huber, M. Lindner, and W. Winter. "Simulation of long-baseline neutrino oscillation experiments with GLoBES (General Long Baseline Experiment Simulator)". In: *Comput. Phys. Commun.* 167 (2005), p. 195. DOI: 10.1016/j.cpc.2005.01.003. arXiv: hep-ph/0407333 [hep-ph].

[151] P. Huber et al. "New features in the simulation of neutrino oscillation experiments with GLoBES 3.0: General Long Baseline Experiment Simulator". In: *Comput. Phys. Commun.* 177 (2007), pp. 432–438. DOI: 10.1016/j.cpc.2007.05.004. arXiv: hep-ph/0701187 [hep-ph].

[152] S. ZELLER. "LBNE-doc-5823-v9". In: (). URL: http://lbne2-docdb.fnal.gov/cgi-bin/ShowDocument?docid=5823.

[153] C. Soumya, K. N. Deepthi, and R. Mohanta. "A comprehensive study of the discovery potential of NOvA, T2K and T2HK experiments". In: *Adv. High Energy Phys.* 2016 (2016), p. 9139402. DOI: 10.1155/2016/9139402. arXiv: 1408.6071 [hep-ph].

[154] R. Acciarri et al. "Long-Baseline Neutrino Facility (LBNF) and Deep Underground Neutrino Experiment (DUNE)". In: (2015). arXiv: 1512.06148 [physics.ins-det].

[155] A. Chatterjee et al. "Octant sensitivity for large theta(13) in atmospheric and long baseline neutrino experiments". In: *JHEP* 06 (2013), p. 010. DOI: 10.1007/JHEP06(2013)010. arXiv: 1302.1370 [hep-ph].

[156] S. K. Agarwalla, S. Prakash, and S. U. Sankar. "Resolving the octant of theta23 with T2K and NOvA". In: *JHEP* 07 (2013), p. 131. DOI: 10.1007/JHEP07(2013)131. arXiv: 1301.2574 [hep-ph].

[157] K. Abe et al. "A Long Baseline Neutrino Oscillation Experiment Using J-PARC Neutrino Beam and Hyper-Kamiokande". In: 2014. arXiv: 1412.4673 [physics.ins-det]. URL: http://inspirehep.net/record/1334360/files/arXiv:1412.4673.pdf.

[158] S. T. Petcov and A. Yu. Smirnov. "Neutrinoless double beta decay and the solar neutrino problem". In: *Phys. Lett.* B322 (1994), pp. 109–118. DOI: 10.1016/0370-2693(94)90498-7. arXiv: hep-ph/9311204 [hep-ph].

[159] S. M. Bilenky, S. Pascoli, and S. T. Petcov. "Majorana neutrinos, neutrino mass spectrum, CP violation and neutrinoless double beta decay. 1. The Three neutrino mixing case". In: *Phys. Rev.* D64 (2001), p. 053010. DOI: 10.1103/PhysRevD.64.053010. arXiv: hep-ph/0102265 [hep-ph].

[160] S. Capelli et al. "CUORICINO last results and CUORE &". In: *Proceedings, 40th Rencontres de Moriond on Electroweak Interactions and Unified Theories: La Thuile, Val d'Aoste, Italy, Mar 5-12, 2005*. 2005, pp. 71–78. arXiv: hep-ex/0505045 [hep-ex]. URL: http://inspirehep.net/record/682665/files/Pages_from_C05-03-05_71.pdf.

[161] R. Brugnera et al. "Status of the GERDA experiment". In: *PoS* Neutel2013 (2013), p. 039.

[162] J. B. Albert et al. "Search for Majorana neutrinos with the first two years of EXO-200 data". In: *Nature* 510 (2014), pp. 229–234. DOI: 10.1038/nature13432. arXiv: 1402.6956 [nucl-ex].

[163] K. Asakura et al. "Results from KamLAND-Zen". In: *AIP Conf. Proc.* 1666 (2015), p. 170003. DOI: 10.1063/1.4915593. arXiv: 1409.0077 [physics.ins-det].

[164] J. Albert. "Status and Results from the EXO Collaboration". In: *EPJ Web Conf.* 66 (2014), p. 08001. DOI: 10.1051/epjconf/20146608001.

[165] D. R. Artusa et al. "Initial performance of the CUORE-0 experiment". In: *Eur. Phys. J.* C74.8 (2014), p. 2956. DOI: 10.1140/epjc/s10052-014-2956-6. arXiv: 1402.0922 [physics.ins-det].

[166] L. Sibley. "SNO+: Physics program and status update". In: *AIP Conf. Proc.* 1604 (2014), pp. 449–455. DOI: 10.1063/1.4883464.

[167] D. Lorca. "The Hunt for neutrinoless double beta decay with the NEXT experiment". In: *Proceedings, 20th International Conference on Particles and Nuclei (PANIC 14): Hamburg, Germany, August 24-29, 2014*. 2014, pp. 321–324. DOI: 10.3204/DESY-PROC-2014-04/65. arXiv: 1411.0475 [physics.ins-det]. URL: http://inspirehep.net/record/1325797/files/arXiv:1411.0475.pdf.

[168] J. J. Gomez-Cadenas. "The NEXT experiment". In: *Nucl. Part. Phys. Proc.* 273-275 (2016), pp. 1732–1739. DOI: 10.1016/j.nuclphysbps.2015.09.279. arXiv: 1411.2433 [physics.ins-det].

[169] M. Fritts and K. Zuber. "Status and perspectives of COBRA". In: *Nucl. Phys. Proc. Suppl.* 237-238 (2013), pp. 37–39. DOI: 10.1016/j.nuclphysbps.2013.04.052.

[170] W. Xu et al. "The *MAJORANA DEMONSTRATOR*: A Search for Neutrinoless Double-beta Decay of ^{76}Ge". In: *J. Phys. Conf. Ser.* 606.1 (2015), p. 012004. DOI: 10.1088/1742-6596/606/1/012004. arXiv: 1501.03089 [nucl-ex].

[171] F. Nova. "NEMO-3 and SuperNEMO: A search for zero neutrino double beta decay". In: *AIP Conf. Proc.* 1560 (2013), pp. 184–186. DOI: 10.1063/1.4826748.

[172] N. Ishihara. "The DCBA experiment searching for neutrinoless double beta decay". In: *Nucl. Phys. Proc. Suppl.* 229-232 (2012), p. 481. DOI: 10.1016/j.nuclphysbps.2012.09.118.

[173] S. M. Bilenky et al. "Short baseline neutrino oscillations and neutrinoless (Beta Beta) decay in schemes with an inverted mass spectrum". In: *Phys. Rev.* D54 (1996), pp. 4432–4444. DOI: 10.1103/PhysRevD.54.4432. arXiv: hep-ph/9604364 [hep-ph].

[174] K. Abe et al. "Measurements of neutrino oscillation in appearance and disappearance channels by the T2K experiment with 6.610^{20} protons on target". In: *Phys. Rev.* D91.7 (2015), p. 072010. DOI: 10.1103/PhysRevD.91.072010. arXiv: 1502.01550 [hep-ex].

[175] I. Baldes, T. Konstandin, and G. Servant. "A First-Order Electroweak Phase Transition in the Standard Model from Varying Yukawas". In: (2016). arXiv: 1604.04526 [hep-ph].

[176] C. Hagedorn and E. Molinaro. "Flavor and CP symmetries for leptogenesis and 0 decay". In: *Nucl. Phys.* B919 (2017), pp. 404–469. DOI: 10.1016/j.nuclphysb.2017.03.015. arXiv: 1602.04206 [hep-ph].

[177] P. Chen, G.-J. Ding, and S. F. King. "Leptogenesis and residual CP symmetry". In: *JHEP* 03 (2016), p. 206. DOI: 10.1007/JHEP03(2016)206. arXiv: 1602.03873 [hep-ph].

[178] T. Araki, J. Kubo, and E. A. Paschos. "S(3) flavor symmetry and leptogenesis". In: *Eur. Phys. J.* C45 (2006), pp. 465–475. DOI: 10.1140/epjc/s2005-02434-3. arXiv: hep-ph/0502164 [hep-ph].

[179] Y. H. Ahn, S. K. Kang, and C. S. Kim. "Spontaneous CP Violation in A_4 Flavor Symmetry and Leptogenesis". In: *Phys. Rev.* D87.11 (2013), p. 113012. DOI: 10.1103/PhysRevD.87.113012. arXiv: 1304.0921 [hep-ph].

[180] R. H. Cyburt et al. "Big Bang Nucleosynthesis: 2015". In: *Rev. Mod. Phys.* 88 (2016), p. 015004. DOI: 10.1103/RevModPhys.88.015004. arXiv: 1505.01076 [astro-ph.CO].

[181] A. D. Dolgov. "Big bang nucleosynthesis". In: *Nucl. Phys. Proc. Suppl.* 110 (2002), pp. 137–143. DOI: 10.1016/S0920-5632(02)01470-6. arXiv: hep-ph/0201107 [hep-ph].

[182] B. D. Fields, P. Molaro, and S. Sarkar. "Big-Bang Nucleosynthesis". In: *Chin. Phys.* C38 (2014), pp. 339–344. arXiv: 1412.1408 [astro-ph.CO].

[183] R. Adam et al. "Planck 2015 results. I. Overview of products and scientific results". In: *Astron. Astrophys.* 594 (2016), A1. DOI: 10.1051/0004-6361/201527101. arXiv: 1502.01582 [astro-ph.CO].

[184] P. A. R. Ade et al. "Planck 2015 results. XIII. Cosmological parameters". In: *Astron. Astrophys.* 594 (2016), A13. DOI: 10.1051/0004-6361/201525830. arXiv: 1502.01589 [astro-ph.CO].

[185] G. F. Smoot et al. "Structure in the COBE differential microwave radiometer first year maps". In: *Astrophys. J.* 396 (1992), pp. L1–L5. DOI: 10.1086/186504.

[186] A. Strumia. "Baryogenesis via leptogenesis". In: *Particle physics beyond the standard model. Proceedings, Summer School on Theoretical Physics, 84th Session, Les Houches, France, August 1-26, 2005*. 2006, pp. 655–680. arXiv: hep-ph/0608347 [hep-ph].

[187] A. D. Sakharov. "Violation of CP Invariance, c Asymmetry, and Baryon Asymmetry of the Universe". In: *Pisma Zh. Eksp. Teor. Fiz.* 5 (1967). [Usp. Fiz. Nauk161,61(1991)], pp. 32–35. DOI: 10.1070/PU1991v034n05ABEH002497.

[188] O. Bertolami et al. "CPT violation and baryogenesis". In: *Phys. Lett.* B395 (1997), pp. 178–183. DOI: 10.1016/S0370-2693(97)00062-2. arXiv: hep-ph/9612437 [hep-ph].

[189] S. Abel. *Lecture notes on Anomalies*. URL: http://www.maths.dur.ac.uk/~dma0saa/lecture_notes.pdf.

[190] A. Lazopoulos. *Lecture notes on Axial Anomaly*. URL: https://people.phys.ethz.ch/~pheno/AFTcourse/notes/lecture2.pdf.

[191] A. A. Belavin et al. "Pseudoparticle Solutions of the Yang-Mills Equations". In: *Phys. Lett.* B59 (1975), pp. 85–87. DOI: 10.1016/0370-2693(75)90163-X.

[192] G. 't Hooft. "Computation of the Quantum Effects Due to a Four-Dimensional Pseudoparticle". In: *Phys. Rev.* D14 (1976). [Erratum: Phys. Rev.D18,2199(1978)],

pp. 3432–3450. DOI: 10.1103/PhysRevD.18.2199.3,10.1103/PhysRevD.14.3432.

[193] M. Shifman. *Advanced Topics in Quantum Field Theory*. Cambridge University Press, 2012.

[194] J. Schaldach. *PhD Thesis, (2002)*. URL: http://www-brs.ub.ruhr-uni-bochum.de/netahtml/HSS/Diss/SchaldachJoerg/diss.pdf.

[195] M. B. Gavela et al. "Standard model CP violation and baryon asymmetry". In: *Mod. Phys. Lett.* A9 (1994), pp. 795–810. DOI: 10.1142/S0217732394000629. arXiv: hep-ph/9312215 [hep-ph].

[196] P. Huet and E. Sather. "Electroweak baryogenesis and standard model CP violation". In: *Phys. Rev.* D51 (1995), pp. 379–394. DOI: 10.1103/PhysRevD.51.379. arXiv: hep-ph/9404302 [hep-ph].

[197] K. Kajantie et al. "The Electroweak phase transition: A Nonperturbative analysis". In: *Nucl. Phys.* B466 (1996), pp. 189–258. DOI: 10.1016/0550-3213(96)00052-1. arXiv: hep-lat/9510020 [hep-lat].

[198] M. Yoshimura. "Unified Gauge Theories and the Baryon Number of the Universe". In: *Phys. Rev. Lett.* 41 (1978). [Erratum: Phys. Rev. Lett.42,746(1979)], pp. 281–284. DOI: 10.1103/PhysRevLett.41.281.

[199] S. Dimopoulos and L. Susskind. "On the Baryon Number of the Universe". In: *Phys. Rev.* D18 (1978), pp. 4500–4509. DOI: 10.1103/PhysRevD.18.4500.

[200] D. Toussaint et al. "Matter - Antimatter Accounting, Thermodynamics, and Black Hole Radiation". In: *Phys. Rev.* D19 (1979), pp. 1036–1045. DOI: 10.1103/PhysRevD.19.1036.

[201] K. Dick et al. "Leptogenesis with Dirac neutrinos". In: *Phys. Rev. Lett.* 84 (2000), pp. 4039–4042. DOI: 10.1103/PhysRevLett.84.4039. arXiv: hep-ph/9907562 [hep-ph].

[202] H. Murayama and A. Pierce. "Realistic Dirac leptogenesis". In: *Phys. Rev. Lett.* 89 (2002), p. 271601. DOI: 10.1103/PhysRevLett.89.271601. arXiv: hep-ph/0206177 [hep-ph].

[203] M. Boz and N. K. Pak. "Dirac Leptogenesis and anomalous U(1)". In: *Eur. Phys. J.* C37 (2004), pp. 507–510. DOI: 10.1140/epjc/s2004-02022-1.

[204] D. G. Cerdeno, A. Dedes, and T. E. J. Underwood. "The Minimal Phantom Sector of the Standard Model: Higgs Phenomenology and Dirac Leptogenesis". In: *JHEP* 09 (2006), p. 067. DOI: 10.1088/1126-6708/2006/09/067. arXiv: hep-ph/0607157 [hep-ph].

[205] B. Thomas and M. Toharia. "Phenomenology of Dirac neutrinogenesis in split supersymmetry". In: *Phys. Rev.* D73 (2006), p. 063512. DOI: 10.1103/PhysRevD.73.063512. arXiv: hep-ph/0511206 [hep-ph].

[206] M. Plumacher. "Baryogenesis and lepton number violation". In: *Z. Phys.* C74 (1997), pp. 549–559. DOI: 10.1007/s002880050418. arXiv: hep-ph/9604229 [hep-ph].

[207] H. A. Weldon. "Effective Fermion Masses of Order gT in High Temperature Gauge Theories with Exact Chiral Invariance". In: *Phys. Rev.* D26 (1982), p. 2789. DOI: 10.1103/PhysRevD.26.2789.

[208] J. M. Cline, K. Kainulainen, and K. A. Olive. "Protecting the primordial baryon asymmetry from erasure by sphalerons". In: *Phys. Rev.* D49 (1994), pp. 6394–6409. DOI: 10.1103/PhysRevD.49.6394. arXiv: hep-ph/9401208 [hep-ph].

[209] L. Covi, E. Roulet, and F. Vissani. "CP violating decays in leptogenesis scenarios". In: *Phys. Lett.* B384 (1996), pp. 169–174. DOI: 10.1016/0370-2693(96)00817-9. arXiv: hep-ph/9605319 [hep-ph].

[210] M. Flanz, E. A. Paschos, and U. Sarkar. "Baryogenesis from a lepton asymmetric universe". In: *Phys. Lett.* B345 (1995). [Erratum: Phys. Lett.B382,447(1996)], pp. 248–252. DOI: 10.1016/0370-2693(96)00866-0, 10.1016/0370-2693(96)00842-8, 10.1016/0370-2693(94)01555-Q. arXiv: hep-ph/9411366 [hep-ph].

[211] A. Pilaftsis and T. E. J. Underwood. "Resonant leptogenesis". In: *Nucl. Phys.* B692 (2004), pp. 303–345. DOI: 10.1016/j.nuclphysb.2004.05.029. arXiv: hep-ph/0309342 [hep-ph].

[212] M. A. Luty. "Baryogenesis via leptogenesis". In: *Phys. Rev.* D45 (1992), pp. 455–465. DOI: 10.1103/PhysRevD.45.455.

[213] W. Buchmuller and M. Plumacher. "Neutrino masses and the baryon asymmetry". In: *Int. J. Mod. Phys.* A15 (2000), pp. 5047–5086. DOI: 10.1016/S0217-751X(00)00293-5,10.1142/S0217751X00002935. arXiv: hep-ph/0007176 [hep-ph].

[214] R. Barbieri et al. "Baryogenesis through leptogenesis". In: *Nucl. Phys.* B575 (2000), pp. 61–77. DOI: 10.1016/S0550-3213(00)00011-0. arXiv: hep-ph/9911315 [hep-ph].

[215] W. Buchmuller, P. Di Bari, and M. Plumacher. "Leptogenesis for pedestrians". In: *Annals Phys.* 315 (2005), pp. 305–351. DOI: 10.1016/j.aop.2004.02.003. arXiv: hep-ph/0401240 [hep-ph].

[216] G. F. Giudice et al. "Towards a complete theory of thermal leptogenesis in the SM and MSSM". In: *Nucl. Phys.* B685 (2004), pp. 89–149. DOI: 10.1016/j.nuclphysb.2004.02.019. arXiv: hep-ph/0310123 [hep-ph].

[217] A. Abada et al. "Flavor issues in leptogenesis". In: *JCAP* 0604 (2006), p. 004. DOI: 10.1088/1475-7516/2006/04/004. arXiv: hep-ph/0601083 [hep-ph].

[218] A. De Simone and A. Riotto. "On the impact of flavour oscillations in leptogenesis". In: *JCAP* 0702 (2007), p. 005. DOI: 10.1088/1475-7516/2007/02/005. arXiv: hep-ph/0611357 [hep-ph].

[219] S. Blanchet, P. Di Bari, and G. G. Raffelt. "Quantum Zeno effect and the impact of flavor in leptogenesis". In: *JCAP* 0703 (2007), p. 012. DOI: 10.1088/1475-7516/2007/03/012. arXiv: hep-ph/0611337 [hep-ph].

[220] S. Blanchet et al. "Leptogenesis with heavy neutrino flavours: from density matrix to Boltzmann equations". In: *JCAP* 1301 (2013), p. 041. DOI: 10.1088/1475-7516/2013/01/041. arXiv: 1112.4528 [hep-ph].

[221] W. Buchmuller and M. Plumacher. "Spectator processes and baryogenesis". In: *Phys. Lett.* B511 (2001), pp. 74–76. DOI: 10.1016/S0370-2693(01)00614-1. arXiv: hep-ph/0104189 [hep-ph].

[222] E. Nardi et al. "On Higgs and sphaleron effects during the leptogenesis era". In: *JHEP* 01 (2006), p. 068. DOI: 10.1088/1126-6708/2006/01/068. arXiv: hep-ph/0512052 [hep-ph].

[223] P. Schwaller. "Scattering rates and spectator effects in leptogenesis". In: *Proceedings, 49th Rencontres de Moriond on Electroweak Interactions and Unified Theories: La Thuile, Italy, March 15-22, 2014*. 2014, pp. 231–236. URL: http://moriond.in2p3.fr/Proceedings/2014/Moriond_EW_2014.pdf.

[224] C. P. Kiessig, M. Plumacher, and M. H. Thoma. "Decay of a Yukawa fermion at finite temperature and applications to leptogenesis". In: *Phys. Rev.* D82 (2010), p. 036007. DOI: 10.1103/PhysRevD.82.036007. arXiv: 1003.3016 [hep-ph].

[225] A. De Simone and A. Riotto. "Quantum Boltzmann Equations and Leptogenesis". In: *JCAP* 0708 (2007), p. 002. DOI: 10.1088/1475-7516/2007/08/002. arXiv: hep-ph/0703175 [hep-ph].

[226] M. Beneke et al. "Flavoured Leptogenesis in the CTP Formalism". In: *Nucl. Phys.* B843 (2011), pp. 177–212. DOI: 10.1016/j.nuclphysb.2010.10.001. arXiv: 1007.4783 [hep-ph].

[227] A. Anisimov et al. "Quantum Leptogenesis I". In: *Annals Phys.* 326 (2011). [Erratum: Annals Phys.338,376(2011)], pp. 1998–2038. DOI: 10.1016/j.aop.2011.02.002,10.1016/j.aop.2013.05.00. arXiv: 1012.5821 [hep-ph].

[228] M. Beneke et al. "Finite Number Density Corrections to Leptogenesis". In: *Nucl. Phys.* B838 (2010), pp. 1–27. DOI: 10.1016/j.nuclphysb.2010.05.003. arXiv: 1002.1326 [hep-ph].

[229] E. Kolb and M. Turner. *The Early Universe (Frontiers in Physics)*. New York: Addison-Wesley Publishing Company, 1990.

[230] W. Buchmuller, P. Di Bari, and M. Plumacher. "The Neutrino mass window for baryogenesis". In: *Nucl. Phys.* B665 (2003), pp. 445–468. DOI: 10.1016/S0550-3213(03)00449-8. arXiv: hep-ph/0302092 [hep-ph].

[231] J. A. Casas and A. Ibarra. "Oscillating neutrinos and muon —¿ e, gamma". In: *Nucl. Phys.* B618 (2001), pp. 171–204. DOI: 10.1016/S0550-3213(01)00475-8. arXiv: hep-ph/0103065 [hep-ph].

[232] S. Pascoli, S. T. Petcov, and A. Riotto. "Leptogenesis and Low Energy CP Violation in Neutrino Physics". In: *Nucl. Phys.* B774 (2007), pp. 1–52. DOI: 10.1016/j.nuclphysb.2007.02.019. arXiv: hep-ph/0611338 [hep-ph].

[233] S. Pascoli, S. T. Petcov, and A. Riotto. "Connecting low energy leptonic CP-violation to leptogenesis". In: *Phys. Rev.* D75 (2007), p. 083511. DOI: 10.1103/PhysRevD.75.083511. arXiv: hep-ph/0609125 [hep-ph].

[234] T. Prokopec. *Lecture notes for Cosmology (ns-tp430m)*. URL: https://www.staff.science.uu.nl/~proko101/2scm.pdf.

[235] D. E. Morrissey and M. J. Ramsey-Musolf. "Electroweak baryogenesis". In: *New J. Phys.* 14 (2012), p. 125003. DOI: 10.1088/1367-2630/14/12/125003. arXiv: 1206.2942 [hep-ph].

[236] M. Trodden. "Electroweak baryogenesis". In: *Rev. Mod. Phys.* 71 (1999), pp. 1463–1500. DOI: 10.1103/RevModPhys.71.1463. arXiv: hep-ph/9803479 [hep-ph].

[237] P. B. Arnold, D. Son, and L. G. Yaffe. "The Hot baryon violation rate is O (alpha-w**5 T**4)". In: *Phys. Rev.* D55 (1997), pp. 6264–6273. DOI: 10.1103/PhysRevD.55.6264. arXiv: hep-ph/9609481 [hep-ph].

[238] T. Cohen, D. E. Morrissey, and A. Pierce. "Electroweak Baryogenesis and Higgs Signatures". In: *Phys. Rev.* D86 (2012), p. 013009. DOI: 10.1103/PhysRevD.86.013009. arXiv: 1203.2924 [hep-ph].

[239] D. Curtin, P. Jaiswal, and P. Meade. "Excluding Electroweak Baryogenesis in the MSSM". In: *JHEP* 08 (2012), p. 005. DOI: 10.1007/JHEP08(2012)005. arXiv: 1203.2932 [hep-ph].

[240] M. Carena et al. "MSSM Electroweak Baryogenesis and LHC Data". In: *JHEP* 02 (2013), p. 001. DOI: 10.1007/JHEP02(2013)001. arXiv: 1207.6330 [hep-ph].

[241] J. Shu and Y. Zhang. "Impact of a CP Violating Higgs Sector: From LHC to Baryogenesis". In: *Phys. Rev. Lett.* 111.9 (2013), p. 091801. DOI: 10.1103/PhysRevLett.111.091801. arXiv: 1304.0773 [hep-ph].

[242] J. M. Cline and K. Kainulainen. "Improved Electroweak Phase Transition with Subdominant Inert Doublet Dark Matter". In: *Phys. Rev.* D87.7 (2013), p. 071701. DOI: 10.1103/PhysRevD.87.071701. arXiv: 1302.2614 [hep-ph].

[243] D. Borah and J. M. Cline. "Inert Doublet Dark Matter with Strong Electroweak Phase Transition". In: *Phys. Rev.* D86 (2012), p. 055001. DOI: 10.1103/PhysRevD.86.055001. arXiv: 1204.4722 [hep-ph].

[244] G. Gil, P. Chankowski, and M. Krawczyk. "Inert Dark Matter and Strong Electroweak Phase Transition". In: *Phys. Lett.* B717 (2012), pp. 396–402. DOI: 10.1016/j.physletb.2012.09.052. arXiv: 1207.0084 [hep-ph].

[245] N. Blinov et al. "Electroweak Baryogenesis from Exotic Electroweak Symmetry Breaking". In: *Phys. Rev.* D92.3 (2015), p. 035012. DOI: 10.1103/PhysRevD.92.035012. arXiv: 1504.05195 [hep-ph].

[246] D. Tong. *Lecture notes on Kinetic Theory*. URL: http://www.damtp.cam.ac.uk/user/tong/kinetic.html.

[247] M. L. Bellac. *Thermal Field Theory*. Cambridge Monographs on Mathematical Physics.

[248] E. A. Calzetta and B.-L. B. Hu. *Nonequilibrium Quantum Field Theory*. Cambridge Monographs on Mathematical Physics.

[249] P. Millington. "Thermal quantum field theory and perturbative non-equilibrium dynamics". PhD thesis. New York: Manchester U., 2012. DOI: 10.1007/978-3-319-01186-8. URL: http://www.springer.com/physics/theoretical%2C+mathematical+%26+computational+physics/book/978-3-319-01185-1.

[250] J. Berges. "Introduction to nonequilibrium quantum field theory". In: *AIP Conf. Proc.* 739 (2005). [,3(2004)], pp. 3–62. DOI: 10.1063/1.1843591. arXiv: hep-ph/0409233 [hep-ph].

[251] M. Drewes. "Quantum aspects of early universe thermodynamics". PhD thesis. Hamburg U., 2010. DOI: 10.3204/DESY-THESIS-2010-010. URL: http://inspirehep.net/record/852627/files/desy-thesis-10-010.pdf.

[252] G. D. Moore and T. Prokopec. "Bubble wall velocity in a first order electroweak phase transition". In: *Phys. Rev. Lett.* 75 (1995), pp. 777–780. DOI: 10.1103/PhysRevLett.75.777. arXiv: hep-ph/9503296 [hep-ph].

[253] G. D. Moore and T. Prokopec. "How fast can the wall move? A Study of the electroweak phase transition dynamics". In: *Phys. Rev.* D52 (1995), pp. 7182–7204. DOI: 10.1103/PhysRevD.52.7182. arXiv: hep-ph/9506475 [hep-ph].

[254] J. M. Cline, K. Kainulainen, and M. Trott. "Electroweak Baryogenesis in Two Higgs Doublet Models and B meson anomalies". In: *JHEP* 11 (2011), p. 089. DOI: 10.1007/JHEP11(2011)089. arXiv: 1107.3559 [hep-ph].

[255] T. Konstandin, G. Nardini, and I. Rues. "From Boltzmann equations to steady wall velocities". In: *JCAP* 1409.09 (2014), p. 028. DOI: 10.1088/1475-7516/2014/09/028. arXiv: 1407.3132 [hep-ph].

[256] J. Kozaczuk. "Bubble Expansion and the Viability of Singlet-Driven Electroweak Baryogenesis". In: *JHEP* 10 (2015), p. 135. DOI: 10.1007/JHEP10(2015)135. arXiv: 1506.04741 [hep-ph].

[257] A. Pilaftsis. "Electroweak Resonant Leptogenesis in the Singlet Majoron Model". In: *Phys. Rev.* D78 (2008), p. 013008. DOI: 10.1103/PhysRevD.78.013008. arXiv: 0805.1677 [hep-ph].

[258] F. F. Deppisch, J. Harz, and M. Hirsch. "Falsifying High-Scale Leptogenesis at the LHC". In: *Phys. Rev. Lett.* 112 (2014), p. 221601. DOI: 10.1103/PhysRevLett.112.221601. arXiv: 1312.4447 [hep-ph].

[259] F. F. Deppisch, J. Harz, and W.-C. Huang. "Impact of Neutrinoless Double Beta Decay on Models of Baryogenesis". In: *PoS* EPS-HEP2015 (2015), p. 078. arXiv: 1510.06305 [hep-ph].